

Measurement of the prompt J/ψ pair production cross-section in pp collisions at $\sqrt{s} = 8$ TeV with the ATLAS detector

ATLAS Collaboration*

CERN, 1211 Geneva 23, Switzerland

Received: 12 December 2016 / Accepted: 24 January 2017 / Published online: 7 February 2017

© CERN for the benefit of the ATLAS collaboration 2017. This article is published with open access at Springerlink.com

Abstract The production of two prompt J/ψ mesons, each with transverse momenta $p_T > 8.5$ GeV and rapidity $|y| < 2.1$, is studied using a sample of proton-proton collisions at $\sqrt{s} = 8$ TeV, corresponding to an integrated luminosity of 11.4 fb^{-1} collected in 2012 with the ATLAS detector at the LHC. The differential cross-section, assuming unpolarised J/ψ production, is measured as a function of the transverse momentum of the lower- p_T J/ψ meson, di- J/ψ p_T and mass, the difference in rapidity between the two J/ψ mesons, and the azimuthal angle between the two J/ψ mesons. The fraction of prompt pair events due to double parton scattering is determined by studying kinematic correlations between the two J/ψ mesons. The total and double parton scattering cross-sections are compared with predictions. The effective cross-section of double parton scattering is measured to be $\sigma_{\text{eff}} = 6.3 \pm 1.6(\text{stat}) \pm 1.0(\text{syst})$ mb.

Contents

1 Introduction	1
2 ATLAS detector	3
3 Event reconstruction and selection	3
4 Signal extraction	3
4.1 Efficiency and acceptance	4
4.2 Non- J/ψ background	4
4.3 Non-prompt background	5
4.4 Pile-up background	7
5 Double parton scattering	9
5.1 Data-driven model-independent approach	9
6 Systematic uncertainties	10
7 Results	12
7.1 Cross-section measurement	12
7.2 Double parton scattering measurement	13
7.2.1 Effective cross-section measurement	16
8 Summary	18
References	20

1 Introduction

The study of the simultaneous production of two prompt J/ψ mesons offers an opportunity to test our understanding of non-perturbative quantum chromodynamics (QCD). These events are also sensitive to next-to-leading-order (NLO) and higher-order perturbative QCD corrections, in addition to providing an opportunity to study and compare J/ψ production models. Di- J/ψ events can be produced from a single gluon-gluon collision via single parton scattering (SPS) or from two independent parton-parton scatters in a single proton-proton collision, known as double parton scattering (DPS).

In particular, the production of di- J/ψ events via double parton scattering presents a unique insight into the structure of the proton and allows a better comprehension of backgrounds to searches for new phenomena. Although the di- J/ψ process has a low production rate in hadron collisions, the high luminosity and energy of the LHC allows a more detailed study than previously possible [1–12]. State-of-the-art techniques have been developed to describe di- J/ψ production in leading-order (LO), NLO, next-to-leading-order colour singlet non-relativistic QCD computations without loops (NLO*), and intrinsic parton transverse momentum calculations. Contributions of gluon fragmentation and quark fragmentation, which occur at even higher order calculations have been shown to make a large difference in the predictions [8].

Prompt J/ψ mesons can be produced directly [13–20] or via a higher-mass charmonium state, such as $\chi_c \rightarrow J/\psi + X$ or $\psi(2S) \rightarrow J/\psi + X$. These feed-down events resemble direct gluon-gluon fusion J/ψ production. Non-prompt events can be identified by their displaced decay vertex from the decay of b -hadrons. The focus of this paper is on prompt-prompt (PP) di- J/ψ production with the decay $J/\psi \rightarrow \mu^+ \mu^-$. This decay channel has the advantage of a clean four-muon signal. Examples of prompt-prompt di- J/ψ production diagrams are shown in Fig. 1.

* e-mail: atlas.publications@cern.ch

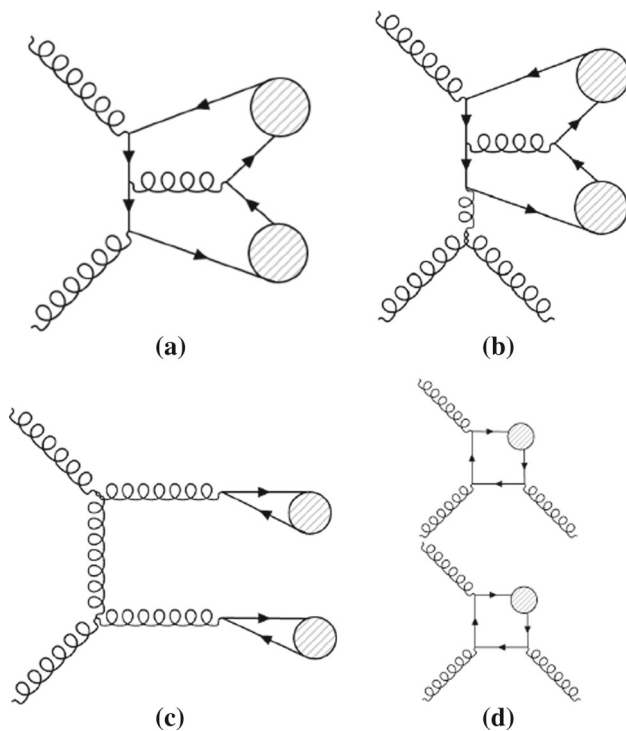


Fig. 1 Examples of Feynman diagrams of prompt-prompt J/ψ pair production in pp collisions for **a** leading-order production and **b** next-to-leading-order production in which the circle represents the J/ψ meson produced in a colour-singlet state, **c** leading-order production where the circles represent a $c\bar{c}$ pair in a colour-octet state, and **d** double parton scattering

It is expected that DPS plays a larger role at high energies and could be increasingly important for $c\bar{c}c\bar{c}$ production [21,22]. DPS can help to explain the cross-section of multi-jet production and the large difference in rapidity¹ for hard interaction processes [23]. As di- J/ψ production is dominated by gluon interactions, it gives information complementary to recent effective cross-section measurements of quark-dominated interactions. The effective cross-section is a factor which relates the production cross-section of the two individual interactions to the total interaction. Due to the low production rate of prompt J/ψ meson pairs, this process has not been studied in as much detail as other DPS processes and can therefore provide a good test of the process dependence of the effective cross-section. Testing possible correlations of non-perturbative origin between the partons

¹ ATLAS uses a right-handed coordinate system where the nominal interaction point (IP) is defined as the origin, the z -axis defines the beam direction, and the x - y plane is transverse to the beam direction. The positive x -axis is defined to point from the IP to the centre of the LHC ring, and the positive y -axis points upward. The azimuthal angle, ϕ , is measured around the beam axis and the polar angle, θ , is measured from the beam axis. The pseudorapidity is defined as $\eta = -\ln[\tan(\theta/2)]$ and for massive particles the rapidity $y = 1/2 \cdot \ln[(E + p_z)/(E - p_z)]$ is used.

in DPS events could lead to a better comprehension of non-perturbative QCD [24].

DPS has been studied in multiple final-states such as $W(\rightarrow \ell\nu) + 2$ jets [25,26], $Z(\rightarrow \ell^+\ell^-) + J/\psi$ [27], quarkonium plus open charm [22,28], double quarkonium [29,30], dijet [31], $\gamma + 3$ jets [32–35], and 4 jets [35–38]. The production of di- J/ψ events via DPS and SPS is described in Refs. [10–12,39–43].

In this paper, the differential cross-sections for PP J/ψ pairs are measured as functions of the transverse momentum of the lower- p_T J/ψ meson, the di- J/ψ transverse momentum, and the di- J/ψ mass. The lower- p_T (sub-leading) J/ψ meson is denoted as J/ψ_2 hereafter. Measurements are presented in two regions of the sub-leading J/ψ meson rapidity both within the muon p_T acceptance and extrapolated to the full acceptance by integrating the muon transverse momentum to zero. Additionally, the differential cross-section over the full J/ψ rapidity region defined by the muon selection criteria is measured for these variables along with the difference in rapidity and the azimuthal angle between the two J/ψ mesons. Using the sub-leading J/ψ meson allows the full range of the muon kinematic region to be explored. As the mass resolution for J/ψ mesons is worse at forward rapidities, the cross-section is measured in two rapidity regions, $|y(J/\psi_2)| < 1.05$ and $1.05 \leq |y(J/\psi_2)| < 2.1$, to increase the sensitivity of the results.

A data-driven method is used to produce background-subtracted SPS-weighted and DPS-weighted distributions of several kinematic variables. The measured distributions are compared with both the leading-order (LO) DPS and NLO* SPS predictions in the same fiducial volume. Finally, using the PP di- J/ψ cross-section, the fraction of DPS events, and the prompt J/ψ cross-section [14], the effective cross-section of DPS is measured and compared to previous measurements.

In data collected at $\sqrt{s} = 7$ TeV during 2011, the CMS experiment measured the cross-section of the pair production of prompt J/ψ mesons extrapolated to a muon p_T of zero assuming unpolarised J/ψ mesons [44]. The D0 experiment measured the fiducial prompt J/ψ pair cross-section using data collected at $\sqrt{s} = 1.96$ TeV [29]. The LHCb experiment measured the pair production of prompt J/ψ mesons in the forward rapidity region using data collected at $\sqrt{s} = 7$ TeV [7]. The present measurement of PP di- J/ψ production uses a different kinematic range and a larger data set.

The rest of this document is organised as follows. In Sect. 2, a brief description of the ATLAS detector and the data samples used in this study is provided. In Sect. 3, the methods used in the event reconstruction as well as the selection criteria used in this analysis are reported. Section 4 focuses on the removal of non- J/ψ , non-prompt J/ψ , and pile-up backgrounds as well as the calculation of the detec-

tor and selection efficiencies used in the extrapolated signal yields. In Sect. 5, double parton scattering and the data-driven method to extract the fraction of DPS events from various kinematic variables are discussed. Section 6 reports the systematic uncertainties. In Sect. 7, the results of the cross-section measurements and DPS study are presented. Finally, the findings are summarised in Sect. 8.

2 ATLAS detector

A full and detailed description of the ATLAS detector can be found in Ref. [45]. The inner detector (ID) is composed of the pixel detector, the semiconductor tracker (SCT), and the transition radiation tracker (TRT). The pixel and SCT detectors cover the range $|\eta| < 2.5$. The barrel is constructed from concentric cylinders around the beam axis and in the end-caps the disks are oriented perpendicular to the beam axis. The TRT is made up of straws filled with gas. It covers a range of $|\eta| \leq 2.0$. The TRT surrounds the SCT and provides r - ϕ information as well as electron identification information from transition radiation photons. The ID is surrounded by a solenoid which provides a 2 T axial magnetic field. The calorimeter has separate electromagnetic and hadronic components. The muon spectrometer (MS) consists of monitored drift tubes for $|\eta| \leq 2.7$ in combination with cathode strip chambers for $2.0 < |\eta| < 2.7$. Additionally, there are two types of triggering chambers, the resistive plate chambers (RPC) and the thin gap chambers (TGC). The MS is designed to provide precise position and momentum measurements in the bending plane and is capable of stand-alone muon reconstruction. The ATLAS trigger system has three levels (Level-1, Level-2, Event Filter). The Level-1 muon trigger uses information from three layers of RPCs in the barrel region ($|\eta| < 1.05$) and three layers of TGCs in the end-cap regions ($1.05 < |\eta| < 2.4$). The geometric coverage of the Level-1 trigger for single muons is about 99% in the end-cap regions and about 80% in the barrel region [46]. Information from the ID and MS is included in the Level-2 and Event Filter triggers.

3 Event reconstruction and selection

The data set used was collected during 2012 at $\sqrt{s} = 8$ TeV for proton–proton collisions. The total integrated luminosity of the data set used is $14.1 \pm 0.3 \text{ fb}^{-1}$, and $11.4 \pm 0.3 \text{ fb}^{-1}$ [47] after accounting for the prescale factor of the J/ψ dimuon trigger.

The selected events satisfy a J/ψ dimuon trigger requiring two muons with $p_T > 4$ GeV and invariant mass in the range $2.5 < m(\mu\mu) < 4.3$ GeV. Two J/ψ candidates reconstructed through their decay to a pair of oppositely

charged muons are required. The reconstruction of the muon tracks is described in Ref. [48]. The offline selection requires that events have at least three muons identified by the MS with matching tracks in the ID. Due to the ID acceptance, the reconstruction of muons is limited to $|\eta^\mu| < 2.5$ and must satisfy the selection criteria described in Ref. [48].

The two J/ψ candidates in each event are ordered by transverse momentum. In the event reconstruction, it is permitted that the two J/ψ candidates are associated with two different proton–proton collision vertices. This is necessary to model the pile-up background. The signed transverse decay length, L_{xy} , of each J/ψ candidate is defined as the projection of the vector from the closest reconstructed hard-scatter vertex candidate along the beam direction to the J/ψ decay vertex onto the J/ψ transverse momentum vector. Events with the two J/ψ candidates originating from different vertices are removed later by imposing a limit on the distance along the beam axis between the two vertices and subtracting the pile-up events that make it through this requirement, as described in Sect. 4.4. After subtracting the remaining multiple vertex events, the primary vertex is the common vertex which is closest to each J/ψ candidate along the beam direction. The following kinematic and geometrical requirements on the muons and J/ψ mesons are applied:

- $|\eta^\mu| < 2.3$ and $p_T^\mu > 2.5$ GeV.
- $2.8 \leq m(\mu\mu) \leq 3.4$ GeV.
- $|y^{J/\psi}| < 2.1$ and $p_T^{J/\psi} > 8.5$ GeV.
- For the triggered J/ψ , both of the reconstructed muons must have an ID track matched to a MS track.
- For the non-triggered J/ψ candidate, at least one of the reconstructed muons must have an ID track matched to a MS track.
- The distance between the two J/ψ decay vertices along the beam direction is required to be $|d_z| < 1.2$ mm. This requirement aims to select two J/ψ mesons that originate from the same proton–proton collision.
- The uncertainty in the measurement of L_{xy} is required to be less than 0.3 mm.

Although the requirement on $|d_z|$ affects events with large decay length, there is negligible bias in the measurement for PP signal events due to the narrow d_z distribution of prompt J/ψ pair production. This is discussed further in Sect. 6.

A total of 1210 events satisfy the above selection criteria.

4 Signal extraction

The PP differential cross-sections are measured in two rapidity regions based on the sub-leading J/ψ rapidity: the central region, $|y(J/\psi_2)| < 1.05$, and the forward region, $1.05 \leq |y(J/\psi_2)| < 2.1$,

$$\frac{\Delta\sigma_i(pp \rightarrow J/\psi J/\psi + X)}{\Delta x} = \frac{N_{\text{sig}}^i}{A_i \times \epsilon_i \times \text{BF}(J/\psi \rightarrow \mu^+\mu^-)^2 \times \Delta x \times \mathcal{L}} \quad (1)$$

In this equation the differential cross-section in bin i , of size Δx , of the kinematic variable x is a function of the number of PP di- J/ψ signal events in the interval, N_{sig}^i ; the kinematic acceptance correction, A_i , which is defined as the probability of a di- J/ψ event in the bin to pass the kinematic requirements; the efficiency, ϵ_i , of the trigger, reconstruction, and selection criteria; the branching fraction of a J/ψ meson to two muons, $\text{BF}(J/\psi \rightarrow \mu^+\mu^-)$; and the total integrated luminosity of the data set, \mathcal{L} .

The main sources of background to PP di- J/ψ production are non- J/ψ events, non-prompt J/ψ events, and events containing J/ψ mesons originating from two separate proton–proton collisions (called pile-up background). This analysis uses a sequential extraction of the di- J/ψ PP signal. First, each event is weighted by the inverse of the trigger, reconstruction and selection efficiencies and the kinematic acceptance. Next the two-dimensional distribution of the mass of the leading J/ψ candidate against the sub-leading J/ψ candidate is fit using a two-dimensional probability density function (PDF) in a maximum-likelihood fit [49] to subtract non- J/ψ background and extract the di- J/ψ signal. The extracted di- J/ψ signal is used to create PP event weights (the probability that the event is prompt–prompt) from the two-dimensional fit of the transverse decay length distribution of the leading J/ψ meson against the sub-leading J/ψ distribution. The extracted di- J/ψ signal is taken in bins Δx of the chosen variable x , weighted by the PP event weight and finally the pile-up background is subtracted.

Results are reported for the fiducial cross-section within the acceptance of the muon requirements as well as that corrected for muons produced outside the muon transverse momentum acceptance, described in detail in Ref. [14]. The world-average branching fraction of a J/ψ meson to two muons, $5.96 \pm 0.03\%$, is used [50].

4.1 Efficiency and acceptance

The PP di- J/ψ signal is corrected for the reconstruction, trigger, and event selection efficiencies, ϵ_i in Eq. (1). To obtain the dimuon trigger efficiency, the first step is to calculate the single-muon-trigger efficiency of each muon, multiply the two efficiencies, and then apply a correction term that accounts for correlations between the vertex resolution and opposite-sign requirements, as well as correcting for configurations in which the muons are too close to each other to be resolved by the Level-1 single-muon trigger. A further correction is applied to account for a bias due to the use of

high- p_T single-muon triggers for the efficiency determination. The correction is determined from the binned ratio of data to Monte Carlo (MC) simulation of an inclusive J/ψ sample generated using PYTHIA 8.186 [51] with the AU2 set of tuned parameters [52] and CTEQ6L1 parton distribution functions [53]. The MC samples are passed through ATLAS detector simulation [54] based on GEANT4 [55], and are reconstructed with the same software as the data. Using the single-muon-trigger efficiencies, the correction term for correlations and the MC correction, the total efficiency for the J/ψ dimuon trigger, ϵ , is then calculated using a modified form of the “tag and probe” method presented in Ref. [56].

A correction to the muon reconstruction efficiency is applied using the efficiency scale factors described in Ref. [48]. Efficiency scale factors have been determined in bins of $q \times \eta$ and ϕ separately for muons with and without an ID track that matches an MS track, where q is the charge of the muon. The scale factors for muons from the triggered J/ψ are taken from the correction that includes ID track matching. Since the other J/ψ meson only requires one of the muons to have an independent ID track matched to a MS track, a combination of the two efficiency corrections is used.

The kinematic acceptance factor, A_i in Eq. (1), is determined from simulation which describes the effect of the muon p_T and η cuts in the fiducial region definition, and corrects the cross-section for a J/ψ observed in the J/ψ p_T and rapidity fiducial region to the full muon geometric and kinematic acceptance. The method is described in detail in Ref. [14], and is applied to the fiducial volume of this analysis. For this correction the J/ψ mesons are assumed to be unpolarised, as the J/ψ polarisation coefficients were found close to zero [57–59]. The additional maximum variation of the polarisation assumption is shown in the differential cross-section distributions.

The final component of the event-weight corrections is the signal efficiency of the selection criteria. The d_z selection efficiency is 99.9 and 96.9% in the central and forward rapidity regions, respectively. The efficiency of the requirement on the L_{xy} uncertainty is 91.1% in the central region and 94.5% in the forward rapidity region. The correction is the inverse of the efficiency and is applied to each event.

4.2 Non- J/ψ background

The non- J/ψ background comes mostly from semileptonic decays of b -hadrons and from dimuon continuum events from Drell–Yan processes. An unbinned two-dimensional (2-D) maximum-likelihood fit [60] of the dimuon invariant mass of the leading J/ψ (J/ψ_1) against the dimuon invariant mass of the sub-leading J/ψ (J/ψ_2) is used to extract the signal. To parameterise the mass distribution of J/ψ signal events, a large inclusive J/ψ sample selected from the 2012 $\sqrt{s} = 8$ TeV ATLAS data is used. It has the same selection criteria,

fiducial volume, and trigger as the di- J/ψ sample with the exception of the cut on d_z which is not applied to the prompt signal.

In the fit of the inclusive J/ψ mass distribution, the signal is modelled by a modified double Crystal Ball function (CB) [61–63] and the background is modelled by a first-order polynomial. The modified double Crystal Ball function has a Gaussian core and power-law low-end and high-end tails that are fixed to have the same rate of decrease, described by the parameter n in the references. The parameter which controls the transition from the core Gaussian to the power-law tails is allowed to be different for each tail.

For the di- J/ψ sample the PDF includes terms for the signal which is parameterised as a product of two normalised CB functions and the normalised background, which is assumed to be constant in the 2-D mass plane. The values of the CB parameters for each J/ψ candidate are set to the values from the inclusive J/ψ sample in the corresponding rapidity region. The term for mixed J/ψ and non- J/ψ contributions is not found to be statistically significant within error and is therefore not included in the PDF. The expression for the PDF used to describe the data is:

$$P = P_{\text{sig}} \times CB(m(J/\psi_1)) \times CB(m(J/\psi_2)) + P_{\text{bkg}} \times P_0, \quad (2)$$

where P_{sig} is the fraction of events attributed to signal, $P_{\text{bkg}} = 1 - P_{\text{sig}}$ is the fraction of events attributed to background, and P_0 is a constant. The two J/ψ masses are not expected to be correlated and no evidence of a correlation is observed in the data.

The average mass and mass resolution of the reconstructed J/ψ meson depend on p_T (both varying by about 3% with p_T in the studied region), but in the di- J/ψ sample there are not enough events to let the mean and width float free for each bin of the chosen distribution. To account for this effect, a correction is applied as a function of p_T . The number of J/ψ signal events obtained from the fit of the inclusive J/ψ sample with and without a fixed mean and width is calculated as a function of p_T and the mass of each J/ψ meson in the di- J/ψ sample is corrected for the mass bias in the corresponding rapidity region.

For the extraction of the signal, the data are split into four rapidity regions based on the rapidities of the two J/ψ mesons. After correcting for the mass bias, the di- J/ψ signal is extracted from the unbinned 2-D maximum-likelihood fit of $m(J/\psi_1)$ against $m(J/\psi_2)$ in the range $2.8 \leq m(J/\psi) \leq 3.4$ GeV. The 1-D projections of the fit onto each J/ψ mass in the central and forward rapidity regions are shown in Fig. 2, and are used as an illustration of the shape of the signal and background distributions. There are 1050 ± 40 non-weighted di- J/ψ events extracted from the 2-D fit of the mass distribution in the fiducial volume.

From the efficiency-weighted unbinned maximum likelihood fit, there are $(15.0 \pm 0.9) \times 10^3$ di- J/ψ signal events in the full inclusive volume; this uncertainty does not include the uncertainty arising from the extrapolation to the inclusive volume. The increase is mainly from the transformation to the inclusive volume in which the p_T of the four muons is extrapolated to zero from the fiducial p_T requirements, in addition to the weights from the other efficiency corrections.

4.3 Non-prompt background

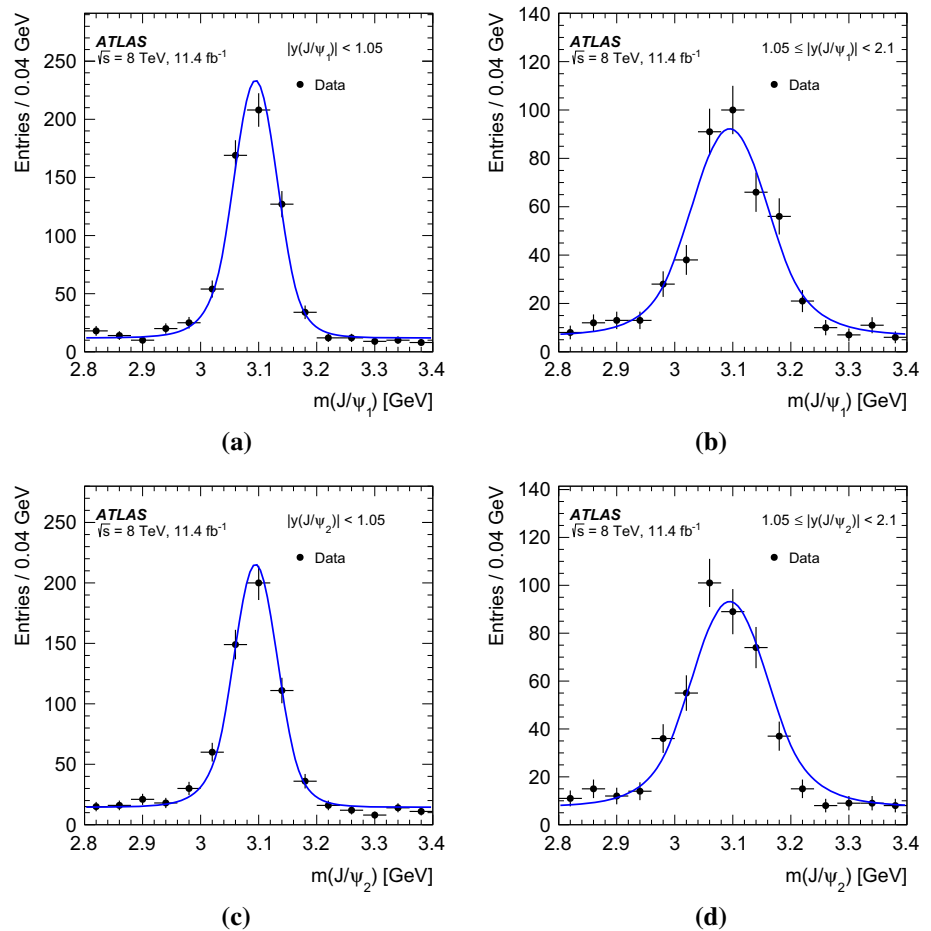
After extracting the inclusive di- J/ψ signal, the next step is to extract the PP signal by creating a PP event weight from a fit of the transverse decay length of each J/ψ meson. The distributions of the transverse decay length L_{xy} resolution, R , the prompt signal, S , and the non-prompt background, N , are defined as:

$$\begin{aligned} R &= G_1(L_{xy}) + G_2(L_{xy}) + G_3(L_{xy}) + G_4(L_{xy}) \\ S &= \delta(L_{xy}) * R \\ N &= \frac{1}{\tau} \exp(-L_{xy}/\tau) * R. \end{aligned} \quad (3)$$

The resolution function is modelled by the sum of four Gaussian functions, $G_i(L_{xy})$, centred at zero. This is determined from a study of the L_{xy} distribution of the inclusive J/ψ sample. The signal PDF is a delta function convolved with the four-Gaussian resolution function, and the non-prompt background PDF is modelled with a single-sided exponential function with decay constant τ , and is convolved with the four-Gaussian resolution function. In the di- J/ψ sample, the PP signal is extracted in four subsamples based on the rapidity of each J/ψ meson. The prompt and non-prompt PDFs are used for both J/ψ , with the parameters of the resolution function set to the values from the inclusive J/ψ sample in the corresponding rapidity region. A 2-D unbinned maximum-likelihood fit of the mass is performed in bins of L_{xy_1} against L_{xy_2} to get the di- J/ψ signal distribution.

In the central–central and forward–forward cases, when both J/ψ are either central or forward, a single value of the decay constant of the non-prompt exponential function is used to describe both J/ψ candidates. For the mixed cases, the two J/ψ candidates are allowed to have non-prompt exponential functions with different decay constants. In these cases, the decay constants of the central–central and forward–forward fits are used as input parameters to a Gaussian penalty function in the fit of the exponential tail of the central and forward J/ψ candidates respectively. The Gaussian penalty with the mean set to the decay constant of the non-prompt exponential function of either the central–central or forward–forward case is applied to the fit of the L_{xy} distributions. The penalty function increases the prob-

Fig. 2 The 1-D projections of the non-weighted invariant mass spectrum fit of the leading J/ψ in the **a** central and **b** forward rapidity regions as well as the sub-leading J/ψ in the **c** central and **d** forward rapidity regions. The fits use the parameters derived from the inclusive J/ψ sample



ability for the decay constant of the exponential tail for the J/ψ candidate to be close to the value of either the central–central or forward–forward case depending on its rapidity. The background-subtracted data are then fit with the product of the prompt PDFs for the two J/ψ mesons and the product of the non-prompt PDFs for the two J/ψ mesons. The mixed prompt and non-prompt terms are not included in the fit as the contribution is not found to be statistically significant. Figure 3 shows the 1-D projections of the results of the fits to data including the projected distributions for the prompt–prompt signal and non-prompt background. Dividing the PP PDF by the total PDF, shown in Fig. 3, gives the likelihood for an event to be PP as a function of the transverse decay length and rapidity of the two J/ψ mesons. By applying the PP probability as a signal weight to each event and then using an unbinned 2-D maximum-likelihood fit of the PP-weighted mass distribution of J/ψ_1 against J/ψ_2 in bins of the given kinematic variable, the projected distribution of that variable for the PP di- J/ψ signal is determined.

Because the PP event weight is determined as a function of the transverse decay length of the two J/ψ mesons in four rapidity regions over the full volume, an average value

is assumed over the differential distributions. Since the fraction of PP events, f_{PP} , can vary, an average f_{PP} leads to a bias of the PP event weight in the differential distributions. An example of the average f_{PP} leading to a bias is the p_T spectra of J/ψ mesons, as f_{PP} decreases with p_T . To determine this bias and to correct for it, MC di- J/ψ samples are used. Three MC samples (prompt–prompt, prompt–non-prompt, and non-prompt–non-prompt) are produced. The particle-level MC samples are produced using the second-hard-process mechanism in PYTHIA 8 [51]. These scale factors are defined as a function of the reconstructed prompt–prompt fraction, f_{PP} .

The resulting bias correction is displayed as a function of the reconstructed f_{PP} in Fig. 4 for the kinematic variables considered in this analysis. The lowest reconstructed f_{PP} is 15%, so the bias correction is only fit above this point. The correction factor is obtained separately for the central and forward rapidity regions of the sub-leading J/ψ meson. The bias correction is flat over a wide range of the reconstructed f_{PP} and drops quickly at low f_{PP} . It is fit with a threshold function defined as $F \times [1 - \text{erf}(x)]$, where F is a free parameter and $\text{erf}(x)$ is the error function obtained by integrating the normal distribution.

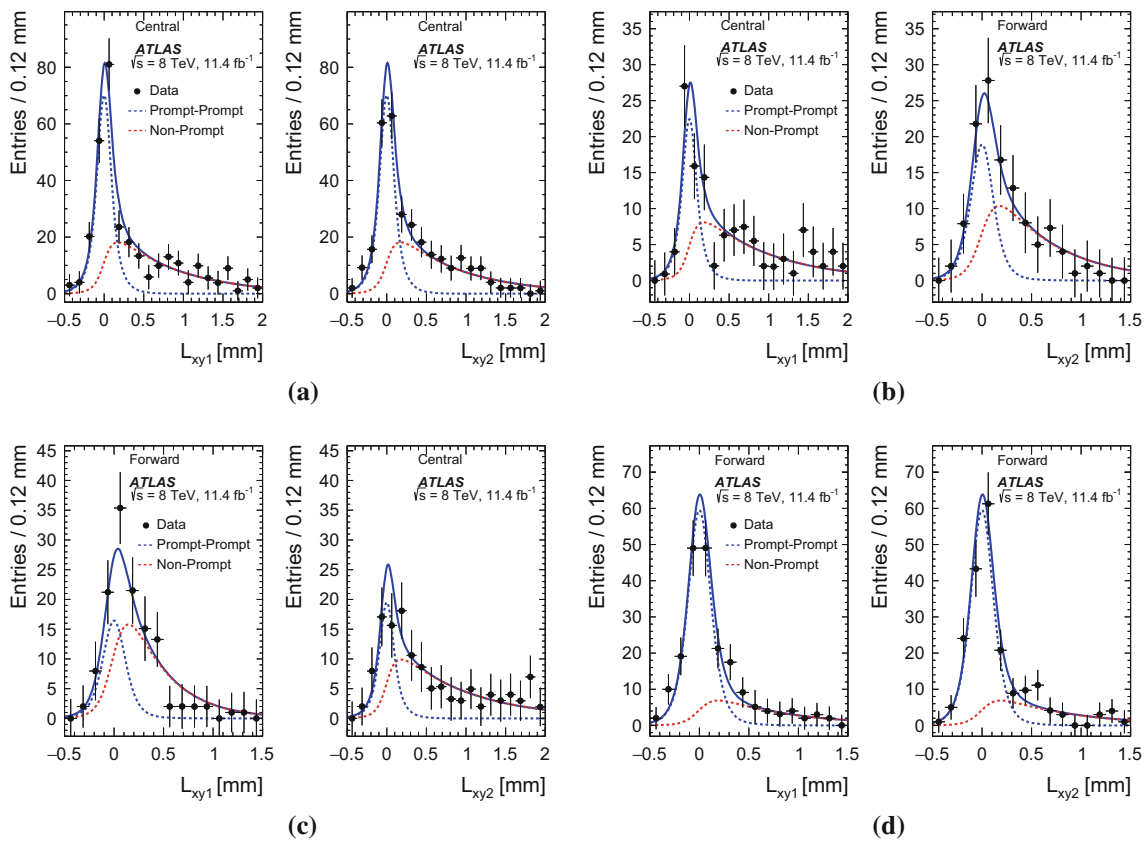


Fig. 3 The background-subtracted non-weighted transverse decay length spectra, L_{xy1} and L_{xy2} , of the leading and sub-leading J/ψ mesons. The data are split into four ranges: **a** central–central, **b** central–

forward, **c** forward–central, and **d** forward–forward. The prompt–prompt signal component and the non-prompt background component in the fiducial volume are shown

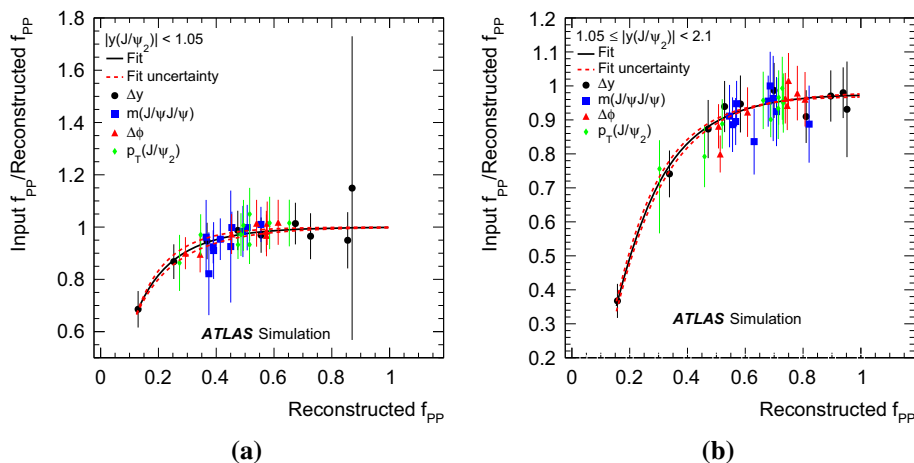


Fig. 4 The PP weight bias correction as a function of the reconstructed f_{PP} in the **a** central and **b** forward rapidity regions for different variables. The Δy distribution is used for the fit

In Fig. 5 the correction is applied to the $p_T(J/\psi_2)$ distribution. The correction factor is found to perform well for each of the variables considered. The original reconstructed distribution is included for comparison. Closure tests with MC samples are performed.

4.4 Pile-up background

The remaining background comes from pile-up events, which are multiple uncorrelated collisions in the same beam crossing. In pile-up events, the two J/ψ mesons originate from

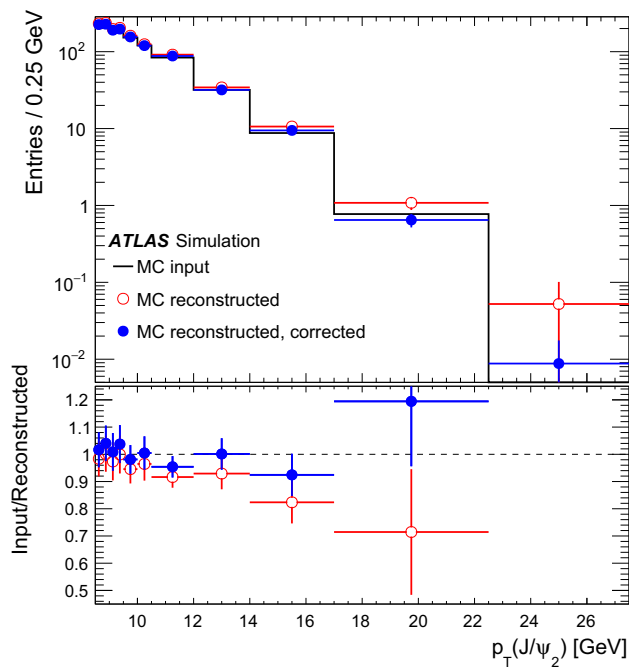


Fig. 5 A comparison of the PP MC input, MC reconstructed, and MC reconstructed corrected distribution of the sub-leading J/ψ p_T , $p_T(J/\psi_2)$. The ratios of the input to the MC reconstructed as well as bias corrected MC reconstructed distributions are shown

two independent proton–proton collisions. These events have distributions similar to those from DPS. The requirement on the distance between the trajectories of the two J/ψ mesons along the beam direction, $|d_z| < 1.2$ mm, is used to remove events that come from two separate primary vertices.

The PP background-subtracted d_z distribution is shown in Fig. 6. To determine the amount of pile-up background

that passes the d_z selection, a double Gaussian function is fit to the data. A narrow Gaussian describes the prompt J/ψ component and a wider Gaussian describes the component due to pile-up. Only the relative normalisation is free in the fit to the di- J/ψ sample. The other parameters of the Gaussian functions are determined from a fit to the large inclusive J/ψ sample over a wide d_z range. In the fit of the inclusive J/ψ sample, the pile-up distribution is found to have a Gaussian width of 49.2 ± 0.8 mm. The background is determined by integrating the fitted function over the selected d_z range of $|d_z| \leq 1.2$ mm.

The amount of pile-up in the accepted sample is $f_{\text{pile-up}} = (0.466 \pm 0.034$ (stat) ± 0.004 (syst))% in the central region and $f_{\text{pile-up}} = (0.802 \pm 0.062$ (stat) ± 0.007 (syst))% in the forward region. The systematic uncertainty is described in Sect. 6. As a check, the signal PP Gaussian width is allowed to be free in the di- J/ψ d_z fit. The width is compatible with the value calculated from the inclusive J/ψ sample but with a much larger uncertainty. Finally, to remove the pile-up background, the pile-up distributions of the kinematic variables are needed. This is achieved by reversing the $|d_z|$ requirement to $|d_z| > 2.0$ mm. The distribution of the chosen variable with this new requirement is then plotted to get the distributions of events coming from two separate primary vertices. The pile-up distributions are normalised to the correct number of events, $n_{\text{Total}} \times f_{\text{pile-up}}$, and subtracted from the PP distributions.

The total number of PP di- J/ψ signal events corrected for the muon acceptance are 3310 ± 330 (central) and 3140 ± 370 (forward) where the uncertainty is extracted from the fit of the weighted data. In the DPS analysis described in Sect. 5, the full muon fiducial volume is used. The number of

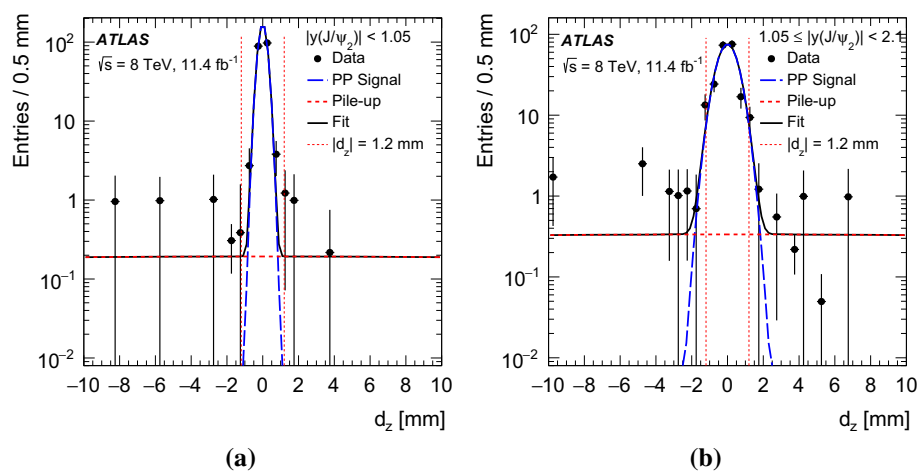


Fig. 6 The distribution of the distance between the trajectories of the two J/ψ mesons along the beam direction, d_z , after subtraction of the non- J/ψ and non-prompt background. A double Gaussian function is fit to the data in order to determine the fraction of pile-up background events in the **a** central and **b** forward rapidity regions. A narrow Gaussian

describes the prompt J/ψ component and a wider Gaussian describes the component due to pile-up. Only the relative normalisation is free in the fit. The parameters of both Gaussian functions are determined from a fit to the inclusive J/ψ sample over a wider range of d_z

PP di- J/ψ signal events in the fiducial volume, not corrected for the acceptance, is 1160 ± 70 .

5 Double parton scattering

Due to the decrease in the average fraction of the incoming proton momentum carried by a parton at large centre-of-mass energies, the parton densities rapidly increase and therefore DPS phenomena can be of substantial importance at the LHC. The DPS cross-section is dependent on the transverse distance between partons, and should decrease quickly as a function of transverse energy. Since at the LHC energies, J/ψ meson production is dominated by gluon-gluon interactions, the DPS cross-section is sensitive to the spatial distribution of gluons in the proton [64].

A simplified ansatz for defining the DPS cross-section in terms of the production cross-sections of the two final states and an effective cross-section is described in Ref. [65] as:

$$\sigma_{\text{eff}} = \frac{1}{2} \frac{\sigma_{J/\psi}^2}{\sigma_{\text{DPS}}^{J/\psi, J/\psi}} = \frac{1}{2} \frac{\sigma_{J/\psi}^2}{f_{\text{DPS}} \times \sigma_{J/\psi J/\psi}}, \quad (4)$$

where f_{DPS} is the fraction of PP di- J/ψ events that are due to DPS. The factor of 1/2 is because the two final states for di- J/ψ events are identical.

The effective cross-section, σ_{eff} , is related to the spatial separation between partons inside the proton. In the derivation of the effective cross-section ansatz, process and energy independence are assumed to be first-order approximations in perturbative QCD predictions. There are possible correlations between the fractional momenta of the incoming partons, the fractional momenta of the partons and the impact parameter, as well as spin and colour correlations that are not addressed in this simplified ansatz. These correlations and a modified effective cross-section ansatz which accounts for these possible correlations are described in Refs. [66–69].

Completely uncorrelated scatterings and the factorisation of the contributions to the cross-section described by the ansatz would lead to a universal effective cross-section which would be close to the inelastic cross-section. The measured values of the effective cross-section from multiple experiments range from about 5 to 20 mb [22, 25–28, 30, 31, 33–35, 37] for centre-of-mass energies of 630 GeV to 8 TeV.

5.1 Data-driven model-independent approach

One of the goals of this analysis is to measure the fraction of DPS events, f_{DPS} , as a function of various parameters such as the mass and p_T of the di- J/ψ system and the difference in rapidity and the azimuthal angle between the two J/ψ mesons in order to probe regions of phase space that are sensitive to different processes. A second goal of this analysis

is to use the di- J/ψ DPS cross-section obtained from the measured f_{DPS} to determine the effective cross-section of DPS. Additionally the modelling and subtraction of the DPS yield can be useful for studies of SPS quarkonium production models.

A common method for extracting the DPS contribution involves fitting DPS and SPS templates to the data. The theoretical predictions for the SPS distributions depend on perturbative QCD corrections of various orders and on J/ψ production models [20, 70–81]. By forming a template based on data, that dependence can be minimised.

In constructing the data-driven DPS template, it is assumed that the two J/ψ candidates are produced independently of each other. The DPS sample is therefore simulated by combining re-sampled J/ψ mesons from two different random events in the di- J/ψ sample which pass the requirements. By using events from the di- J/ψ sample, it is ensured that the J/ψ candidates in the DPS sample have the same kinematics as the data. The distribution of the absolute difference between the rapidities, Δy , against the absolute difference between the azimuthal angles, $\Delta\phi$, of the two J/ψ candidates for this DPS sample is shown in Fig. 7a. The template for the SPS component, shown in Fig. 7b, is obtained by subtracting the DPS template from the Δy against $\Delta\phi$ distribution of the background-subtracted data. The DPS contribution is normalised to the data in the region $\Delta y \geq 1.8$ and $\Delta\phi \leq \pi/2$, where DPS is assumed to dominate and SPS is assumed to be negligible. The DPS-dominated region is determined after a careful study of the data. The Δy requirement is determined as before this region the data drops off quickly with Δy and after it flattens out which is indicative of a dominant DPS contribution. After examining the data, it is observed that the peak at $\Delta\phi = \pi$ has a large tail in Δy and therefore an additional requirement is placed to avoid this tail. Additionally, theoretical predictions [10, 11] show that SPS is negligible in this region. The assumption of and sensitivity to the definition of the DPS-dominated region is tested by increasing the Δy and varying the $\Delta\phi$ requirements. By increasing the Δy requirement to a smaller region in which SPS is known to be negligible, the possibility of a SPS tail making it into the normalisation region is determined. Tests of the normalisation are included in Sect. 7.2. At low $\Delta\phi$ and large Δy , DPS dominates and this validates the choice of region used to normalise the DPS template to the data ($\Delta y \geq 1.8, \Delta\phi \leq \pi/2$).

From the 2-D data-driven templates of the SPS and DPS distribution, the DPS and SPS event weights, w_{DPS} and w_{SPS} , are:

$$\begin{aligned} w_{\text{DPS}}(\Delta\phi, \Delta y) &= \frac{N_{\text{DPS}}(\Delta\phi, \Delta y)}{N_{\text{Data}}(\Delta\phi, \Delta y)}, \\ w_{\text{SPS}}(\Delta\phi, \Delta y) &= \frac{N_{\text{SPS}}(\Delta\phi, \Delta y)}{N_{\text{Data}}(\Delta\phi, \Delta y)}, \end{aligned} \quad (5)$$

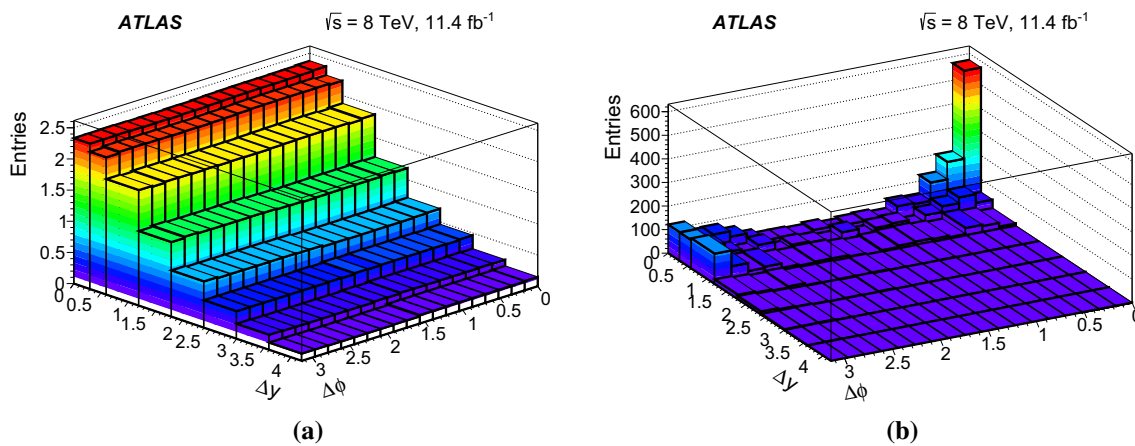


Fig. 7 The 2-D data-driven templates of Δy against $\Delta\phi$ for **a** DPS obtained by combining J/ψ pairs from different events and normalising to the data and **b** SPS obtained by subtracting the normalised DPS

template from the data. The data-driven templates are used to calculate the DPS and SPS event weights

where N_{Data} is the number of the background-subtracted and bias corrected di- J/ψ data events, and $N_{\text{DPS(SPS)}}$ are the number of background-subtracted and corrected DPS (SPS) events in the normalised template.

By applying these weights as well as the PP weight, and then extracting the di- J/ψ signal from the 2-D mass fits in bins of the chosen variable one can extract the PP SPS-weighted and DPS-weighted distributions of the kinematic variables studied.

From these weights, the value of f_{DPS} is determined. These weighted distributions are then compared to the sum of the LO DPS and NLO* SPS predicted distributions with f_{DPS} fixed to the measured experimental value. Finally, the effective cross-section is calculated and compared to the current measured values.

6 Systematic uncertainties

Sources of systematic uncertainty and their relative percentage are summarised in Table 1 for the di- J/ψ cross-section and Table 2 for the f_{DPS} measurement. Many of the systematic uncertainties cancel in the f_{DPS} measurement.

Trigger The systematic uncertainty due to the trigger selection is estimated by creating one thousand MC templates, varying each bin within the statistical uncertainty of the trigger efficiency and determining the effect on the yield. Additionally the spatial and vertex correction are varied within their uncertainty. Finally, a conservative uncertainty for the MC correction is determined by calculating the efficiency weighted yield without the application of the MC correction. This systematic uncertainty accounts for the use of different low- p_T single-muon triggers in the MC simulation that are not present in data and covers the possible range of trigger

Table 1 The summary of relative systematic uncertainties in the di- J/ψ cross-section in the central and forward rapidity regions of the sub-leading J/ψ . The systematic uncertainties for the branching fraction and luminosity are treated separately

Systematic uncertainty: di- J/ψ cross-section [%]		
Source	$ y(J/\psi_2) < 1.05$	$1.05 \leq y(J/\psi_2) < 2.1$
Trigger	± 7.5	± 8.3
Muon reconstruction	± 1.1	± 1.3
Kinematic acceptance	± 0.4	± 1.1
Mass model	± 0.1	± 0.1
Mass bias	± 0.2	± 0.2
Prompt–prompt model	± 0.2	± 0.01
Differential f_{PP} corr.	± 0.6	± 0.3
Pile-up	± 0.03	± 0.4
Total	± 7.7	± 8.5
Branching fraction	± 1.1	± 1.1
Luminosity	± 1.9	± 1.9

corrections. This is the dominant source of the systematic uncertainty due to the trigger selection.

Muon reconstruction The estimation of the systematic uncertainty due to the two muon reconstruction efficiency correction used in the analysis, described in Sect. 4.1, uses the same MC method as for the trigger efficiency measurement. The dominant source uncertainty comes from the statistical error in the tag-and-probe fit of $Z \rightarrow \mu\mu$ data for high- p_T muons and $J/\psi \rightarrow \mu\mu$ data for low- p_T muons.

Kinematic acceptance Comparing the ratio with and without the acceptance correction for the SPS and DPS MC samples gives the systematic uncertainty for the assumption that the acceptance correction can be applied independently for each J/ψ candidate. This assumption affects only SPS

Table 2 The summary of the relative systematic uncertainties for the data-driven f_{DPS} measurement. Several systematic uncertainties cancel in the ratio

Systematic uncertainty: f_{DPS} [%]	
Source	Relative uncertainty [%]
Trigger	± 0.7
Muon reconstruction	± 0.1
Mass model	± 0.01
Mass bias	± 0.02
Prompt–prompt model	± 0.1
Differential f_{PP} corr.	± 0.1
Pile-up	± 0.8
DPS model	± 5.6
Total	± 5.7

production. To measure the systematic uncertainty from bin migration effects due to the detector resolution, the method outlined in Ref. [14] is used in which the J/ψ p_{T} and rapidity spectra with and without convolution the experimental resolution are compared. The systematic uncertainty as a function of the rapidity is negligible and the systematic uncertainty as a function of the p_{T} is small relative to the SPS correction.

Mass model To extract signal di- J/ψ events, a 2-D fit of $m(J/\psi_1)$ against $m(J/\psi_2)$ is used. The signal parameters are determined from inclusive J/ψ samples in the central and forward rapidity regions. The mass fit parameters are varied within their uncertainties to estimate the systematic uncertainty due to the choice of the mass model. Alternative characterisations of the background, such as linear and exponential functions, were tested and were found to have negligible differences.

Mass bias The mean and width of the J/ψ mass fit are not constant as a function of p_{T} . The correction for fixing these values is the ratio of the number of J/ψ from the inclusive J/ψ sample with fixed mean and width parameters to the number with the mean and width allowed to be free, as a function of p_{T} . To find the systematic uncertainty of the mass bias correction, the correction is varied within its uncertainties in each bin.

Prompt–Prompt model A 2-D fit of the transverse decay length, L_{xy} , for signal di- J/ψ events is used to extract the PP distributions described in Sect. 4.3. The dependence of the PP model on the resolution function is tested using a triple-Gaussian function and assigning the difference from the default model as a systematic uncertainty. The systematic uncertainty is larger in the central rapidity region due to the smaller fraction of non-prompt events in the forward region from the event selection requirements. This allowed for more freedom in the fit of the PP component in the central region and a larger uncertainty from the model.

Differential f_{PP} correction The systematic uncertainty for the correction factor of the differential f_{PP} bias, described in Sect. 4.3, is determined by varying the fit of the bias correction and measuring the difference in the correction factor. A covariance matrix of the partial derivative of the likelihood function, used to determine the correction, with respect to the free parameters of the fit is used to extract the maximal deviation of the fit of the bias against the measured f_{PP} . The correction factor is refit with the varied parameters and the difference from the nominal final result is taken as the systematic uncertainty of the correction.

Pile-up The fit of the d_z distribution is varied by adjusting the pile-up Gaussian width within its uncertainty. As another test, a constant is used instead of a Gaussian function for the pile-up PDF. Any bias from the requirement of $|d_z| < 1.2$ mm on PP events is tested by adding a requirement of $|\Delta z_0| < \sqrt{2} \times 1.2$ mm for the inclusive J/ψ sample and propagating the change in the prompt PDF to the 2-D fit of the $L_{\text{xy}1}$ against $L_{\text{xy}2}$. Here, Δz_0 is defined as the difference in the impact parameter of an object with respect to the primary vertex in the r - z plane for each muon, and the factor of $\sqrt{2}$ is because the di- J/ψ sample has twice the muons of the inclusive J/ψ sample.

Branching fraction and luminosity The J/ψ meson to dimuon branching fraction systematic uncertainty is taken from the world-average [50]. The uncertainty in the integrated luminosity of 1.9% comes from Ref. [47] and is propagated through to the cross-section calculation.

DPS model The DPS-dominated region of the 2-D template used to create the SPS and DPS event weights, described in Sect. 5.1, is varied in both $\Delta\phi$ and Δy to test the dependence of f_{DPS} on the assumption and definition of the DPS-dominated region. For $\Delta\phi$ the DPS-dominated region is varied by $\pi/9$, the width of a bin in the DPS-dominated region. For Δy , the strictness of the DPS-dominated requirement is only increased to avoid including the SPS tail in the defined DPS-dominated region. It is increased by a single bin of Δy in the DPS-dominated region to 2.4. In this region, predictions show that SPS is negligible. The systematic uncertainty due to the contribution from the tail of the SPS distribution extending into the normalisation region has been determined by reducing the size of the normalisation region.

DPS binning As a cross-check, the dependence of f_{DPS} on the binning of the 2-D template used to create the SPS and DPS event weights is tested. A finer bin width is used where the distribution falls off more steeply around the NLO SPS peak and the DPS-dominated region is set to avoid the tail of the SPS distribution. The change in the f_{DPS} value is well within the uncertainty of f_{DPS} .

7 Results

The PP di- J/ψ and DPS differential cross-sections in the central and forward rapidity regions are measured for the sub-leading J/ψ p_T , the di- J/ψ p_T , and the di- J/ψ invariant mass corrected for the muon kinematic acceptance. Also shown are the results over the full J/ψ rapidity range in the muon fiducial volume: the total and DPS cross-sections for the difference in rapidity between the two J/ψ mesons, the azimuthal angle between the two J/ψ mesons, the di- J/ψ invariant mass, and the di- J/ψ p_T . The fraction of DPS events is calculated for each distribution, and the distributions are compared to the LO DPS and NLO* SPS+DPS predictions. For this comparison, the DPS predictions are normalised to the measured fraction of DPS events and the NLO* SPS predictions are multiplied by the feed-down correction factor from $\psi(2S)$ described in Ref. [10], which assumes that feed-down has the same distribution as the NLO* SPS predictions. For the data, feed-down is part of the PP signal. Finally, the effective cross-section of DPS is calculated and compared with previous measurements.

7.1 Cross-section measurement

The fiducial PP cross-section for the region $p_T(J/\psi) > 8.5$ GeV, $|y(J/\psi)| < 2.1$, $p_T(\mu) \geq 2.5$ GeV and $|\eta(\mu)| < 2.3$ with the two muons from the triggered J/ψ candidate having $p_T(\mu) \geq 4$ GeV is:

$$\sigma_{\text{Fid}}(pp \rightarrow J/\psi J/\psi + X) = \begin{cases} 15.6 \pm 1.3 \text{ (stat)} \pm 1.2 \text{ (syst)} \pm 0.2 \text{ (BF)} \\ \quad \pm 0.3 \text{ (lumi) pb, for } |y| < 1.05, \\ 13.5 \pm 1.3 \text{ (stat)} \pm 1.1 \text{ (syst)} \pm 0.2 \text{ (BF)} \\ \quad \pm 0.3 \text{ (lumi) pb, for } 1.05 \leq |y| < 2.1. \end{cases}$$

The above results are measured in two rapidity regions which are defined in terms of the sub-leading J/ψ meson. The systematic uncertainties for the branching fraction and luminosity are quoted separately. The extrapolated cross-section is measured by including the acceptance correction and assuming unpolarised J/ψ production. This cross-section is measured in the J/ψ fiducial volume $p_T > 8.5$ GeV, $|y| < 2.1$ with no requirement on the kinematics of the muon in the final state. The total cross-section over the full fiducial J/ψ rapidity is 160 ± 12 (stat) ± 14 (syst) ± 2 (BF) ± 3 (lumi) pb. The PP cross-section in the two rapidity regions of the sub-leading J/ψ meson is:

$$\sigma(pp \rightarrow J/\psi J/\psi + X) = \begin{cases} 82.2 \pm 8.3 \text{ (stat)} \pm 6.3 \text{ (syst)} \pm 0.9 \text{ (BF)} \\ \quad \pm 1.6 \text{ (lumi) pb, for } |y| < 1.05, \\ 78.3 \pm 9.2 \text{ (stat)} \pm 6.6 \text{ (syst)} \pm 0.9 \text{ (BF)} \\ \quad \pm 1.5 \text{ (lumi) pb, for } 1.05 \leq |y| < 2.1. \end{cases}$$

The differential cross-sections as a function of the sub-leading J/ψ p_T are shown for the central and forward rapidity regions in Fig. 8. The DPS-weighted distribution created using the data-driven method within the muon kinematic acceptance, which is described in Sect. 5.1, is weighted by the acceptance correction to get the inclusive cross-section and is included in the figure. It is assumed that the DPS weights created within the muon kinematic acceptance can be applied to the acceptance-corrected distributions. An in-depth discussion of the DPS-weighted distribution is given in Sect. 7.2.

The cross-section results are reported under the assumption of unpolarised J/ψ mesons as the J/ψ polarisation coefficients are close to zero [57–59]. As an additional test, the variation of the cross-section has been determined for four extreme cases of J/ψ spin-alignment, one with full longitudinal polarisation and three with different transverse polarisations. Both J/ψ candidates are assumed to have the same polarisation. These are maximal polarisations compared to the small possible polarisation at the low- p_T range studied in this analysis. The maximum deviations from the unpolarised case are given in Tables 3 and 4 for the total and DPS di- J/ψ cross-sections, respectively. The differential variations due to the maximal polarisation scenarios are included separately in the figures for the differential di- J/ψ cross-section.

Additionally, the cross-section in the two rapidity regions is measured as a function of the di- J/ψ transverse momentum as well as the invariant mass. The differential cross-sections as a function of $p_T(J/\psi J/\psi)$ and $m(J/\psi J/\psi)$ are shown in Figs. 9 and 10 respectively, along with the DPS-weighted distribution. There are two peaks in the di- J/ψ p_T distribution. The peak near zero is due to events in which the J/ψ are produced back-to-back in an *away* topology and the peak at higher p_T is due to events that have a *towards* topology in which the two J/ψ are produced in the same direction and are back-to-back with respect to an additional gluon. The large separation is due to the requirement that each J/ψ have $p_T > 8.5$ GeV.

Table 3 The maximum variation of the di- J/ψ cross-section determined for four extreme cases of J/ψ spin-alignment of maximal polarisation, one with full longitudinal polarisation and three with different full transverse polarisations, relative to the nominal unpolarised assumption. Both J/ψ candidates are assumed to have the same polarisation

Maximum spin-alignment scenarios: di- J/ψ cross-section		
Scenario	$ y(J/\psi_2) \leq 1.05$	$1.05 \leq y(J/\psi_2) < 2.1$
Longitudinal	−47%	−45%
Transverse positive	+68%	+82%
Transverse negative	+39%	+28%
Transverse zero	+51%	+47%

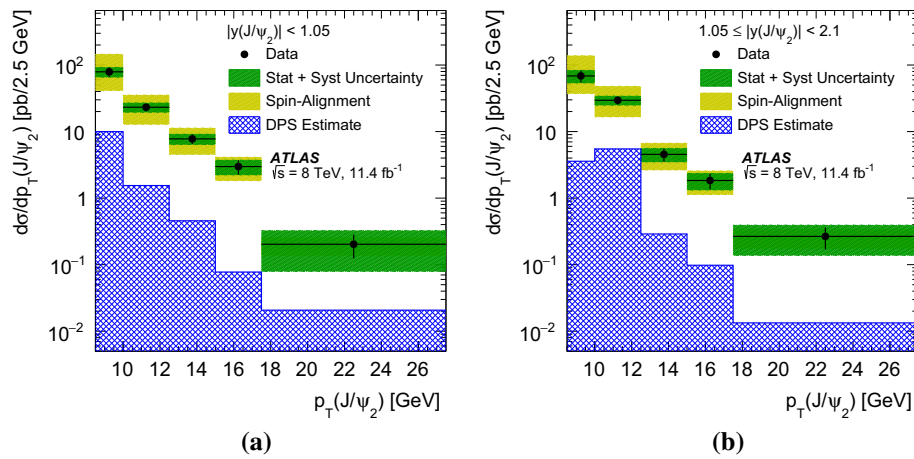


Fig. 8 The differential cross-section, $d\sigma/dp_T(J/\psi_2)$, in the **a** central and **b** forward rapidity regions. The variation due to the choice of J/ψ spin-alignment is shown separately. The longitudinal polarisation is found to minimise the di- J/ψ cross-section and the positive transverse polarisation is found to maximise the di- J/ψ cross-section. Also shown

Table 4 The maximum variation of the DPS di- J/ψ cross-section determined for four extreme cases of J/ψ spin-alignment of maximal polarisation, one with full longitudinal polarisation and three with different full transverse polarisations, relative to the nominal unpolarised assumption. Both J/ψ candidates are assumed to have the same polarisation

Maximum spin-alignment scenarios: di- J/ψ DPS cross-section		
Scenario	$ y(J/\psi_2) \leq 1.05$	$1.05 \leq y(J/\psi_2) < 2.1$
Longitudinal	-47%	-45%
Transverse positive	+79%	+65%
Transverse negative	+35%	+35%
Transverse zero	+54%	+48%

7.2 Double parton scattering measurement

Using the DPS and SPS event weights, which are described in Sect. 5.1, DPS-weighted and SPS-weighted differential distributions are derived. Due to the limited size of the data set, there are large fluctuations in the acceptance-corrected distributions. Therefore the muon fiducial volume is used, which does not include the acceptance weight and hence no assumptions about the J/ψ polarisation are made. Because the SPS and DPS fractions add to unity by construction, only the DPS-weighted distributions are shown in Fig. 11. Since the total distribution and DPS-weighted distribution are shown, the SPS-weighted distribution is understood to be the remainder of the events that are not DPS.

The centre-of-mass energy and fiducial volume requirements of the analysis are applied to the NLO* SPS predictions in Refs. [10, 11]. These predictions are generated using HELAC-Onia, which is described in Refs. [82, 83], and used

is the data-driven DPS distribution derived with the method described in the text. It is assumed that the DPS weights created within the muon kinematic acceptance can be applied to the acceptance-corrected distributions

CTEQ6L1 for LO and CTEQ6M [53] for NLO* parton distribution functions. The colour octet contributions and the intrinsic parton transverse momentum are not included in the predictions. The DPS predictions in Refs. [10, 11] are based on the models from Refs. [39, 43], which assume factorisation of perturbative QCD and use an approximate prompt single- J/ψ matrix element modelled from combined fits of data from multiple experiments. For comparison, the DPS predictions from Ref. [43] are used. The DPS predictions are created using the MSTW2008 NLO [84] parton distribution function. The theory predictions are made in the muon fiducial volume and assume unpolarised J/ψ mesons, and therefore the acceptance correction is not needed for comparison with the predictions. In Fig. 11, the DPS-weighted distribution produced from the event weights of the data-driven method and the total distribution are compared to the LO DPS and sum of the LO DPS and NLO* SPS predictions. The DPS predictions are normalised to the f_{DPS} value measured with the data-driven model. For the NLO* SPS predictions, a constant correction factor of 1.85 is applied for feed-down [10] from $\psi(2S)$ which is present in the data. Changes in SPS predictions from varying the factorisation and renormalisation scales of perturbative QCD, as well as the mass of the charm quark are assigned as systematic uncertainties.

In each of the plots in Fig. 11, the shape of the data-driven DPS distribution approximately agrees with the shape of the DPS predictions. However, there is disagreement between the total data distribution and the total theory predictions at large Δy , large invariant mass, and in the low- p_T region that corresponds to di- J/ψ production in an away topology.

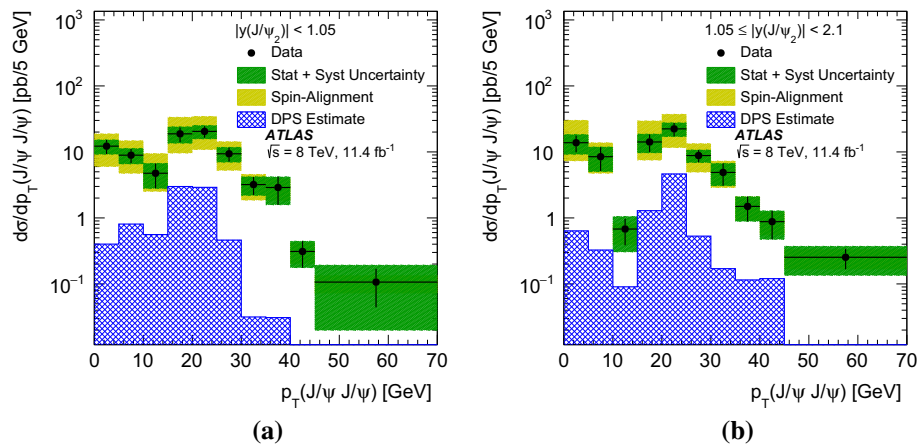


Fig. 9 The differential cross-section, $d\sigma/dp_T(J/\psi J/\psi)$, in the **a** central and **b** forward rapidity. The variation due to the choice of J/ψ spin-alignment is shown separately. The longitudinal polarisation is found to minimise the di- J/ψ cross-section and the positive transverse polarisation is found to maximise the di- J/ψ cross-section. Also shown is the data-driven DPS distribution derived with the method described in the

text. It is assumed that the DPS weights created within the muon kinematic acceptance can be applied to the acceptance-corrected distributions. The two peaks at low and high p_T are due to the away and towards event topologies respectively. The separation is due to the requirement that each J/ψ have $p_T > 8.5$ GeV

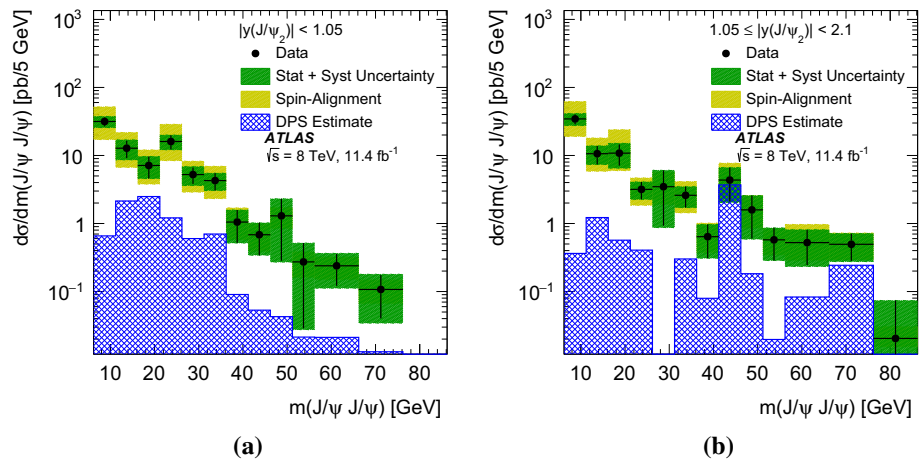


Fig. 10 The differential cross-section, $d\sigma/dm(J/\psi J/\psi)$, in the **a** central and **b** forward rapidity regions. The variation due to the choice of J/ψ spin-alignment is shown separately. The longitudinal polarisation is found to minimise the di- J/ψ cross-section and the positive transverse polarisation is found to maximise the di- J/ψ cross-

section. Also shown is the data-driven DPS distribution derived with the method described in the text. It is assumed that the DPS weights created within the muon kinematic acceptance can be applied to the acceptance-corrected distributions

The distributions in Fig. 11 show that a significant fraction of events have a towards topology where the NLO SPS contributions dominate: specifically events in the low- $\Delta\phi$ region of Fig. 11b and the peak of the di- J/ψ p_T distribution in Fig. 11d at around $p_T = 22$ GeV. Therefore LO predictions alone, which do not include the towards topology, are not enough to describe PP di- J/ψ production.

Most of the NLO* SPS predictions would appear to require a larger value of f_{DPS} than the values measured from the data-driven distributions to fit the data. A possible reason for the discrepancies may be that the NLO* predictions assume a constant correction factor for feed-down from higher-mass charmonium states, which could change

the kinematic properties of the SPS distributions. Requiring $p_T(J/\psi) > 8.5$ GeV limits feed-down, but a change in the kinematic properties of the feed-down component could lead to a wider SPS tail [12,42]. The wide peak at low di- J/ψ p_T could be explained by a large effect due to the inclusion of the intrinsic parton transverse momentum, a non-constant feed-down component, or a combination of the two.

To study the properties of the discrepancies seen, a requirement of $\Delta y \geq 1.8$ is imposed. The corresponding distributions are shown in Fig. 12, where for a better comparison the same binning as in Fig. 11 is used. Because the SPS and DPS distributions are determined from a data-driven method, the statistics are the same as the data. For better clarity the errors

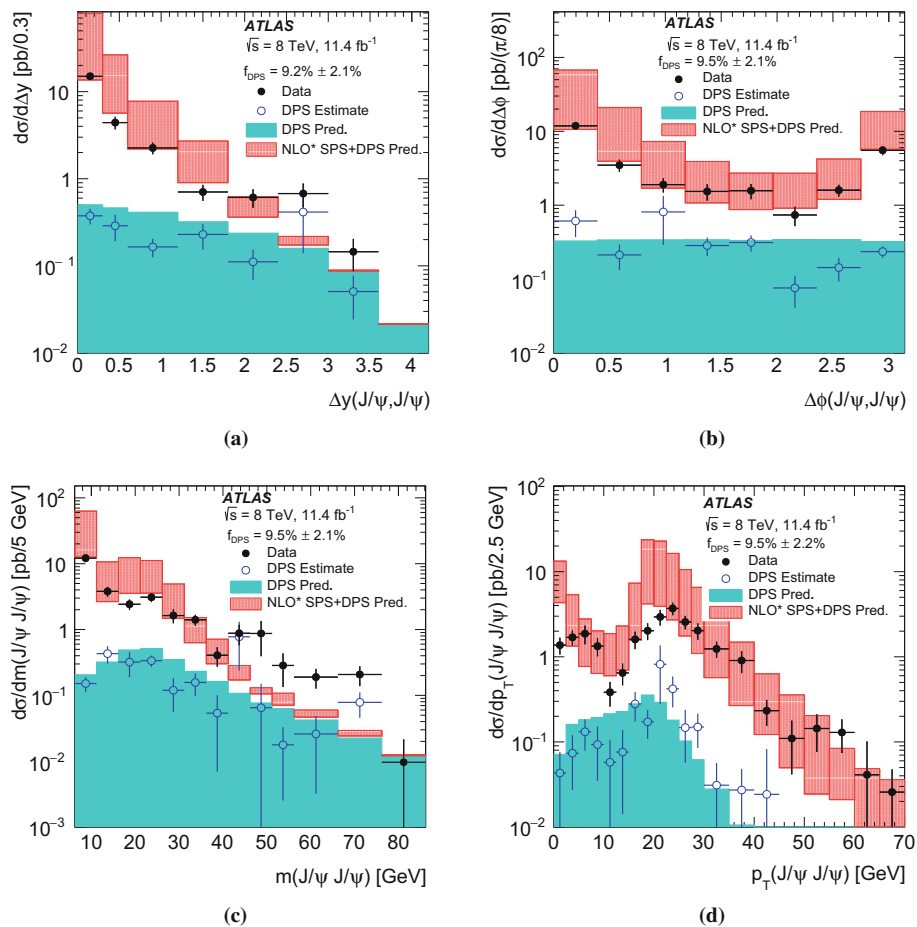


Fig. 11 The DPS and total differential cross-sections as a function of **a** the difference in rapidity between the two J/ψ mesons, **b** the azimuthal angle between the two J/ψ mesons, **c** the invariant mass of the di- J/ψ , **d** the transverse momentum of the di- J/ψ . Shown are the data as well as the LO DPS [43] + NLO* SPS [10, 11] predictions. The

DPS predictions are normalised to the value of f_{DPS} found in the data and the NLO* SPS predictions are multiplied by a constant feed-down correction factor. The data-driven DPS-weighted distribution and the total data distribution are compared to the DPS theory prediction and the total SPS+DPS prediction

in the SPS and DPS distributions are not included in these figures.

A comparison of the di- J/ψ invariant mass distribution in Fig. 11c with that in Fig. 12a shows that the events in the region of excess ($\Delta y \geq 1.8$) have large di- J/ψ invariant mass, as expected from the relationship between the invariant mass and the difference in rapidity. The di- J/ψ transverse momentum, shown in Fig. 12b, has an SPS peak near zero and then falls off monotonically while the DPS peaks at a slightly larger p_T . This indicates that the two J/ψ mesons are produced in an away topology. The $\Delta\phi$ distribution in this region, shown in Fig. 12c, is not uniform as would be expected for a pure DPS: there is a large SPS peak from the away topology peaked at $\Delta\phi \approx \pi$. To make this comparison easier, the $\Delta\phi$ distribution is also shown on linear vertical scale in Fig. 12d. A plausible explanation for the excess of SPS in the distribution is the presence of a non-constant contribution to the di- J/ψ final state from feed-down of back-to-back SPS pair production from excited charmonium states

which could change the kinematic properties of the SPS distribution [12, 42].

To further understand the relative SPS and DPS composition of events in the normalisation region, the distributions of di- J/ψ invariant mass, Δy and di- J/ψ p_T are shown in Fig. 13 for events in the kinematic region $\Delta\phi \leq \pi/2$. There is a clear difference in the shape of the SPS and DPS distributions. The SPS estimate has a much larger peak at low mass, and the DPS distribution falls off much more quickly as a function of the di- J/ψ p_T . The SPS Δy distribution has a large peak near zero and the DPS distribution is flatter. The different shapes of the distributions, as well as the DPS domination at large Δy in this region, further confirms the choice of the normalisation region.

Reference [10] states that if the data are SPS-dominated, feed-down events should be primarily from LO $\psi(2S)$ and J/ψ production and can make up 40% of the SPS cross-section. This matches the peaks due to events with an away topology observed in the $\Delta\phi$ and di- J/ψ p_T distributions at

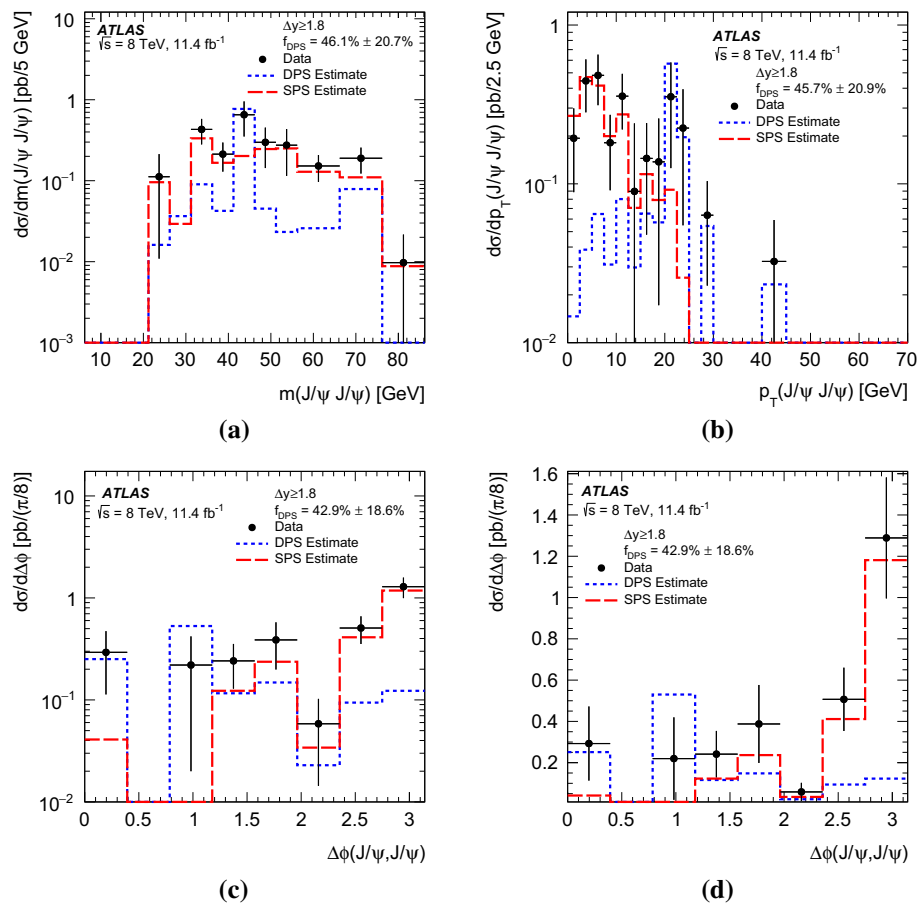


Fig. 12 The PP, DPS, and SPS total cross-section distributions in the reduced kinematic region of $\Delta y \geq 1.8$ for **a** the di- J/ψ invariant mass, **b** the di- J/ψ transverse momentum, **c** the azimuthal angle between the two J/ψ mesons and **d** the same distribution as **c** shown with a linear scale on the vertical axis. The same binning as in Fig. 11 is used.

large Δy in Fig. 12. Additionally, in Ref. [10] the Δy and di- J/ψ mass from the CMS di- J/ψ measurement [44] are fit with DPS and NLO* SPS predictions. The CMS data also show an excess at large Δy and di- J/ψ mass. In Ref. [12] a comparison of the predicted NLO* SPS, feed-down, and DPS distributions is shown. The predicted di- J/ψ mass and Δy distributions from feed-down have a wider tail than the NLO* SPS distributions, similar to what is observed in the DPS distributions. The increase at large di- J/ψ mass and Δy is also predicted in Ref. [42], which studied all possible Fock state contributions to the SPS production of prompt J/ψ meson pairs. A significant non-constant contribution from feed-down is a possible explanation of the much quicker drop off of the tail in the NLO* SPS predictions relative to the data-driven distribution, seen in Fig. 11a–d. Because feed-down can have a distribution similar to DPS, it can explain why the predictions seem to require a larger f_{DPS} value than measured by the data-driven distribution. A larger f_{DPS} would not explain the peak at $\Delta\phi \approx \pi$ for $\Delta y \geq 1.8$, which can be

explained by SPS from a non-constant feed-down contribution. Additionally, the wide peak seen at low di- J/ψ p_T can be explained either by a large effect due to the inclusion of the intrinsic parton transverse momentum, smearing due to a non-constant feed-down component, or a combination of the two.

7.2.1 Effective cross-section measurement

With the measured inclusive di- J/ψ cross-section and the fraction of DPS events as well as the prompt J/ψ cross-section in the corresponding fiducial volume, the effective cross-section can be derived using Eq. (4). The prompt J/ψ differential cross-section is obtained from measurements in Ref. [14] by integrating over p_T and extrapolating to the rapidity acceptance region of this analysis ($|y(J/\psi)| \leq 2.1$ cf. $|y(J/\psi)| \leq 2.0$ in Ref. [14]). The extrapolation uses a linear fit to the cross-section as a function of the absolute rapidity. The statistical and systematic uncertainties are scaled to keep

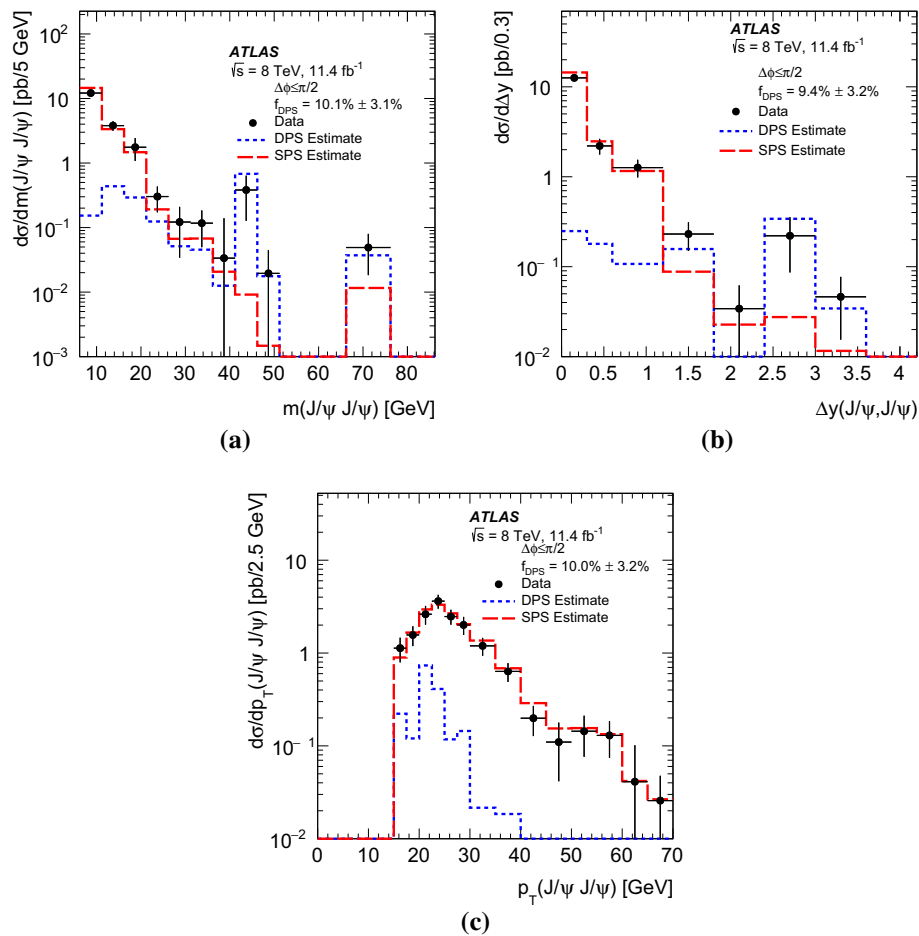


Fig. 13 The PP, DPS, and SPS total cross-section distributions in the reduced kinematic region of $\Delta\phi \leq \pi/2$ for **a** the di- J/ψ invariant mass, **b** the difference in rapidity between the two J/ψ mesons, and **c** the di- J/ψ transverse momentum. The same binning as in Fig. 11 is used.

Because the SPS and DPS distributions are determined from a data-driven method, the statistics are the same as the data. Therefore the errors in the SPS and DPS distributions are not included in these figures as they are derived from the data and would obscure the data distribution

the relative uncertainties the same before and after extrapolation. The cross-section in the fiducial volume of this analysis is $\sigma_{J/\psi} = 429.8 \pm 0.1$ (stat) ± 38.6 (syst) nb.

The value of f_{DPS} is taken from the Δy distribution since it has a well-known DPS distribution, and the other distributions are used as a cross-check. Using the Δy distribution the fraction is measured to be:

$$f_{DPS} = (9.2 \pm 2.1 \text{ (stat)} \pm 0.5 \text{ (syst)})\%.$$

The DPS cross-section, corrected for the muon acceptance in the full J/ψ rapidity range is measured to be:

$$\sigma_{DPS}^{J/\psi, J/\psi} = 14.8 \pm 3.5 \text{ (stat)} \pm 1.5 \text{ (syst)} \pm 0.2 \text{ (BF)} \pm 0.3 \text{ (lumi) pb.}$$

A small difference is found between the DPS cross-section measured in the inclusive volume and the cross-section extrapolated from the fiducial volume. This difference is introduced by fluctuations in the DPS distributions from the

acceptance weight which is used to extrapolate to the inclusive volume, and is smaller than the statistical error. The effective cross-section obtained from these inputs is measured to be:

$$\sigma_{\text{eff}} = 6.3 \pm 1.6 \text{ (stat)} \pm 1.0 \text{ (syst)} \pm 0.1 \text{ (BF)} \pm 0.1 \text{ (lumi) mb.}$$

The effective cross-section measured in this analysis is compared to measurements from other experiments and processes in Fig. 14. In Fig. 15 the effective cross-sections are shown as a function of \sqrt{s} . In defining the effective cross-section, assumptions are made which lead to process and energy independence although there is no theoretical need for this independence. More measurements of the effective cross-section at different energies will be helpful to test this assumption. The ATLAS and D0 [29] analyses provide a hint that the effective cross-section measured from the prompt di- J/ψ final state could be lower than that measured for the other final

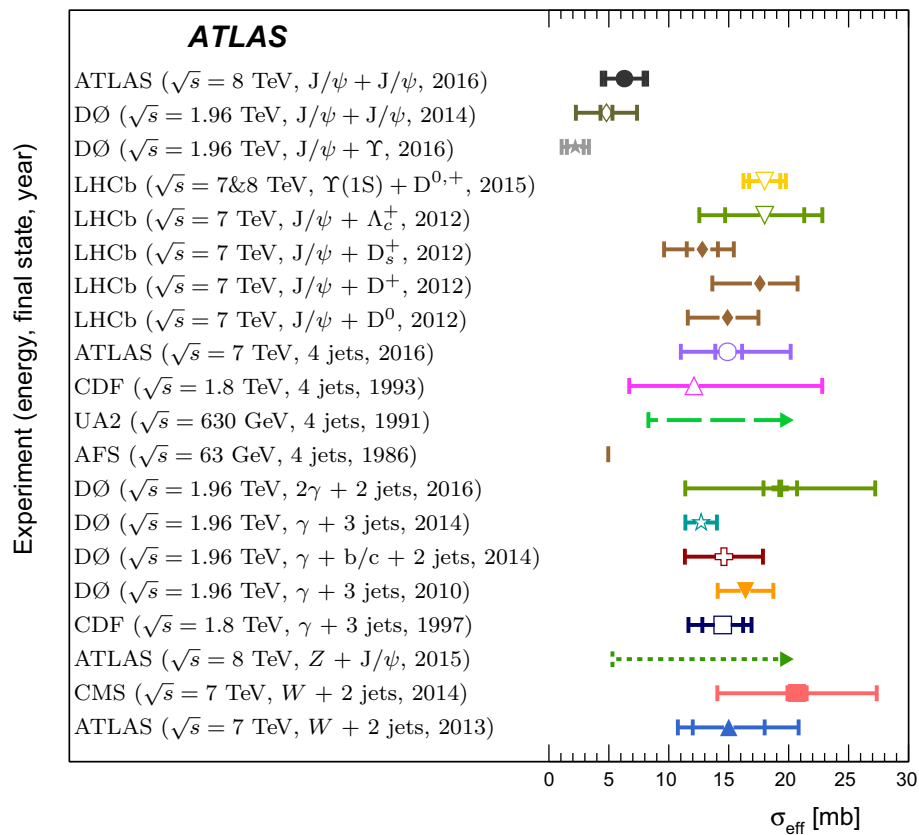


Fig. 14 The effective cross-section of DPS from different energies and final states measured by the AFS experiment [36], the UA2 experiment [37], the CDF experiment [32,35], the D0 experiment [29–31,33,34], the CMS experiment [26], the LHCb experiment [22,28], and the ATLAS experiment [25,27,38]. The *inner error bars* represent

the statistical uncertainties and the *outer error bars* represent the sum in quadrature of the statistical and systematic uncertainties. *Dashed arrows* indicate *lower limits* and the *vertical line* represents the AFS measurement published without uncertainties

states. It is interesting to note that the di- J/ψ , $J/\psi + \Upsilon$ [30], and 4-jet [35,37,38] processes are each dominated by gluon interactions and therefore should directly probe the gluon distribution in the proton [40,64,85]. However other analyses of gluon dominated processes [22,28] measured a larger effective cross-sections in these states. Additional studies could help to learn more about DPS and the dependencies of the effective cross-section. The pion cloud model [86] predicts a smaller average transverse distance between gluons in the nucleon than between quarks. Such a difference could produce a lower effective cross-section for gluon-dominated processes.

8 Summary

In summary, using 11.4 fb^{-1} of $\sqrt{s} = 8 \text{ TeV}$ proton–proton collision data, the first study of prompt J/ψ pairs from the ATLAS detector at the LHC is presented. The differential cross-section as a function of the sub-leading

J/ψ p_T , di- J/ψ p_T , and di- J/ψ mass are measured for two rapidity regions of the sub-leading J/ψ meson: $|y(J/\psi_2)| < 1.05$ and $1.05 \leq |y(J/\psi_2)| < 2.1$. Integrating over the p_T of the muons, the cross-section is 82.2 ± 8.3 (stat) ± 6.3 (syst) ± 0.9 (BF) ± 1.6 (lumi) pb in the central region and 78.3 ± 9.2 (stat) ± 6.6 (syst) ± 0.9 (BF) ± 1.5 (lumi) pb in the forward region. This measurement assumes unpolarised J/ψ mesons and does not include the J/ψ spin-alignment systematic uncertainty. In the muon fiducial volume, $p_T(\mu) > 2.5 \text{ GeV}$, $|\eta(\mu)| < 2.3$, and the triggered J/ψ having both muons with $p_T(\mu) > 4.0 \text{ GeV}$, the cross-section is 15.6 ± 1.3 (stat) ± 1.2 (syst) ± 0.2 (BF) ± 0.3 (lumi) pb for $|y(J/\psi_2)| < 1.05$ and 13.5 ± 1.3 (stat) ± 1.1 (syst) ± 0.2 (BF) ± 0.3 (lumi) pb for $1.05 \leq |y(J/\psi_2)| < 2.1$. No assumptions are made about the J/ψ polarisation in the muon fiducial volume.

Using a data-driven method, the fraction of double parton scattering processes in a single proton–proton collision is measured to be $f_{\text{DPS}} = (9.2 \pm 2.1$ (stat) ± 0.5 (syst))% in the muon fiducial volume. The shapes of the measured double

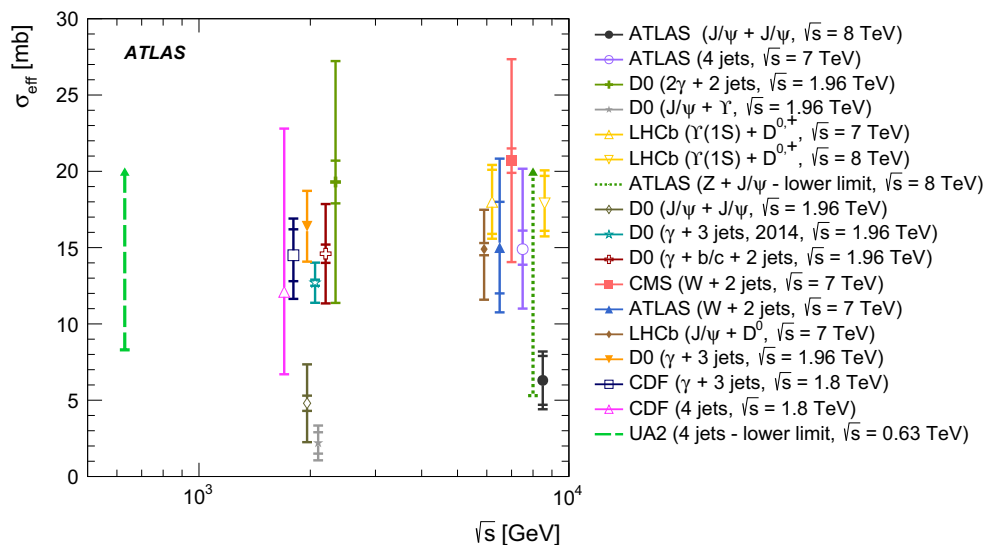


Fig. 15 The effective cross-section of DPS as a function of the centre-of-mass energy, \sqrt{s} , for the UA2 experiment [37], the CDF experiment [32,35], the D0 experiment [29–31,33,34], the CMS experiment [26], the LHCb experiment [22,28], and the ATLAS experiment [25,27,38]. The inner error bars represent the statistical uncertainties and the outer error bars represent the sum in quadrature of the statistical and systematic uncertainties. Dashed arrows indicate lower limits. For clarity, measurements at identical centre-of-mass energies are slightly offset in \sqrt{s}

parton scattering distributions are consistent with model predictions. For single parton scattering, the results are characterised by distributions wider than the next-to-leading-order predictions as seen in the absolute difference between the rapidities of the two J/ψ , the absolute difference between the azimuthal angles, the invariant mass of the di- J/ψ , and the di- J/ψ transverse momentum.

A significant fraction of events appear to correspond to a topology in which the two colour singlet J/ψ mesons are produced in the same direction and back-to-back with respect to an additional gluon. This topology is only included in next-to-leading-order calculations. A theoretical model based on leading-order DPS plus next-to-leading-order-colour singlet model SPS predictions without loops (NLO*) describes the data well, including in the kinematic regions where NLO contributions dominate. Possible explanations for the difference between the data and theoretical predictions at large Δy and invariant mass might be the need to include a large effect due to the inclusion of the intrinsic parton transverse momentum or a contribution via feed-down from a colour-singlet $\psi(2S)$ meson which does not have the same kinematic properties as the NLO* SPS predictions. The contribution from feed-down can amount to 40% of the single parton scattering cross-section. Further studies of the pair production of J/ψ mesons would give an opportunity to further constrain quarkonium production models and provide information on spin physics and heavy ion physics.

From these inputs, the effective cross-section for prompt J/ψ meson pair production at $\sqrt{s} = 8$ TeV is measured

to be $\sigma_{\text{eff}} = 6.3 \pm 1.6$ (stat) ± 1.0 (syst) ± 0.1 (BF) ± 0.1 (lumi) mb. The data suggest that the effective cross-section measured from the prompt di- J/ψ final state could be lower than that measured for the other final states.

to be $\sigma_{\text{eff}} = 6.3 \pm 1.6$ (stat) ± 1.0 (syst) ± 0.1 (BF) ± 0.1 (lumi) mb. The data suggest that the effective cross-section measured from the prompt di- J/ψ final state could be lower than that measured for the other final states.

Acknowledgements We thank CERN for the very successful operation of the LHC, as well as the support staff from our institutions without whom ATLAS could not be operated efficiently. We acknowledge the support of ANPCyT, Argentina; YerPhI, Armenia; ARC, Australia; BMWFW and FWF, Austria; ANAS, Azerbaijan; SSTC, Belarus; CNPq and FAPESP, Brazil; NSERC, NRC and CFI, Canada; CERN; CONICYT, Chile; CAS, MOST and NSFC, China; COLCIENCIAS, Colombia; MSMT CR, MPO CR and VSC CR, Czech Republic; DNRF and DNSRC, Denmark; IN2P3-CNRS, CEA-DSM/IRFU, France; GNSF, Georgia; BMBF, HGF, and MPG, Germany; GSRT, Greece; RGC, Hong Kong SAR, China; ISF, I-CORE and Benozio Center, Israel; INFN, Italy; MEXT and JSPS, Japan; CNRST, Morocco; FOM and NWO, Netherlands; RCN, Norway; MNiSW and NCN, Poland; FCT, Portugal; MNE/IFA, Romania; MES of Russia and NRC KI, Russian Federation; JINR; MESTD, Serbia; MSSR, Slovakia; ARRS and MIZŠ, Slovenia; DST/NRF, South Africa; MINECO, Spain; SRC and Wallenberg Foundation, Sweden; SERI, SNSF and Cantons of Bern and Geneva, Switzerland; MOST, Taiwan; TAEK, Turkey; STFC, United Kingdom; DOE and NSF, United States of America. In addition, individual groups and members have received support from BCKDF, the Canada Council, CANARIE, CRC, Compute Canada, FQRNT, and the Ontario Innovation Trust, Canada; EPLANET, ERC, ERDF, FP7, Horizon 2020 and Marie Skłodowska-Curie Actions, European Union; Investissements d’Avenir Labex and Idex, ANR, Région Auvergne and Fondation Partager le Savoir, France; DFG and AvH Foundation, Germany; Herakleitos, Thales and Aristeia programmes co-financed by EU-ESF and the Greek NSRF; BSF, GIF and Minerva, Israel; BRF, Norway; CERCA Programme Generalitat de Catalunya, Generalitat Valenciana, Spain; the Royal Society and Leverhulme Trust, United Kingdom. The crucial computing support from all WLCG partners is acknowledged grate-

fully, in particular from CERN, the ATLAS Tier-1 facilities at TRIUMF (Canada), NDGF (Denmark, Norway, Sweden), CC-IN2P3 (France), KIT/GridKA (Germany), INFN-CNAF (Italy), NL-T1 (Netherlands), PIC (Spain), ASGC (Taiwan), RAL (UK) and BNL (USA), the Tier-2 facilities worldwide and large non-WLCG resource providers. Major contributors of computing resources are listed in Ref. [87].

Open Access This article is distributed under the terms of the Creative Commons Attribution 4.0 International License (<http://creativecommons.org/licenses/by/4.0/>), which permits unrestricted use, distribution, and reproduction in any medium, provided you give appropriate credit to the original author(s) and the source, provide a link to the Creative Commons license, and indicate if changes were made. Funded by SCOAP³.

References

- V.G. Kartvelishvili, S.M. Esakiya, On hadron induced production of J/ψ meson pairs. *Yad. Fiz.* **38**, 722 (1983)
- B. Humpert, P. Mery, $\psi\psi$ production at collider energies. *Z. Phys. C.* **20**, 83 (1983)
- NA3 Collaboration, J. Badier et al., Evidence for $\psi\psi$ production in π^- interactions at 150 GeV/c and 280 GeV/c, *Phys. Lett. B* **114** (1982) 457
- NA3 Collaboration, J. Badier et al., $\psi\psi$ production and limits on beauty meson production from 400 GeV/c protons, *Physics Letters B* **158** (1985) 85
- P. Ko, C. Yu, J. Lee, Inclusive double-quarkonium production at the Large Hadron Collider. *JHEP* **01**, 70 (2011). [arXiv:1007.3095](https://arxiv.org/abs/1007.3095) [hep-ph]
- A.V. Berezhnoy et al., Double J/ψ -meson Production at LHC and 4c-tetraquark state. *Phys. Rev. D* **84**, 094023 (2011). [arXiv:1101.5881](https://arxiv.org/abs/1101.5881) [hep-ph]
- LHCb Collaboration, R. Aaij et al., Observation of J/ψ pair production in pp collisions at $\sqrt{s} = 7\text{ TeV}$, *Phys. Lett. B* **707** (2012) 52, [arXiv:1109.0963](https://arxiv.org/abs/1109.0963) [hep-ex]
- L.P. Sun, H. Han, K.T. Chao, Impact of J/ψ pair production at the LHC and predictions in nonrelativistic QCD. *Phys. Rev. D* **94**, 074033 (2016). [arXiv:1404.4042](https://arxiv.org/abs/1404.4042) [hep-ph]
- S.P. Baranov, A.H. Rezaeian, Prompt double J/ψ production in proton-proton collisions at the LHC. *Phys. Rev. D* **93**, 114011 (2016). [arXiv:1511.04089](https://arxiv.org/abs/1511.04089) [hep-ph]
- J.P. Lansberg, H.S. Shao, J/ψ -pair production at large momenta: Indications for double-parton scatterings and large α_s^5 contributions. *Phys. Lett. B* **751**, 479 (2015). [arXiv:1410.8822](https://arxiv.org/abs/1410.8822) [hep-ph]
- J.P. Lansberg, H.S. Shao, Production of $J/\psi + \eta_c$ versus $J/\psi + J/\psi$ at the LHC: Importance of real α_s^5 corrections. *Phys. Rev. Lett.* **111**, 122001 (2013). [arXiv:1308.0474](https://arxiv.org/abs/1308.0474) [hep-ph]
- A.K. Likhoded, A.V. Luchinsky, S.V. Poslavsky, Production of $J/\psi + \chi_c$ and $J/\psi + J/\psi$ with real gluon emission at LHC. *Phys. Rev. D* **94**, 054017 (2016). [arXiv:1606.06767](https://arxiv.org/abs/1606.06767) [hep-ph]
- ATLAS Collaboration, Measurement of the differential cross-sections of inclusive, prompt and non-prompt J/ψ production in proton-proton collisions at $\sqrt{s} = 7\text{ TeV}$, *Nucl. Phys. B* **850** (2011) 387, [arXiv:1104.3038](https://arxiv.org/abs/1104.3038) [hep-ex]
- ATLAS Collaboration, Measurement of the differential cross-sections of prompt and non-prompt production of J/ψ and $\psi(2S)$ in pp collisions at $\sqrt{s} = 7$ and 8 TeV with the ATLAS detector, *Eur. Phys. J. C* **76** (2016) 283, [arXiv:1512.03657](https://arxiv.org/abs/1512.03657) [hep-ex]
- LHCb Collaboration, R. Aaij et al., Measurement of J/ψ production in pp collisions at $\sqrt{s} = 7\text{ TeV}$, *Eur. Phys. J. C* **71** (2011) 1645, [arXiv:1103.0423](https://arxiv.org/abs/1103.0423) [hep-ex]
- LHCb Collaboration, R. Aaij et al., Production of J/ψ and Υ mesons in pp collisions at $\sqrt{s} = 8\text{ TeV}$, *JHEP* **06** (2013) 64, [arXiv:1304.6977](https://arxiv.org/abs/1304.6977) [hep-ex]
- CMS Collaboration, J/ψ and $\psi(2S)$ production in pp collisions at $\sqrt{s} = 7\text{ TeV}$. *JHEP* **02**, 11 (2012). [arXiv:1111.1557](https://arxiv.org/abs/1111.1557) [hep-ex]
- CMS Collaboration, Measurement of J/ψ and $\psi(2S)$ Prompt Double-Differential Cross Sections in pp Collisions at $\sqrt{s} = 7\text{ TeV}$. *Phys. Rev. Lett.* **114**, 191802 (2015). [arXiv:1502.04155](https://arxiv.org/abs/1502.04155) [hep-ex]
- ALICE Collaboration, A. Jarošlav et al., Inclusive, prompt and non-prompt J/ψ production at mid-rapidity in Pb-Pb collisions at $\sqrt{s_{NN}} = 2.76\text{ TeV}$, *JHEP* **07** (2015) 51, [arXiv:1504.07151](https://arxiv.org/abs/1504.07151) [nucl-ex]
- N. Brambilla et al., Heavy quarkonium: progress, puzzles, and opportunities. *Eur. Phys. J. C* **71**, 1534 (2011). [arXiv:1010.5827](https://arxiv.org/abs/1010.5827) [hep-ph]
- A. Szczurek, Double parton scattering at high energies. *Acta Phys. Polon. B* **46**, 1415 (2015). [arXiv:1504.06491](https://arxiv.org/abs/1504.06491) [hep-ph]
- LHCb Collaboration, R. Aaij et al., Observation of double charm production involving open charm in pp collisions at $\sqrt{s} = 7\text{ TeV}$, *JHEP* **06** (2012) 141, [Addendum: *JHEP* **03** (2014) 108], [arXiv:1205.0975](https://arxiv.org/abs/1205.0975) [hep-ex]
- P. Bartalini et al., Multi-Parton interactions at the LHC, (2011), [arXiv:1111.0469](https://arxiv.org/abs/1111.0469) [hep-ph]
- H. Abramowicz et al., Summary of the Workshop on Multi-Parton Interactions (MPI@LHC 2012), (2013), [arXiv:1306.5413](https://arxiv.org/abs/1306.5413) [hep-ph]
- ATLAS Collaboration, Measurement of hard double-parton interactions in $W(\rightarrow lv) + 2\text{ jet}$ events at $\sqrt{s} = 7\text{ TeV}$ with the ATLAS detector, *New J. Phys.* **15** (2013) 033038, [arXiv:1301.6872](https://arxiv.org/abs/1301.6872) [hep-ex]
- CMS Collaboration, Study of double parton scattering using $W + 2\text{-jet}$ events in proton-proton collisions at $\sqrt{s} = 7\text{ TeV}$. *JHEP* **03**, 32 (2014). [arXiv:1312.5729](https://arxiv.org/abs/1312.5729) [hep-ex]
- ATLAS Collaboration, Observation and measurements of the production of prompt and non-prompt J/ψ mesons in association with a Z boson in pp collisions at $\sqrt{s} = 8\text{ TeV}$ with the ATLAS detector, *Eur. Phys. J. C* **75** (2015) 229, [arXiv:1412.6428](https://arxiv.org/abs/1412.6428) [hep-ex]
- LHCb Collaboration, R. Aaij et al., Production of associated Υ and open charm hadrons in pp collisions at $\sqrt{s} = 7$ and 8 TeV via double parton scattering, *JHEP* **07** (2016) 52, [arXiv:1510.05949](https://arxiv.org/abs/1510.05949) [hep-ex]
- D0 Collaboration, V. M. Abazov et al., Observation and studies of double J/ψ production at the Tevatron. *Phys. Rev. D* **90**, 111101 (2014). [arXiv:1406.2380](https://arxiv.org/abs/1406.2380) [hep-ex]
- D0 Collaboration, V. M. Abazov et al., Evidence for simultaneous production of J/ψ and Υ mesons. *Phys. Rev. Lett.* **116**, 082002 (2016). [arXiv:1511.02428](https://arxiv.org/abs/1511.02428) [hep-ex]
- D0 Collaboration, V. M. Abazov et al., Study of double parton interactions in diphoton + dijet events in $p\bar{p}$ collisions at $\sqrt{s} = 1.96\text{ TeV}$. *Phys. Rev. D* **93**, 052008 (2016). [arXiv:1512.05291](https://arxiv.org/abs/1512.05291) [hep-ex]
- CDF Collaboration, F. Abe et al., Measurement of double parton scattering in $p\bar{p}$ collisions at $\sqrt{s} = 1.8\text{ TeV}$. *Phys. Rev. Lett.* **79**, 584 (1997)
- D0 Collaboration, V. M. Abazov et al., Double parton interactions in $\gamma+3\text{ jet}$ events in $p\bar{p}$ collisions at $\sqrt{s} = 1.96\text{ TeV}$. *Phys. Rev. D* **81**, 052012 (2010). [arXiv:0912.5104](https://arxiv.org/abs/0912.5104) [hep-ex]
- D0 Collaboration, V. M. Abazov et al., Double parton interactions in $\gamma + 3\text{ jet}$ and $\gamma + b/c\text{ jet} + 2\text{ jet}$ events in $p\bar{p}$ collisions at $\sqrt{s} = 1.96\text{ TeV}$. *Phys. Rev. D* **89**, 072006 (2014). [arXiv:1402.1550](https://arxiv.org/abs/1402.1550) [hep-ex]
- CDF Collaboration, F. Abe et al., Study of four jet events and evidence for double parton interactions in $p\bar{p}$ collisions at $\sqrt{s} = 1.8\text{ TeV}$. *Phys. Rev. D* **47**, 4857 (1993)
- AFS Collaboration, T. Akesson et al., Double Parton Scattering in pp Collisions at $\sqrt{s} = 63\text{ GeV}$. *Z. Phys. C* **34**, 163 (1987)

37. UA2 Collaboration, J. Alitti et al., A Study of multi-jet events at the CERN anti-p p collider and a search for double parton scattering, Phys. Lett. B **268** (1991) 145
38. ATLAS Collaboration, Study of hard double-parton scattering in four-jet events in pp collisions at $\sqrt{s} = 7$ TeV with the ATLAS experiment, JHEP **11** (2016) 110. [arXiv:1608.01857](#) [hep-ex]
39. C.H. Kom, A. Kulesza, W.J. Stirling, Pair Production of J/ψ as a probe of double parton scattering at LHCb. Phys. Rev. Lett. **107**, 082002 (2011). [arXiv:1105.4186](#) [hep-ph]
40. S.P. Baranov et al., Interparticle correlations in the production of J/ψ pairs in proton-proton collisions. Phys. Rev. D **87**, 034035 (2013). [arXiv:1210.1806](#) [hep-ph]
41. D. d'Enterria, A.M. Snigirev, Enhanced J/ψ -pair production from double parton scatterings in nucleus-nucleus collisions at the Large Hadron Collider. Phys. Lett. B **727**, 157 (2013). [arXiv:1301.5845](#) [hep-ph]
42. Z.G. He, B.A. Kniehl, Complete Nonrelativistic-QCD Prediction for Prompt Double J/ψ Hadroproduction. Phys. Rev. Lett. **115**, 022002 (2015). [arXiv:1609.02786](#) [hep-ph]
43. C. Borschensky and A. Kulesza, Double parton scattering in pair-production of J/ψ mesons at the LHC revisited, (2016), [arXiv:1610.00666](#) [hep-ph]
44. CMS Collaboration, Measurement of prompt J/ψ pair production in pp collisions at $\sqrt{s} = 7$ TeV. JHEP **09**, 94 (2014). [arXiv:1406.0484](#) [hep-ex]
45. ATLAS Collaboration, The ATLAS Experiment at the CERN Large Hadron Collider, JINST **3** (2008) S08003
46. ATLAS Collaboration, Performance of the ATLAS muon trigger in pp collisions at $\sqrt{s} = 8$ TeV, Eur. Phys. J. C **75** (2015) 120, [arXiv:1408.3179](#) [hep-ex]
47. ATLAS Collaboration, Luminosity determination in pp collisions at $\sqrt{s} = 8$ TeV using the ATLAS detector at the LHC, (2016), [arXiv:1608.03953](#) [hep-ex]
48. ATLAS Collaboration, Measurement of the muon reconstruction performance of the ATLAS detector using 2011 and 2012 LHC proton-proton collision data, Eur. Phys. J. C **74** (2014) 3130, [arXiv:1407.3935](#) [hep-ex]
49. W. Verkerke and D. P. Kirkby, The RooFit toolkit for data modeling, (2003), [arXiv:physics/0306116](#)
50. K.A. Olive et al., Review of Particle Physics. Chin. Phys. C **38**, 090001 (2014)
51. T. Sjöstrand, S. Mrenna, P.Z. Skands, A. Brief, Introduction to PYTHIA 8.1. Comput. Phys. Commun. **178**, 852 (2008). [arXiv:0710.3820](#) [hep-ph]
52. ATLAS Collaboration, Summary of ATLAS Pythia 8 tunes, ATL-PHYS-PUB-2012-003, 2012, url: <https://cds.cern.ch/record/1474107>
53. D. Stump et al., Inclusive jet production, parton distributions, and the search for new physics. JHEP **10**, 46 (2003). [arXiv:hep-ph/0303013](#)
54. ATLAS Collaboration, The ATLAS Simulation Infrastructure, Eur. Phys. J. C **70** (2010) 823, [arXiv:1005.4568](#) [hep-ex]
55. S. Agostinelli et al., GEANT4: A Simulation toolkit. Nucl. Instrum. Meth. A **506**, 250 (2003)
56. ATLAS Collaboration, Measurement of Upsilon production in 7 TeV pp collisions at ATLAS, Phys. Rev. D **87** (2013) 052004, [arXiv:1211.7255](#) [hep-ex]
57. CDF Collaboration, A. Abulencia et al., Polarization of J/ψ and $\psi(2S)$ mesons produced in $p\bar{p}$ collisions at $\sqrt{s} = 1.96$ TeV. Phys. Rev. Lett. **99**, 132001 (2007). [arXiv:0704.0638](#) [hep-ex]
58. LHCb Collaboration, R. Aaij et al., Measurement of J/ψ polarization in pp collisions at $\sqrt{s} = 7$ TeV, Eur. Phys. J. C **73** (2013) 2631, [arXiv:1307.6379](#) [hep-ex]
59. CMS Collaboration, Measurement of the prompt J/ψ and $\psi(2S)$ polarizations in pp collisions at $\sqrt{s} = 7$ TeV. Phys. Lett. B **727**, 381 (2013). [arXiv:1307.6070](#) [hep-ex]
60. G. Cowan et al., Asymptotic formulae for likelihood-based tests of new physics, Eur. Phys. J. C **71** (2011) 1554, [Erratum: Eur. Phys. J. C **73** (2013) 2501], [arXiv:1007.1727](#) [physics.data-an]
61. M. Oreglia, A Study of the Reactions $\psi' \rightarrow \gamma\gamma\psi$, SLAC-R-236 (1980). <http://www.slac.stanford.edu/cgi-wrap/getdoc/slac-r-236.pdf>
62. J. Gaiser, Charmonium Spectroscopy From Radiative Decays of the J/ψ and ψ' , SLAC-R-255 (1982). <http://www.slac.stanford.edu/cgi-wrap/getdoc/slac-r-255.pdf>
63. T. Skwarnicki, A study of the radiative CASCADE transitions between the Upsilon-Prime and Upsilon resonances, DESY-F31-86-02 (1986). http://lss.fnal.gov/cgi-bin/find_paper.pl?other/thesis/skwarnicki.pdf
64. B. Blok et al., The four jet production at LHC and Tevatron in QCD. Phys. Rev. D **83**, 071501 (2011). [arXiv:1009.2714](#) [hep-ph]
65. B. Humpert, Are there multi-quark interactions? Phys. Lett. B **131**, 461 (1983)
66. M. Diehl, Correlation effects in multiple hard scattering, (2013), [arXiv:1306.6480](#) [hep-ph]
67. M. Diehl, T. Kasemets, S. Keane, Correlations in double parton distributions: effects of evolution. JHEP **05**, 118 (2014). [arXiv:1401.1233](#) [hep-ph]
68. T. Kasemets, P.J. Mulders, Constraining double parton correlations and interferences. Phys. Rev. D **91**, 014015 (2015). [arXiv:1411.0726](#) [hep-ph]
69. A. V. Manohar, W.J. Waalewijn, A QCD Analysis of Double Parton Scattering: Color Correlations, Interference Effects and Evolution. Phys. Rev. D **85**, 114009 (2012). [arXiv:1202.3794](#) [hep-ph]
70. H. Fritzsche, Producing Heavy Quark Flavors in Hadronic Collisions: A Test of Quantum Chromodynamics. Phys. Lett. B **67**, 217 (1977)
71. F. Halzen, Cvc for Gluons and Hadroproduction of Quark Flavors. Phys. Lett. B **69**, 105 (1977)
72. C.-H. Chang, Hadronic Production of J/ψ Associated With a Gluon. Nucl. Phys. B **172**, 425 (1980)
73. R. Baier, R. Ruckl, Hadronic Production of J/ψ and Υ : Transverse Momentum Distributions. Phys. Lett. B **102**, 364 (1981)
74. E. Braaten, S. Fleming, Color octet fragmentation and the ψ' surplus at the Tevatron. Phys. Rev. Lett. **74**, 3327 (1995). [arXiv:hep-ph/9411365](#)
75. P.L. Cho, A.K. Leibovich, Color octet quarkonia production. Phys. Rev. D **53**, 150 (1996). [arXiv:hep-ph/9505329](#)
76. P.L. Cho, A.K. Leibovich, Color octet quarkonia production. 2. Phys. Rev. D **53**, 6203 (1996). [arXiv:hep-ph/9511315](#)
77. E. Braaten, S. Fleming, T.C. Yuan, Production of heavy quarkonium in high-energy colliders. Ann. Rev. Nucl. Part. Sci. **46**, 197 (1996). [arXiv:hep-ph/9602374](#)
78. M. Kramer, Quarkonium production at high-energy colliders. Prog. Part. Nucl. Phys. **47**, 141 (2001). [arXiv:hep-ph/0106120](#)
79. N. Brambilla et al., Heavy quarkonium physics, (2004), [arXiv:hep-ph/0412158](#)
80. J.P. Lansberg, J/ψ , ψ' and Υ production at hadron colliders: A Review. Int. J. Mod. Phys. A **21**, 3857 (2006). [arXiv:hep-ph/0602091](#)
81. A. Andronic et al., Heavy-flavour and quarkonium production in the LHC era: from proton-proton to heavy-ion collisions. Eur. Phys. J. C **76**, 107 (2016). [arXiv:1506.03981](#) [nucl-ex]
82. H.S. Shao, HELAC-Onia: An automatic matrix element generator for heavy quarkonium physics. Comput. Phys. Commun. **184**, 2562 (2013). [arXiv:1212.5293](#) [hep-ph]
83. H.S. Shao, HELAC-Onia 2.0: an upgraded matrix-element and event generator for heavy quarkonium physics. Comput. Phys. Commun. **198**, 238 (2016). [arXiv:1507.03435](#) [hep-ph]
84. A.D. Martin et al., Parton distributions for the LHC. Eur. Phys. J. C **63**, 189 (2009). [arXiv:0901.0002](#) [hep-ph]

85. M. Vanttinen et al., Hadroproduction and polarization of charmium. *Phys. Rev. D* **51**, 3332 (1995). [arXiv:hep-ph/9410237](https://arxiv.org/abs/hep-ph/9410237)
86. M. Strikman, C. Weiss, Chiral dynamics and partonic structure at large transverse distances. *Phys. Rev. D* **80**, 114029 (2009). [arXiv:0906.3267](https://arxiv.org/abs/0906.3267) [hep-ph]
87. ATLAS Collaboration, ATLAS Computing Acknowledgements 2016–2017, ATL-GEN-PUB-2016-002. <http://cds.cern.ch/record/2202407>

ATLAS Collaboration

M. Aaboud^{137d}, G. Aad⁸⁸, B. Abbott¹¹⁵, J. Abdallah⁸, O. Abdinov¹², B. Abeloos¹¹⁹, R. Aben¹⁰⁹, O. S. AbouZeid¹³⁹, N. L. Abraham¹⁵¹, H. Abramowicz¹⁵⁵, H. Abreu¹⁵⁴, R. Abreu¹¹⁸, Y. Abulaiti^{148a,148b}, B. S. Acharya^{167a,167b,a}, S. Adachi¹⁵⁷, L. Adamczyk^{41a}, D. L. Adams²⁷, J. Adelman¹¹⁰, S. Adomeit¹⁰², T. Adye¹³³, A. A. Affolder⁷⁷, T. Agatonovic-Jovin¹⁴, J. A. Aguilar-Saavedra^{128a,128f}, S. P. Ahlen²⁴, F. Ahmadov^{68,b}, G. Aielli^{135a,135b}, H. Akerstedt^{148a,148b}, T. P. A. Åkesson⁸⁴, A. V. Akimov⁹⁸, G. L. Alberghi^{22a,22b}, J. Albert¹⁷², S. Albrand⁵⁸, M. J. Alconada Verzini⁷⁴, M. Aleksa³², I. N. Aleksandrov⁶⁸, C. Alexa^{28b}, G. Alexander¹⁵⁵, T. Alexopoulos¹⁰, M. Alhroob¹¹⁵, B. Ali¹³⁰, M. Aliev^{76a,76b}, G. Alimonti^{94a}, J. Alison³³, S. P. Alkire³⁸, B. M. M. Allbrooke¹⁵¹, B. W. Allen¹¹⁸, P. P. Allport¹⁹, A. Aloisio^{106a,106b}, A. Alonso³⁹, F. Alonso⁷⁴, C. Alpigiani¹⁴⁰, A. A. Alshehri⁵⁶, M. Alstary⁸⁸, B. Alvarez Gonzalez³², D. Álvarez Piqueras¹⁷⁰, M. G. Alviggi^{106a,106b}, B. T. Amadio¹⁶, Y. Amaral Coutinho^{26a}, C. Amelung²⁵, D. Amidei⁹², S. P. Amor Dos Santos^{128a,128c}, A. Amorim^{128a,128b}, S. Amoroso³², G. Amundsen²⁵, C. Anastopoulos¹⁴¹, L. S. Ancu⁵², N. Andari¹⁹, T. Andeen¹¹, C. F. Anders^{60b}, G. Anders³², J. K. Anders⁷⁷, K. J. Anderson³³, A. Andreazza^{94a,94b}, V. Andrei^{60a}, S. Angelidakis⁹, I. Angelozzi¹⁰⁹, A. Angerami³⁸, F. Anghinolfi³², A. V. Anisenkov^{111,c}, N. Anjos¹³, A. Annovi^{126a,126b}, C. Antel^{60a}, M. Antonelli⁵⁰, A. Antonov^{100,*}, D. J. Antrim¹⁶⁶, F. Anulli^{134a}, M. Aoki⁶⁹, L. Aperio Bella¹⁹, G. Arabidze⁹³, Y. Arai⁶⁹, J. P. Araque^{128a}, A. T. H. Arce⁴⁸, F. A. Arduh⁷⁴, J.-F. Arguin⁹⁷, S. Argyropoulos⁶⁶, M. Arik^{20a}, A. J. Armbruster¹⁴⁵, L. J. Armitage⁷⁹, O. Arnaez³², H. Arnold⁵¹, M. Arratia³⁰, O. Arslan²³, A. Artamonov⁹⁹, G. Artoni¹²², S. Artz⁸⁶, S. Asai¹⁵⁷, N. Asbah⁴⁵, A. Ashkenazi¹⁵⁵, B. Åsman^{148a,148b}, L. Asquith¹⁵¹, K. Assamagan²⁷, R. Astalos^{146a}, M. Atkinson¹⁶⁹, N. B. Atlay¹⁴³, K. Augsten¹³⁰, G. Avolio³², B. Axen¹⁶, M. K. Ayoub¹¹⁹, G. Azuelos^{97,d}, M. A. Baak³², A. E. Baas^{60a}, M. J. Baca¹⁹, H. Bachacou¹³⁸, K. Bachas^{76a,76b}, M. Backes¹²², M. Backhaus³², P. Bagiachi^{134a,134b}, P. Bagnaia^{134a,134b}, Y. Bai^{35a}, J. T. Baines¹³³, M. Bajic³⁹, O. K. Baker¹⁷⁹, E. M. Baldwin^{111,c}, P. Balek¹⁷⁵, T. Balestri¹⁵⁰, F. Balli¹³⁸, W. K. Balunas¹²⁴, E. Banas⁴², Sw. Banerjee^{176,e}, A. A. E. Bannoura¹⁷⁸, L. Barak³², E. L. Barberio⁹¹, D. Barberis^{53a,53b}, M. Barbero⁸⁸, T. Barillari¹⁰³, M.-S. Barisits³², T. Barklow¹⁴⁵, N. Barlow³⁰, S. L. Barnes⁸⁷, B. M. Barnett¹³³, R. M. Barnett¹⁶, Z. Barnovska-Blenessy^{36a}, A. Baroncelli^{136a}, G. Barone²⁵, A. J. Barr¹²², L. Barranco Navarro¹⁷⁰, F. Barreiro⁸⁵, J. Barreiro Guimarães da Costa^{35a}, R. Bartoldus¹⁴⁵, A. E. Barton⁷⁵, P. Bartos^{146a}, A. Basalae¹²⁵, A. Bassalat^{119,f}, R. L. Bates⁵⁶, S. J. Batista¹⁶¹, J. R. Batley³⁰, M. Battaglia¹³⁹, M. Bause^{134a,134b}, F. Bauer¹³⁸, H. S. Bawa^{145,g}, J. B. Beacham¹¹³, M. D. Beattie⁷⁵, T. Beau⁸³, P. H. Beauchemin¹⁶⁵, P. Bechtel²³, H. P. Beck^{18,h}, K. Becker¹²², M. Becker⁸⁶, M. Beckingham¹⁷³, C. Becot¹¹², A. J. Beddall^{20d}, A. Beddall^{20b}, V. A. Bednyakov⁶⁸, M. Bedognetti¹⁰⁹, C. P. Bee¹⁵⁰, L. J. Beemster¹⁰⁹, T. A. Beermann³², M. Begel²⁷, J. K. Behr⁴⁵, A. S. Bell⁸¹, G. Bella¹⁵⁵, L. Bellagamba^{22a}, A. Bellerive³¹, M. Bellomo⁸⁹, K. Belotskiy¹⁰⁰, O. Beltramello³², N. L. Belyaev¹⁰⁰, O. Benary^{155,*}, D. Bencheekroun^{137a}, M. Bender¹⁰², K. Bendtz^{148a,148b}, N. Benekos¹⁰, Y. Benhammou¹⁵⁵, E. Benhar Nocchioli¹⁷⁹, J. Benitez⁶⁶, D. P. Benjamin⁴⁸, J. R. Bensinger²⁵, S. Bentvelsen¹⁰⁹, L. Beresford¹²², M. Beretta⁵⁰, D. Berge¹⁰⁹, E. Bergeas Kuutmann¹⁶⁸, N. Berger⁵, J. Beringer¹⁶, S. Berlendis⁵⁸, N. R. Bernard⁸⁹, C. Bernius¹¹², F. U. Bernlochner²³, T. Berry⁸⁰, P. Berta¹³¹, C. Bertella⁸⁶, G. Bertoli^{148a,148b}, F. Bertolucci^{126a,126b}, I. A. Bertram⁷⁵, C. Bertsche⁴⁵, D. Bertsche¹¹⁵, G. J. Besjes³⁹, O. Bessidskaia Bylund^{148a,148b}, M. Bessner⁴⁵, N. Besson¹³⁸, C. Betancourt⁵¹, A. Bethani⁵⁸, S. Bethke¹⁰³, A. J. Bevan⁷⁹, R. M. Bianchi¹²⁷, M. Bianco³², O. Biebel¹⁰², D. Biedermann¹⁷, R. Bielski⁸⁷, N. V. Biesuz^{126a,126b}, M. Biglietti^{136a}, J. Bilbao De Mendizabal⁵², T. R. V. Billoud⁹⁷, H. Bilokon⁵⁰, M. Bindi⁵⁷, S. Binet¹¹⁹, A. Bingul^{20b}, C. Bini^{134a,134b}, S. Biondi^{22a,22b}, T. Bisanz⁵⁷, D. M. Bjergaard⁴⁸, C. W. Black¹⁵², J. E. Black¹⁴⁵, K. M. Black²⁴, D. Blackburn¹⁴⁰, R. E. Blair⁶, T. Blazek^{146a}, I. Bloch⁴⁵, C. Blocker²⁵, A. Blue⁵⁶, W. Blum^{86,*}, U. Blumenschein⁵⁷, S. Blunier^{34a}, G. J. Bobbink¹⁰⁹, V. S. Bobrovnikov^{111,c}, S. S. Bocchetta⁸⁴, A. Bocchi⁴⁸, C. Bock¹⁰², M. Boehler⁵¹, D. Boerner¹⁷⁸, J. A. Bogaerts³², D. Bogavac¹⁴, A. G. Bogdanchikov¹¹¹, C. Bohm^{148a}, V. Boisvert⁸⁰, P. Bokan¹⁴, T. Bold^{41a}, A. S. Boldyrev^{167a,167c}, M. Bomben⁸³, M. Bona⁷⁹, M. Boonekamp¹³⁸, A. Borisov¹³², G. Borissov⁷⁵, J. Bortfeldt³², D. Bortoletto¹²², V. Bortolotto^{62a,62b,62c}, K. Bos¹⁰⁹, D. Boscherini^{22a}, M. Bosman¹³, J. D. Bossio Sola²⁹, J. Boudreau¹²⁷, J. Bouffard², E. V. Bouhova-Thacker⁷⁵, D. Boumediene³⁷, C. Bourdarios¹¹⁹, S. K. Boutle⁵⁶, A. Boveia³², J. Boyd³², I. R. Boyko⁶⁸, J. Bracinik¹⁹, A. Brandt⁸, G. Brandt⁵⁷, O. Brandt^{60a}, U. Bratzler¹⁵⁸, B. Brau⁸⁹, J. E. Brau¹¹⁸, W. D. Breaden Madden⁵⁶, K. Brendlinger¹²⁴, A. J. Brennan⁹¹, L. Brenner¹⁰⁹, R. Brenner¹⁶⁸, S. Bressler¹⁷⁵, T. M. Bristow⁴⁹

D. Britton⁵⁶, D. Britzger⁴⁵, F. M. Brochu³⁰, I. Brock²³, R. Brock⁹³, G. Brooijmans³⁸, T. Brooks⁸⁰, W. K. Brooks^{34b}, J. Brosamer¹⁶, E. Brost¹¹⁰, J.H Broughton¹⁹, P. A. Bruckman de Renstrom⁴², D. Bruncko^{146b}, R. Bruneliere⁵¹, A. Bruni^{22a}, G. Bruni^{22a}, L. S. Bruni¹⁰⁹, BH Brunt³⁰, M. Bruschi^{22a}, N. Brusino²³, P. Bryant³³, L. Bryngemark⁸⁴, T. Buanes¹⁵, Q. Buat¹⁴⁴, P. Buchholz¹⁴³, A. G. Buckley⁵⁶, I. A. Budagov⁶⁸, F. Buehrer⁵¹, M. K. Bugge¹²¹, O. Bulekov¹⁰⁰, D. Bullock⁸, H. Burckhart³², S. Burdin⁷⁷, C. D. Burgard⁵¹, A. M. Burger⁵, B. Burghgrave¹¹⁰, K. Burka⁴², S. Burke¹³³, I. Burmeister⁴⁶, J. T. P. Burr¹²², E. Busato³⁷, D. Büscher⁵¹, V. Büscher⁸⁶, P. Bussey⁵⁶, J. M. Butler²⁴, C. M. Buttar⁵⁶, J. M. Butterworth⁸¹, P. Butti¹⁰⁹, W. Buttinger²⁷, A. Buzatu⁵⁶, A. R. Buzykaev^{111.c}, S. Cabrera Urbán¹⁷⁰, D. Caforio¹³⁰, V. M. Cairo^{40a,40b}, O. Cakir^{4a}, N. Calace⁵², P. Calafiura¹⁶, A. Calandri⁸⁸, G. Calderini⁸³, P. Calfayan⁶⁴, G. Callea^{40a,40b}, L. P. Caloba^{26a}, S. Calvente Lopez⁸⁵, D. Calvet³⁷, S. Calvet³⁷, T. P. Calvet⁸⁸, R. Camacho Toro³³, S. Camarda³², P. Camarri^{135a,135b}, D. Cameron¹²¹, R. Caminal Armadans¹⁶⁹, C. Camincher⁵⁸, S. Campana³², M. Campanelli⁸¹, A. Camplani^{94a,94b}, A. Campoverde¹⁴³, V. Canale^{106a,106b}, A. Canepa^{163a}, M. Cano Bret^{36c}, J. Cantero¹¹⁶, T. Cao¹⁵⁵, M. D. M. Capeans Garrido³², I. Caprini^{28b}, M. Caprini^{28b}, M. Capua^{40a,40b}, R. M. Carbone³⁸, R. Cardarelli^{135a}, F. Cardillo⁵¹, I. Carli¹³¹, T. Carli³², G. Carlino^{106a}, L. Carminati^{94a,94b}, R. M. D. Carney^{148a,148b}, S. Caron¹⁰⁸, E. Carquin^{34b}, G. D. Carrillo-Montoya³², J. R. Carter³⁰, J. Carvalho^{128a,128c}, D. Casadei¹⁹, M. P. Casado^{13.i}, M. Casolino¹³, D. W. Casper¹⁶⁶, E. Castaneda-Miranda^{147a}, R. Castelijm¹⁰⁹, A. Castelli¹⁰⁹, V. Castillo Gimenez¹⁷⁰, N. F. Castro^{128a,j}, A. Catinaccio³², J. R. Catmore¹²¹, A. Cattai³², J. Caudron²³, V. Cavaliere¹⁶⁹, E. Cavallaro¹³, D. Cavalli^{94a}, M. Cavalli-Sforza¹³, V. Cavalinni^{126a,126b}, F. Ceradini^{136a,136b}, L. Cerda Alberich¹⁷⁰, A. S. Cerqueira^{26b}, A. Cerri¹⁵¹, L. Cerrito^{135a,135b}, F. Cerutti¹⁶, A. Cervelli¹⁸, S. A. Cetin^{20c}, A. Chafaq^{137a}, D. Chakraborty¹¹⁰, S. K. Chan⁵⁹, Y. L. Chan^{62a}, P. Chang¹⁶⁹, J. D. Chapman³⁰, D. G. Charlton¹⁹, A. Chatterjee⁵², C. C. Chau¹⁶¹, C. A. Chavez Barajas¹⁵¹, S. Che¹¹³, S. Cheatham^{167a,167c}, A. Chegwidan⁹³, S. Chekanov⁶, S. V. Chekulaev^{163a}, G. A. Chelkov^{68,k}, M. A. Chelstowska⁹², C. Chen⁶⁷, H. Chen²⁷, K. Chen¹⁵⁰, S. Chen^{35b}, S. Chen¹⁵⁷, X. Chen^{35c}, Y. Chen⁷⁰, H. C. Cheng⁹², H. J. Cheng^{35a}, Y. Cheng³³, A. Cheplakov⁶⁸, E. Cheremushkina¹³², R. Cherkaoui El Moursli^{137e}, V. Chernyatin^{27,*}, E. Cheu⁷, L. Chevalier¹³⁸, V. Chiarella⁵⁰, G. Chiarelli^{126a,126b}, G. Chiodini^{76a}, A. S. Chisholm³², A. Chitan^{28b}, M. V. Chizhov⁶⁸, K. Choi⁶⁴, A. R. Chomont³⁷, S. Chouridou⁹, B. K. B. Chow¹⁰², V. Christodoulou⁸¹, D. Chromek-Burckhart³², J. Chudoba¹²⁹, A. J. Chuinard⁹⁰, J. J. Chwastowski⁴², L. Chytka¹¹⁷, G. Ciapetti^{134a,134b}, A. K. Ciftci^{4a}, D. Cinca⁴⁶, V. Cindro⁷⁸, I. A. Cioara²³, C. Ciocca^{22a,22b}, A. Ciocio¹⁶, F. Ciotto^{106a,106b}, Z. H. Citron¹⁷⁵, M. Citterio^{94a}, M. Ciubancan^{28b}, A. Clark⁵², B. L. Clark⁵⁹, M. R. Clark³⁸, P. J. Clark⁴⁹, R. N. Clarke¹⁶, C. Clement^{148a,148b}, Y. Coadou⁸⁸, M. Cobal^{167a,167c}, A. Coccaro⁵², J. Cochran⁶⁷, L. Colasurdo¹⁰⁸, B. Cole³⁸, A. P. Colijn¹⁰⁹, J. Collot⁵⁸, T. Colombo¹⁶⁶, G. Compostella¹⁰³, P. Conde Muiño^{128a,128b}, E. Coniavitis⁵¹, S. H. Connell^{147b}, I. A. Connelly⁸⁰, V. Consorti⁵¹, S. Constantinescu^{28b}, G. Conti³², F. Conventi^{106a,l}, M. Cooke¹⁶, B. D. Cooper⁸¹, A. M. Cooper-Sarkar¹²², F. Cormier¹⁷¹, K. J. R. Cormier¹⁶¹, T. Cornelissen¹⁷⁸, M. Corradi^{134a,134b}, F. Corriveau^{90,m}, A. Cortes-Gonzalez³², G. Cortiana¹⁰³, G. Costa^{94a}, M. J. Costa¹⁷⁰, D. Costanzo¹⁴¹, G. Cottin³⁰, G. Cowan⁸⁰, B. E. Cox⁸⁷, K. Cranmer¹¹², S. J. Crawley⁵⁶, G. Cree³¹, S. Crépe-Renaudin⁵⁸, F. Crescioli⁸³, W. A. Cribbs^{148a,148b}, M. Crispin Ortuzar¹²², M. Cristinziani²³, V. Croft¹⁰⁸, G. Crosetti^{40a,40b}, A. Cueto⁸⁵, T. Cuhadar Donszelmann¹⁴¹, J. Cummings¹⁷⁹, M. Curatolo⁵⁰, J. Cúth⁸⁶, H. Czirr¹⁴³, P. Czodrowski³, G. D'amen^{22a,22b}, S. D'Auria⁵⁶, M. D'Onofrio⁷⁷, M. J. Da Cunha Sargedas De Sousa^{128a,128b}, C. Da Via⁸⁷, W. Dabrowski^{41a}, T. Dado^{146a}, T. Dai⁹², O. Dale¹⁵, F. Dallaire⁹⁷, C. Dallapiccola⁸⁹, M. Dam³⁹, J. R. Dandoy³³, N. P. Dang⁵¹, A. C. Daniells¹⁹, N. S. Dann⁸⁷, M. Danninger¹⁷¹, M. Dano Hoffmann¹³⁸, V. Dao⁵¹, G. Darbo^{53a}, S. Darmora⁸, J. Dassoulas³, A. Dattagupta¹¹⁸, W. Davey²³, C. David¹⁷², T. Davidek¹³¹, M. Davies¹⁵⁵, P. Davison⁸¹, E. Dawe⁹¹, I. Dawson¹⁴¹, K. De⁸, R. de Asmundis^{106a}, A. De Benedetti¹¹⁵, S. De Castro^{22a,22b}, S. De Cecco⁸³, N. De Groot¹⁰⁸, P. de Jong¹⁰⁹, H. De la Torre⁹³, F. De Lorenzi⁶⁷, A. De Maria⁵⁷, D. De Pedis^{134a}, A. De Salvo^{134a}, U. De Sanctis¹⁵¹, A. De Santo¹⁵¹, J. B. De Vivie De Regie¹¹⁹, W. J. Dearnaley⁷⁵, R. Debbe²⁷, C. Debenedetti¹³⁹, D. V. Dedovich⁶⁸, N. Dehghanian³, I. Deigaard¹⁰⁹, M. Del Gaudio^{40a,40b}, J. Del Peso⁸⁵, T. Del Prete^{126a,126b}, D. Delgove¹¹⁹, F. Deliot¹³⁸, C. M. Delitzsch⁵², A. Dell'Acqua³², L. Dell'Asta²⁴, M. Dell'Orso^{126a,126b}, M. Della Pietra^{106a,l}, D. della Volpe⁵², M. Delmastro⁵, P. A. Delsart⁵⁸, D. A. DeMarco¹⁶¹, S. Demers¹⁷⁹, M. Demichev⁶⁸, A. Demilly⁸³, S. P. Denisov¹³², D. Denysiuk¹³⁸, D. Derendarz⁴², J. E. Derkaoui^{137d}, F. Derue⁸³, P. Dervan⁷⁷, K. Desch²³, C. Deterre⁴⁵, K. Dette⁴⁶, P. O. Deviveiros³², A. Dewhurst¹³³, S. Dhaliwal²⁵, A. Di Ciaccio^{135a,135b}, L. Di Ciaccio⁵, W. K. Di Clemente¹²⁴, C. Di Donato^{106a,106b}, A. Di Girolamo³², B. Di Girolamo³², B. Di Micco^{136a,136b}, R. Di Nardo³², A. Di Simone⁵¹, R. Di Sipio¹⁶¹, D. Di Valentino³¹, C. Diaconu⁸⁸, M. Diamond¹⁶¹, F. A. Dias⁴⁹, M. A. Diaz^{34a}, E. B. Diehl⁹², J. Dietrich¹⁷, S. Díez Cornell⁴⁵, A. Dimitrievska¹⁴, J. Dingfelder²³, P. Dita^{28b}, S. Dita^{28b}, F. Dittus³², F. Djama⁸⁸, T. Djobava^{54b}, J. I. Djuvsland^{60a}, M. A. B. do Vale^{26c}, D. Dobos³², M. Dobre^{28b}, C. Doglioni⁸⁴, J. Dolejsi¹³¹, Z. Dolezal¹³¹, M. Donadelli^{26d}, S. Donati^{126a,126b}, P. Dondero^{123a,123b}, J. Donini³⁷, J. Dopke¹³³, A. Doria^{106a}, M. T. Dova⁷⁴, A. T. Doyle⁵⁶, E. Drechsler⁵⁷, M. Dris¹⁰, Y. Du^{36b}, J. Duarte-Camperderros¹⁵⁵, E. Duchovni¹⁷⁵, G. Duckeck¹⁰², O. A. Ducu^{97,n}, D. Duda¹⁰⁹, A. Dudarev³², A. Chr. Dudder⁸⁶, E. M. Duffield¹⁶, L. Duflot¹¹⁹, M. Dührssen³²,

M. Dumancic¹⁷⁵, A. K. Duncan⁵⁶, M. Dunford^{60a}, H. Duran Yildiz^{4a}, M. Düren⁵⁵, A. Durglishvili^{54b}, D. Duschinger⁴⁷, B. Dutta⁴⁵, M. Dyndal⁴⁵, C. Eckardt⁴⁵, K. M. Ecker¹⁰³, R. C. Edgar⁹², N. C. Edwards⁴⁹, T. Eifert³², G. Eigen¹⁵, K. Einsweiler¹⁶, T. Ekelof¹⁶⁸, M. El Kacimi^{137c}, V. Ellajosyula⁸⁸, M. Ellert¹⁶⁸, S. Elles⁵, F. Ellinghaus¹⁷⁸, A. A. Elliot¹⁷², N. Ellis³², J. Elmsheuser²⁷, M. Elsing³², D. Emeliyanov¹³³, Y. Enari¹⁵⁷, O. C. Endner⁸⁶, J. S. Ennis¹⁷³, J. Erdmann⁴⁶, A. Ereditato¹⁸, G. Ernis¹⁷⁸, J. Ernst², M. Ernst²⁷, S. Errede¹⁶⁹, E. Ertel⁸⁶, M. Escalier¹¹⁹, H. Esch⁴⁶, C. Escobar¹²⁷, B. Esposito⁵⁰, A. I. Etienne¹³⁸, E. Etzion¹⁵⁵, H. Evans⁶⁴, A. Ezhilov¹²⁵, M. Ezzi^{137e}, F. Fabbri^{22a,22b}, L. Fabbri^{22a,22b}, G. Facini³³, R. M. Fakhruddinov¹³², S. Falciano^{134a}, R. J. Falla⁸¹, J. Faltova³², Y. Fang^{35a}, M. Fanti^{94a,94b}, A. Farbin⁸, A. Farilla^{136a}, C. Farina¹²⁷, E. M. Farina^{123a,123b}, T. Farooque¹³, S. Farrell¹⁶, S. M. Farrington¹⁷³, P. Farthouat³², F. Fassi^{137e}, P. Fassnacht³², D. Fassouliotis⁹, M. Fauci Giannelli⁸⁰, A. Favareto^{53a,53b}, W. J. Fawcett¹²², L. Fayard¹¹⁹, O. L. Fedin^{125,o}, W. Fedorko¹⁷¹, S. Feigl¹²¹, L. Felgioni⁸⁸, C. Feng^{36b}, E. J. Feng³², H. Feng⁹², A. B. Fenyuk¹³², L. Feremenga⁸, P. Fernandez Martinez¹⁷⁰, S. Fernandez Perez¹³, J. Ferrando⁴⁵, A. Ferrari¹⁶⁸, P. Ferrari¹⁰⁹, R. Ferrari^{123a}, D. E. Ferreira de Lima^{60b}, A. Ferrer¹⁷⁰, D. Ferrere⁵², C. Ferretti⁹², F. Fiedler⁸⁶, A. Filipčić⁷⁸, M. Filipuzzi⁴⁵, F. Filthaut¹⁰⁸, M. Fincke-Keeler¹⁷², K. D. Finelli¹⁵², M. C. N. Fiolhais^{128a,128c}, L. Fiorini¹⁷⁰, A. Fischer², C. Fischer¹³, J. Fischer¹⁷⁸, W. C. Fisher⁹³, N. Flaschel⁴⁵, I. Fleck¹⁴³, P. Fleischmann⁹², G. T. Fletcher¹⁴¹, R. R. M. Fletcher¹²⁴, T. Flick¹⁷⁸, B. M. Flierl¹⁰², L. R. Flores Castillo^{62a}, M. J. Flowerdew¹⁰³, G. T. Forcolin⁸⁷, A. Formica¹³⁸, A. Forti⁸⁷, A. G. Foster¹⁹, D. Fournier¹¹⁹, H. Fox⁷⁵, S. Fracchia¹³, P. Francavilla⁸³, M. Franchini^{22a,22b}, D. Francis³², L. Franconi¹²¹, M. Franklin⁵⁹, M. Frate¹⁶⁶, M. Fraternali^{123a,123b}, D. Freeborn⁸¹, S. M. Fressard-Batranceanu³², F. Friedrich⁴⁷, D. Froidevaux³², J. A. Frost¹²², C. Fukunaga¹⁵⁸, E. Fullana Torregrosa⁸⁶, T. Fusayasu¹⁰⁴, J. Fuster¹⁷⁰, C. Gabaldon⁵⁸, O. Gabizon¹⁵⁴, A. Gabrielli^{22a,22b}, A. Gabrielli¹⁶, G. P. Gach^{41a}, S. Gadatsch³², G. Gagliardi^{53a,53b}, L. G. Gagnon⁹⁷, P. Gagnon⁶⁴, C. Galea¹⁰⁸, B. Galhardo^{128a,128c}, E. J. Gallas¹²², B. J. Gallop¹³³, P. Gallus¹³⁰, G. Galster³⁹, K. K. Gan¹¹³, S. Ganguly³⁷, J. Gao^{36a}, Y. Gao⁴⁹, Y. S. Gao^{145,g}, F. M. Garay Walls⁴⁹, C. García¹⁷⁰, J. E. García Navarro¹⁷⁰, M. Garcia-Sciveres¹⁶, R. W. Gardner³³, N. Garelli¹⁴⁵, V. Garonne¹²¹, A. Gascon Bravo⁴⁵, K. Gasnikova⁴⁵, C. Gatti⁵⁰, A. Gaudiello^{53a,53b}, G. Gaudio^{123a}, L. Gauthier⁹⁷, I. L. Gavrilenko⁹⁸, C. Gay¹⁷¹, G. Gaycken²³, E. N. Gazis¹⁰, Z. Gece¹⁷¹, C. N. P. Gee¹³³, Ch. Geich-Gimbel²³, M. Geisen⁸⁶, M. P. Geisler^{60a}, K. Gellerstedt^{148a,148b}, C. Gemme^{53a}, M. H. Genest⁵⁸, C. Geng^{36a,p}, S. Gentile^{134a,134b}, C. Gentsos¹⁵⁶, S. George⁸⁰, D. Gerbaudo¹³, A. Gershon¹⁵⁵, S. Ghasemi¹⁴³, M. Ghneimat²³, B. Giacobbe^{22a}, S. Giagu^{134a,134b}, P. Giannetti^{126a,126b}, S. M. Gibson⁸⁰, M. Gignac¹⁷¹, M. Gilchriese¹⁶, T. P. S. Gillam³⁰, D. Gillberg³¹, G. Gilles¹⁷⁸, D. M. Gingrich^{3,d}, N. Giokaris^{9,*}, M. P. Giordani^{167a,167c}, F. M. Giorgi^{22a}, P. F. Giraud¹³⁸, P. Giromini⁵⁹, D. Giugni^{94a}, F. Giuli¹²², C. Giuliani¹⁰³, M. Giulini^{60b}, B. K. Gjelsten¹²¹, S. Gkaitatzis¹⁵⁶, I. Gkialas¹⁵⁶, E. L. Gkougkousis¹¹⁹, L. K. Gladilin¹⁰¹, C. Glasman⁸⁵, J. Glatzer¹³, P. C. F. Glaysher⁴⁹, A. Glazov⁴⁵, M. Goblirsch-Kolb²⁵, J. Godlewski⁴², S. Goldfarb⁹¹, T. Golling⁵², D. Golubkov¹³², A. Gomes^{128a,128b,128d}, R. Gonçalo^{128a}, J. Goncalves Pinto Firmino DaCosta¹³⁸, G. Gonella⁵¹, L. Gonella¹⁹, A. Gongadze⁶⁸, S. González de la Hoz¹⁷⁰, S. Gonzalez-Sevilla⁵², L. Goossens³², P. A. Gorbounov⁹⁹, H. A. Gordon²⁷, I. Gorelov¹⁰⁷, B. Gorini³², E. Gorini^{76a,76b}, A. Gorišek⁷⁸, E. Gornicki⁴², A. T. Goshaw⁴⁸, C. Gössling⁴⁶, M. I. Gostkin⁶⁸, C. R. Goudet¹¹⁹, D. Goujdami^{137c}, A. G. Goussiou¹⁴⁰, N. Govender^{147b,q}, E. Gozani¹⁵⁴, L. Graber⁵⁷, I. Grabowska-Bold^{41a}, P. O. J. Gradin⁵⁸, P. Grafström^{22a,22b}, J. Gramling⁵², E. Gramstad¹²¹, S. Grancagnolo¹⁷, V. Gratchev¹²⁵, P. M. Gravila^{28e}, H. M. Gray³², E. Graziani^{136a}, Z. D. Greenwood^{82,r}, C. Greife²³, K. Gregersen⁸¹, I. M. Gregor⁴⁵, P. Grenier¹⁴⁵, K. Grevtsov⁵, J. Griffiths⁸, A. A. Grillo¹³⁹, K. Grimm⁷⁵, S. Grinstein^{13,s}, Ph. Gris³⁷, J.-F. Grivaz¹¹⁹, S. Groh⁸⁶, E. Gross¹⁷⁵, J. Grosse-Knetter⁵⁷, G. C. Grossi⁸², Z. J. Grout⁸¹, L. Guan⁹², W. Guan¹⁷⁶, J. Guenther⁶⁵, F. Guescini⁵², D. Guest¹⁶⁶, O. Gueta¹⁵⁵, B. Gui¹¹³, E. Guido^{53a,53b}, T. Guillemain⁵, S. Guindon², U. Gul⁵⁶, C. Gumpert³², J. Guo^{36c}, Y. Guo^{36a,p}, R. Gupta⁴³, S. Gupta¹²², G. Gustavino^{134a,134b}, P. Gutierrez¹¹⁵, N. G. Gutierrez Ortiz⁸¹, C. Gutsche⁸¹, C. Guyot¹³⁸, C. Gwenlan¹²², C. B. Gwilliam⁷⁷, A. Haas¹¹², C. Haber¹⁶, H. K. Hadavand⁸, N. Haddad^{137e}, A. Hader⁸⁸, S. Hageböck²³, M. Hagihara¹⁶⁴, Z. Hajduk⁴², H. Hakobyan^{180,*}, M. Haleem⁴⁵, J. Haley¹¹⁶, G. Halladjian⁹³, G. D. Hallewell⁸⁸, K. Hamacher¹⁷⁸, P. Hamal¹¹⁷, K. Hamano¹⁷², A. Hamilton^{147a}, G. N. Hamity¹⁴¹, P. G. Hamnett⁴⁵, L. Han^{36a}, K. Hanagaki^{69,t}, K. Hanawa¹⁵⁷, M. Hance¹³⁹, B. Haney¹²⁴, P. Hanke^{60a}, R. Hanna¹³⁸, J. B. Hansen³⁹, J. D. Hansen³⁹, M. C. Hansen²³, P. H. Hansen³⁹, K. Hara¹⁶⁴, A. S. Hard¹⁷⁶, T. Harenberg¹⁷⁸, F. Hariri¹¹⁹, S. Harkusha⁹⁵, R. D. Harrington⁴⁹, P. F. Harrison¹⁷³, F. Hartjes¹⁰⁹, N. M. Hartmann¹⁰², M. Hasegawa⁷⁰, Y. Hasegawa¹⁴², A. Hasib¹¹⁵, S. Hassani¹³⁸, S. Haug¹⁸, R. Hauser⁹³, L. Hauswald⁴⁷, M. Havranek¹²⁹, C. M. Hawkes¹⁹, R. J. Hawkings³², D. Hayakawa¹⁵⁹, D. Hayden⁹³, C. P. Hays¹²², J. M. Hays⁷⁹, H. S. Hayward⁷⁷, S. J. Haywood¹³³, S. J. Head¹⁹, T. Heck⁸⁶, V. Hedberg⁸⁴, L. Heelan⁸, S. Heim¹²⁴, T. Heim¹⁶, B. Heinemann¹⁶, J. J. Heinrich¹⁰², L. Heinrich¹¹², C. Heinz⁵⁵, J. Hejbal¹²⁹, L. Helary³², S. Hellman^{148a,148b}, C. Helsens³², J. Henderson¹²², R. C. W. Henderson⁷⁵, Y. Heng¹⁷⁶, S. Henkelmann¹⁷¹, A. M. Henriques Correia³², S. Henrot-Versille¹¹⁹, G. H. Herbert¹⁷, H. Herde²⁵, V. Herget¹⁷⁷, Y. Hernández Jiménez^{147c}, G. Herten⁵¹, R. Hertenberger¹⁰², L. Hervas³², G. G. Hesketh⁸¹, N. P. Hessey¹⁰⁹, J. W. Hetherly⁴³, E. Higón-Rodríguez¹⁷⁰, E. Hill¹⁷², J. C. Hill³⁰, K. H. Hiller⁴⁵, S. J. Hillier¹⁹

I. Hinchliffe¹⁶, E. Hines¹²⁴, M. Hirose⁵¹, D. Hirschbuehl¹⁷⁸, X. Hoad⁴⁹, J. Hobbs¹⁵⁰, N. Hod^{163a}, M. C. Hodgkinson¹⁴¹, P. Hodgson¹⁴¹, A. Hoecker³², M. R. Hoferkamp¹⁰⁷, F. Hoenic¹⁰², D. Hohn²³, T. R. Holmes¹⁶, M. Homann⁴⁶, T. Honda⁶⁹, T. M. Hong¹²⁷, B. H. Hooberman¹⁶⁹, W. H. Hopkins¹¹⁸, Y. Horii¹⁰⁵, A. J. Horton¹⁴⁴, J.-Y. Hostachy⁵⁸, S. Hou¹⁵³, A. Hoummada^{137a}, J. Howarth⁴⁵, J. Hoya⁷⁴, M. Hrabovsky¹¹⁷, I. Hristova¹⁷, J. Hrivnac¹¹⁹, T. Hryn'ova⁵, A. Hrynevich⁹⁶, P. J. Hsu⁶³, S.-C. Hsu¹⁴⁰, Q. Hu^{36a}, S. Hu^{36c}, Y. Huang⁴⁵, Z. Hubacek¹³⁰, F. Hubaut⁸⁸, F. Huegging²³, T. B. Huffman¹²², E. W. Hughes³⁸, G. Hughes⁷⁵, M. Huhtinen³², P. Huo¹⁵⁰, N. Huseynov^{68,b}, J. Huston⁹³, J. Huth⁵⁹, G. Iacobucci⁵², G. Iakovidis²⁷, I. Ibragimov¹⁴³, L. Iconomidou-Fayard¹¹⁹, E. Ideal¹⁷⁹, Z. Idrissi^{137e}, P. Iengo³², O. Igonkina^{109,u}, T. Iizawa¹⁷⁴, Y. Ikegami⁶⁹, M. Ikeno⁶⁹, Y. Ilchenko^{11,v}, D. Iliadis¹⁵⁶, N. Ilic¹⁴⁵, G. Introzzi^{123a,123b}, P. Ioannou^{9,*}, M. Iodice^{136a}, K. Iordanidou³⁸, V. Ippolito⁵⁹, N. Ishijima¹²⁰, M. Ishino¹⁵⁷, M. Ishitsuka¹⁵⁹, R. Ishmukhametov¹¹³, C. Issever¹²², S. Istin^{20a}, F. Ito¹⁶⁴, J. M. Iturbe Ponce⁸⁷, R. Iuppa^{162a,162b}, W. Iwanski⁶⁵, H. Iwasaki⁶⁹, J. M. Izen⁴⁴, V. Izzo^{106a}, S. Jabbar³, B. Jackson¹²⁴, P. Jackson¹, V. Jain², K. B. Jakobi⁸⁶, K. Jakobs⁵¹, S. Jakobsen³², T. Jakoubek¹²⁹, D. O. Jamin¹¹⁶, D. K. Jana⁸², R. Jansky⁶⁵, J. Janssen²³, M. Janus⁵⁷, P. A. Janus^{41a}, G. Jarlskog⁸⁴, N. Javadov^{68,b}, T. Javůrek⁵¹, F. Jeanneau¹³⁸, L. Jeanty¹⁶, J. Jejelava^{54a,w}, G.-Y. Jeng¹⁵², D. Jennens⁹¹, P. Jenni^{51,x}, C. Jeske¹⁷³, S. Jézéquel⁵, H. Ji¹⁷⁶, J. Jia¹⁵⁰, H. Jiang⁶⁷, Y. Jiang^{36a}, Z. Jiang¹⁴⁵, S. Jiggins⁸¹, J. Jimenez Pena¹⁷⁰, S. Jin^{35a}, A. Jinaru^{28b}, O. Jinnouchi¹⁵⁹, H. Jivan^{147c}, P. Johansson¹⁴¹, K. A. Johns⁷, W. J. Johnson¹⁴⁰, K. Jon-And^{148a,148b}, G. Jones¹⁷³, R. W. L. Jones⁷⁵, S. Jones⁷, T. J. Jones⁷⁷, J. Jongmanns^{60a}, P. M. Jorge^{128a,128b}, J. Jovicevic^{163a}, X. Ju¹⁷⁶, A. Juste Rozas^{13,s}, M. K. Köhler¹⁷⁵, A. Kaczmarzka⁴², M. Kado¹¹⁹, H. Kagan¹¹³, M. Kagan¹⁴⁵, S. J. Kahn⁸⁸, T. Kaji¹⁷⁴, E. Kajomovitz⁴⁸, C. W. Kalderon¹²², A. Kaluza⁸⁶, S. Kama⁴³, A. Kamenshchikov¹³², N. Kanaya¹⁵⁷, S. Kaneti³⁰, L. Kanjir⁷⁸, V. A. Kantserov¹⁰⁰, J. Kanzaki⁶⁹, B. Kaplan¹¹², L. S. Kaplan¹⁷⁶, A. Kapliy³³, D. Kar^{147c}, K. Karakostas¹⁰, A. Karamaoun³, N. Karastathis¹⁰, M. J. Kareem⁵⁷, E. Karentzos¹⁰, M. Karnevskiy⁸⁶, S. N. Karpov⁶⁸, Z. M. Karpova⁶⁸, K. Karthik¹¹², V. Kartvelishvili⁷⁵, A. N. Karyukhin¹³², K. Kasahara¹⁶⁴, L. Kashif¹⁷⁶, R. D. Kass¹¹³, A. Kastanas¹⁴⁹, Y. Kataoka¹⁵⁷, C. Kato¹⁵⁷, A. Katre⁵², J. Katzy⁴⁵, K. Kawade¹⁰⁵, K. Kawagoe⁷³, T. Kawamoto¹⁵⁷, G. Kawamura⁵⁷, V. F. Kazanin^{111,c}, R. Keeler¹⁷², R. Kehoe⁴³, J. S. Keller⁴⁵, J. J. Kempster⁸⁰, H. Keoshkerian¹⁶¹, O. Kepka¹²⁹, B. P. Kerševan⁷⁸, S. Kersten¹⁷⁸, R. A. Keyes⁹⁰, M. Khader¹⁶⁹, F. Khalil-zada¹², A. Khanov¹¹⁶, A. G. Kharlamov^{111,c}, T. Kharlamova¹¹¹, T. J. Khoo⁵², V. Khovanskij⁹⁹, E. Khramov⁶⁸, J. Khubua^{54b,y}, S. Kido⁷⁰, C. R. Kilby⁸⁰, H. Y. Kim⁸, S. H. Kim¹⁶⁴, Y. K. Kim³³, N. Kimura¹⁵⁶, O. M. Kind¹⁷, B. T. King⁷⁷, M. King¹⁷⁰, J. Kirk¹³³, A. E. Kiryunin¹⁰³, T. Kishimoto¹⁵⁷, D. Kisielewska^{41a}, F. Kiss⁵¹, K. Kiuchi¹⁶⁴, O. Kivernyk¹³⁸, E. Kladiva^{146b}, M. H. Klein³⁸, M. Klein⁷⁷, U. Klein⁷⁷, K. Kleinknecht⁸⁶, P. Klimek¹¹⁰, A. Klimentov²⁷, R. Klingenberg⁴⁶, T. Klioutchnikova³², E.-E. Kluge^{60a}, P. Kluit¹⁰⁹, S. Kluth¹⁰³, J. Knapik⁴², E. Kneringer⁶⁵, E. B. F. G. Knoops⁸⁸, A. Knue⁵⁶, A. Kobayashi¹⁵⁷, D. Kobayashi¹⁵⁹, T. Kobayashi¹⁵⁷, M. Kobel⁴⁷, M. Kocian¹⁴⁵, P. Kodys¹³¹, T. Koffas³¹, E. Koffeman¹⁰⁹, N. M. Köhler¹⁰³, T. Koi¹⁴⁵, H. Kolanoski¹⁷, M. Kolb^{60b}, I. Koletsou⁵, A. A. Komar^{98,*}, Y. Komori¹⁵⁷, T. Kondo⁶⁹, N. Kondrashova^{36c}, K. Köneke⁵¹, A. C. König¹⁰⁸, T. Kono^{69,z}, R. Konoplich^{112,aa}, N. Konstantinidis⁸¹, R. Kopeliansky⁶⁴, S. Koperny^{41a}, L. Köpke⁸⁶, A. K. Kopp⁵¹, K. Korcyl⁴², K. Kordas¹⁵⁶, A. Korn⁸¹, A. A. Korol^{111,c}, I. Korolkov¹³, E. V. Korolkova¹⁴¹, O. Kortner¹⁰³, S. Kortner¹⁰³, T. Kosek¹³¹, V. V. Kostyukhin²³, A. Kotwal⁴⁸, A. Koulouris¹⁰, A. Kourkoumeli-Charalampidi^{123a,123b}, C. Kourkoumelis⁹, V. Kouskoura²⁷, A. B. Kowalewska⁴², R. Kowalewski¹⁷², T. Z. Kowalski^{41a}, C. Kozakai¹⁵⁷, W. Kozanecki¹³⁸, A. S. Kozhin¹³², V. A. Kramarenko¹⁰¹, G. Kramberger⁷⁸, D. Krasnopevtsev¹⁰⁰, M. W. Krasny⁸³, A. Krasznahorkay³², A. Kravchenko²⁷, M. Kretz^{60c}, J. Kretzschmar⁷⁷, K. Kreutzfeldt⁵⁵, P. Krieger¹⁶¹, K. Krizka³³, K. Kroeninger⁴⁶, H. Kroha¹⁰³, J. Kroll¹²⁴, J. Kroseberg²³, J. Krstic¹⁴, U. Kruchonak⁶⁸, H. Krüger²³, N. Krumnack⁶⁷, M. C. Kruse⁴⁸, M. Kruskal²⁴, T. Kubota⁹¹, H. Kucuk⁸¹, S. Kuday^{4b}, J. T. Kuechler¹⁷⁸, S. Kuehn⁵¹, A. Kugel^{60c}, F. Kuger¹⁷⁷, T. Kuhl⁴⁵, V. Kukhtin⁶⁸, R. Kukla¹³⁸, Y. Kulchitsky⁹⁵, S. Kuleshov^{34b}, M. Kuna^{134a,134b}, T. Kunigo⁷¹, A. Kupco¹²⁹, H. Kurashige⁷⁰, L. L. Kurchaninov^{163a}, Y. A. Kurochkin⁹⁵, M. G. Kurth⁴⁴, V. Kus¹²⁹, E. S. Kuwertz¹⁷², M. Kuze¹⁵⁹, J. Kvitka¹¹⁷, T. Kwan¹⁷², D. Kyriazopoulos¹⁴¹, A. La Rosa¹⁰³, J. L. La Rosa Navarro^{26d}, L. La Rotonda^{40a,40b}, C. Lacasta¹⁷⁰, F. Lacava^{134a,134b}, J. Lacey³¹, H. Lacker¹⁷, D. Lacour⁸³, V. R. Lacuesta¹⁷⁰, E. Ladygin⁶⁸, R. Lafaye⁵, B. Laforge⁸³, T. Lagouri¹⁷⁹, S. Lai⁵⁷, S. Lammers⁶⁴, W. Lampl⁷, E. Lançon¹³⁸, U. Landgraf⁵¹, M. P. J. Landon⁷⁹, M. C. Lanfermann⁵², V. S. Lang^{60a}, J. C. Lange¹³, A. J. Lankford¹⁶⁶, F. Lanni²⁷, K. Lantzsch²³, A. Lanza^{123a}, S. Laplace⁸³, C. Lapoire³², J. F. Laporte¹³⁸, T. Lari^{94a}, F. Lasagni Manghi^{22a,22b}, M. Lassnig³², P. Laurelli⁵⁰, W. Lavrijsen¹⁶, A. T. Law¹³⁹, P. Laycock⁷⁷, T. Lazovich⁵⁹, M. Lazzaroni^{94a,94b}, B. Le⁹¹, O. Le Dortz⁸³, E. Le Guirriec⁸⁸, E. P. Le Quilleuc¹³⁸, M. LeBlanc¹⁷², T. LeCompte⁶, F. Ledroit-Guillon⁵⁸, C. A. Lee²⁷, S. C. Lee¹⁵³, L. Lee¹, B. Lefebvre⁹⁰, G. Lefebvre⁸³, M. Lefebvre¹⁷², F. Legger¹⁰², C. Leggett¹⁶, A. Lehan⁷⁷, G. Lehmann Miotto³², X. Lei⁷, W. A. Leight³¹, A. G. Leister¹⁷⁹, M. A. L. Leite^{26d}, R. Leitner¹³¹, D. Lellouch¹⁷⁵, B. Lemmer⁵⁷, K. J. C. Leney⁸¹, T. Lenz²³, B. Lenzi³², R. Leone⁷, S. Leone^{126a,126b}, C. Leonidopoulos⁴⁹, S. Leontsinis¹⁰, G. Lerner¹⁵¹, C. Leroy⁹⁷, A. A. J. Lesage¹³⁸, C. G. Lester³⁰, M. Levchenko¹²⁵, J. Levêque⁵, D. Levin⁹², L. J. Levinson¹⁷⁵, M. Levy¹⁹, D. Lewis⁷⁹, M. Leyton⁴⁴, B. Li^{36a,p}, C. Li^{36a}, H. Li¹⁵⁰, L. Li⁴⁸, L. Li^{36c}, Q. Li^{35a}, S. Li⁴⁸, X. Li⁸⁷, Y. Li¹⁴³, Z. Liang^{35a}, B. Liberti^{135a}, A. Liblong¹⁶¹, P. Lichard³², K. Lie¹⁶⁹, J. Liebal²³, W. Liebig¹⁵, A. Limosani¹⁵²

S. C. Lin^{153,ab}, T. H. Lin⁸⁶, B. E. Lindquist¹⁵⁰, A. E. Lioni⁵², E. Lipeles¹²⁴, A. Lipniacka¹⁵, M. Lisovsky^{60b}, T. M. Liss¹⁶⁹, A. Lister¹⁷¹, A. M. Litke¹³⁹, B. Liu^{153,ac}, D. Liu¹⁵³, H. Liu⁹², H. Liu²⁷, J. Liu^{36b}, J. B. Liu^{36a}, K. Liu⁸⁸, L. Liu¹⁶⁹, M. Liu^{36a}, Y. L. Liu^{36a}, Y. Liu^{36a}, M. Livan^{123a,123b}, A. Lleres⁵⁸, J. Llorente Merino^{35a}, S. L. Lloyd⁷⁹, F. Lo Sterzo¹⁵³, E. M. Lobodzinska⁴⁵, P. Loch⁷, F. K. Loebinger⁸⁷, K. M. Loew²⁵, A. Loginov^{179,*}, T. Lohse¹⁷, K. Lohwasser⁴⁵, M. Lokajicek¹²⁹, B. A. Long²⁴, J. D. Long¹⁶⁹, R. E. Long⁷⁵, L. Longo^{76a,76b}, K. A. Looper¹¹³, J. A. Lopez Lopez^{34b}, D. Lopez Mateos⁵⁹, B. Lopez Paredes¹⁴¹, I. Lopez Paz¹³, A. Lopez Solis⁸³, J. Lorenz¹⁰², N. Lorenzo Martinez⁶⁴, M. Losada²¹, P. J. Lösel¹⁰², X. Lou^{35a}, A. Lounis¹¹⁹, J. Love⁶, P. A. Love⁷⁵, H. Lu^{62a}, N. Lu⁹², H. J. Lubatti¹⁴⁰, C. Luci^{134a,134b}, A. Lucotte⁵⁸, C. Luedtke⁵¹, F. Luehring⁶⁴, W. Lukas⁶⁵, L. Luminari^{134a}, O. Lundberg^{148a,148b}, B. Lund-Jensen¹⁴⁹, P. M. Luzi⁸³, D. Lynn²⁷, R. Lysak¹²⁹, E. Lytken⁸⁴, V. Lyubushkin⁶⁸, H. Ma²⁷, L. L. Ma^{36b}, Y. Ma^{36b}, G. Maccarrone⁵⁰, A. Macchiolo¹⁰³, C. M. Macdonald¹⁴¹, B. Maček⁷⁸, J. Machado Miguens^{124,128b}, D. Madaffari⁸⁸, R. Madar³⁷, H. J. Maddocks¹⁶⁸, W. F. Mader⁴⁷, A. Madsen⁴⁵, J. Maeda⁷⁰, S. Maeland¹⁵, T. Maeno²⁷, A. Maevskiy¹⁰¹, E. Magradze⁵⁷, J. Mahlstedt¹⁰⁹, C. Maiani¹¹⁹, C. Maidantchik^{26a}, A. A. Maier¹⁰³, T. Maier¹⁰², A. Maio^{128a,128b,128d}, S. Majewski¹¹⁸, Y. Makida⁶⁹, N. Makovec¹¹⁹, B. Malaescu⁸³, Pa. Malecki⁴², V. P. Maleev¹²⁵, F. Malek⁵⁸, U. Mallik⁶⁶, D. Malon⁶, C. Malone¹⁴⁵, C. Malone³⁰, S. Maltezos¹⁰, S. Malyukov³², J. Mamuzic¹⁷⁰, G. Mancini⁵⁰, L. Mandelli^{94a}, I. Mandić⁷⁸, J. Maneira^{128a,128b}, L. Manhaes de Andrade Filho^{26b}, J. Manjarres Ramos^{163b}, A. Mann¹⁰², A. Manousos³², B. Mansoulie¹³⁸, J. D. Mansour^{35a}, R. Mantifel⁹⁰, M. Mantoani⁵⁷, S. Manzoni^{94a,94b}, L. Mapelli³², G. Marceca²⁹, L. March⁵², G. Marchiori⁸³, M. Marcisovsky¹²⁹, M. Marjanovic¹⁴, D. E. Marley⁹², F. Marroquim^{26a}, S. P. Marsden⁸⁷, Z. Marshall¹⁶, S. Marti-Garcia¹⁷⁰, B. Martin⁹³, T. A. Martin¹⁷³, V. J. Martin⁴⁹, B. Martin dit Latour¹⁵, M. Martinez^{13,s}, V. I. Martinez Outschoorn¹⁶⁹, S. Martin-Haugh¹³³, V. S. Martoiu^{28b}, A. C. Martyniuk⁸¹, A. Marzin³², L. Masetti⁸⁶, T. Mashimo¹⁵⁷, R. Mashinistov⁹⁸, J. Masik⁸⁷, A. L. Maslennikov^{111,c}, I. Massa^{22a,22b}, L. Massa^{22a,22b}, P. Mastrandrea⁵, A. Mastroberardino^{40a,40b}, T. Masubuchi¹⁵⁷, P. Mättig¹⁷⁸, J. Mattmann⁸⁶, J. Maurer^{28b}, S. J. Maxfield⁷⁷, D. A. Maximov^{111,c}, R. Mazini¹⁵³, I. Maznas¹⁵⁶, S. M. Mazza^{94a,94b}, N. C. Mc Fadden¹⁰⁷, G. Mc Goldrick¹⁶¹, S. P. Mc Kee⁹², A. McCarn⁹², R. L. McCarthy¹⁵⁰, T. G. McCarthy¹⁰³, L. I. McClymont⁸¹, E. F. McDonald⁹¹, J. A. Mcfayden⁸¹, G. Mchedlidze⁵⁷, S. J. McMahon¹³³, R. A. McPherson^{172,m}, M. Medinnis⁴⁵, S. Meehan¹⁴⁰, S. Mehlhase¹⁰², A. Mehta⁷⁷, K. Meier^{60a}, C. Meineck¹⁰², B. Meirose⁴⁴, D. Melini¹⁷⁰, B. R. Mellado Garcia^{147c}, M. Melo^{146a}, F. Meloni¹⁸, S. B. Menary⁸⁷, L. Meng⁷⁷, X. T. Meng⁹², A. Mengarelli^{22a,22b}, S. Menke¹⁰³, E. Meoni¹⁶⁵, S. Mergelmeyer¹⁷, P. Mermod⁵², L. Merola^{106a,106b}, C. Meroni^{94a}, F. S. Merritt³³, A. Messina^{134a,134b}, J. Metcalfe⁶, A. S. Mete¹⁶⁶, C. Meyer⁸⁶, C. Meyer¹²⁴, J-P. Meyer¹³⁸, J. Meyer¹⁰⁹, H. Meyer Zu Theenhausen^{60a}, F. Miano¹⁵¹, R. P. Middleton¹³³, S. Miglioranza^{53a,53b}, L. Mijović⁴⁹, G. Mikenberg¹⁷⁵, M. Mikestikova¹²⁹, M. Mikuz⁷⁸, M. Milesi⁹¹, A. Milic²⁷, D. W. Miller³³, C. Mills⁴⁹, A. Milov¹⁷⁵, D. A. Milstead^{148a,148b}, A. A. Minaenko¹³², Y. Minami¹⁵⁷, I. A. Minashvili⁶⁸, A. I. Mincer¹¹², B. Mindur^{41a}, M. Mineev⁶⁸, Y. Minegishi¹⁵⁷, Y. Ming¹⁷⁶, L. M. Mir¹³, K. P. Mistry¹²⁴, T. Mitani¹⁷⁴, J. Mitrevski¹⁰², V. A. Mitsou¹⁷⁰, A. Miucci¹⁸, P. S. Miyagawa¹⁴¹, A. Mizukami⁶⁹, J. U. Mjörnmark⁸⁴, M. Mlynarikova¹³¹, T. Moa^{148a,148b}, K. Mochizuki⁹⁷, P. Mogg⁵¹, S. Mohapatra³⁸, S. Molander^{148a,148b}, R. Moles-Valls²³, R. Monden⁷¹, M. C. Mondragon⁹³, K. Mönig⁴⁵, J. Monk³⁹, E. Monnier⁸⁸, A. Montalbano¹⁵⁰, J. Montejo Berlingen³², F. Monticelli⁷⁴, S. Monzani^{94a,94b}, R. W. Moore³, N. Morange¹¹⁹, D. Moreno²¹, M. Moreno Llacer⁵⁷, P. Morettini^{53a}, S. Morgenstern³², D. Mori¹⁴⁴, T. Mori¹⁵⁷, M. Morii⁵⁹, M. Morinaga¹⁵⁷, V. Morisbak¹²¹, S. Moritz⁸⁶, A. K. Morley¹⁵², G. Mornacchi³², J. D. Morris⁷⁹, S. S. Mortensen³⁹, L. Morvaj¹⁵⁰, P. Moschovakos¹⁰, M. Mosidze^{54b}, H. J. Moss¹⁴¹, J. Moss^{145,ad}, K. Motohashi¹⁵⁹, R. Mount¹⁴⁵, E. Mountricha²⁷, E. J. W. Moyse⁸⁹, S. Muanza⁸⁸, R. D. Mudd¹⁹, F. Mueller¹⁰³, J. Mueller¹²⁷, R. S. P. Mueller¹⁰², T. Mueller³⁰, D. Muenstermann⁷⁵, P. Mullen⁵⁶, G. A. Mullier¹⁸, F. J. Munoz Sanchez⁸⁷, J. A. Murillo Quijada¹⁹, W.J. Murray^{133,173}, H. Musheghyan⁵⁷, M. Muškinja⁷⁸, A. G. Myagkov^{132,ae}, M. Myska¹³⁰, B. P. Nachman¹⁴⁵, O. Nackenhorst⁵², K. Nagai¹²², R. Nagai^{69,z}, K. Nagano⁶⁹, Y. Nagasaka⁶¹, K. Nagata¹⁶⁴, M. Nagel⁵¹, E. Nagy⁸⁸, A. M. Nairz³², Y. Nakahama¹⁰⁵, K. Nakamura⁶⁹, T. Nakamura¹⁵⁷, I. Nakano¹¹⁴, R. F. Naranjo Garcia⁴⁵, R. Narayan¹¹, D. I. Narrias Villar^{60a}, I. Naryshkin¹²⁵, T. Naumann⁴⁵, G. Navarro²¹, R. Nayyar⁷, H. A. Neal⁹², P. Yu. Nechaeva⁹⁸, T. J. Neep⁸⁷, A. Negri^{123a,123b}, M. Negrini^{22a}, S. Nektarijevic¹⁰⁸, C. Nellist¹¹⁹, A. Nelson¹⁶⁶, S. Nemecek¹²⁹, P. Nemethy¹¹², A. A. Nepomuceno^{26a}, M. Nessi^{32,af}, M. S. Neubauer¹⁶⁹, M. Neumann¹⁷⁸, R. M. Neves¹¹², P. Nevski²⁷, P. R. Newman¹⁹, D. H. Nguyen⁶, T. Nguyen Manh⁹⁷, R. B. Nickerson¹²², R. Nicolaidou¹³⁸, J. Nielsen¹³⁹, A. Nikiforov¹⁷, V. Nikolaenko^{132,ae}, I. Nikolic-Audit⁸³, K. Nikolopoulos¹⁹, J. K. Nilsen¹²¹, P. Nilsson²⁷, Y. Ninomiya¹⁵⁷, A. Nisati^{134a}, R. Nisius¹⁰³, T. Nobe¹⁵⁷, M. Nomachi¹²⁰, I. Nomidis³¹, T. Nooney⁷⁹, S. Norberg¹¹⁵, M. Nordberg³², N. Norjoharuddeen¹²², O. Novgorodova⁴⁷, S. Nowak¹⁰³, M. Nozaki⁶⁹, L. Nozka¹¹⁷, K. Ntekas¹⁶⁶, E. Nurse⁸¹, F. Nuti⁹¹, F. O'grady⁷, D. C. O'Neil¹⁴⁴, A. A. O'Rourke⁴⁵, V. O'Shea⁵⁶, F. G. Oakham^{31,d}, H. Oberlack¹⁰³, T. Obermann²³, J. Ocariz⁸³, A. Ochi⁷⁰, I. Ochoa³⁸, J. P. Ochoa-Ricoux^{34a}, S. Oda⁷³, S. Odaka⁶⁹, H. Ogren⁶⁴, A. Oh⁸⁷, S. H. Oh⁴⁸, C. C. Ohm¹⁶, H. Ohman¹⁶⁸, H. Oide^{53a,53b}, H. Okawa¹⁶⁴, Y. Okumura¹⁵⁷, T. Okuyama⁶⁹, A. Olariu^{28b}, L. F. Oleiro Seabra^{128a}, S. A. Olivares Pino⁴⁹, D. Oliveira Damazio²⁷, A. Olszewski⁴², J. Olszowska⁴²

A. Onofre^{128a,128e}, K. Onogi¹⁰⁵, P. U. E. Onyisi^{11.v}, M. J. Oreglia³³, Y. Oren¹⁵⁵, D. Orestano^{136a,136b}, N. Orlando^{62b}, R. S. Orr¹⁶¹, B. Osculati^{53a,53b,*}, R. Ospanov⁸⁷, G. Otero y Garzon²⁹, H. Otono⁷³, M. Ouchrif^{137d}, F. Ould-Saada¹²¹, A. Ouraou¹³⁸, K. P. Oussoren¹⁰⁹, Q. Ouyang^{35a}, M. Owen⁵⁶, R. E. Owen¹⁹, V. E. Ozcan^{20a}, N. Ozturk⁸, K. Pachal¹⁴⁴, A. Pacheco Pages¹³, L. Pacheco Rodriguez¹³⁸, C. Padilla Aranda¹³, M. Pagáčová⁵¹, S. Pagan Griso¹⁶, M. Paganini¹⁷⁹, F. Paige²⁷, P. Pais⁸⁹, K. Pajchel¹²¹, G. Palacino⁶⁴, S. Palazzo^{40a,40b}, S. Palestini³², M. Palka^{41b}, D. Pallin³⁷, E. St. Panagiotopoulou¹⁰, C. E. Pandini⁸³, J. G. Panduro Vazquez⁸⁰, P. Pani^{148a,148b}, S. Panitkin²⁷, D. Pantea^{28b}, L. Paolozzi⁵², Th. D. Papadopoulou¹⁰, K. Papageorgiou¹⁵⁶, A. Paramonov⁶, D. Paredes Hernandez¹⁷⁹, A. J. Parker⁷⁵, M. A. Parker³⁰, K. A. Parker¹⁴¹, F. Parodi^{53a,53b}, J. A. Parsons³⁸, U. Parzefall⁵¹, V. R. Pascuzzi¹⁶¹, E. Pasqualucci^{134a}, S. Passaggio^{53a}, Fr. Pastore⁸⁰, G. Pásztor^{31.ag}, S. Patariaia¹⁷⁸, J. R. Pater⁸⁷, T. Pauly³², J. Pearce¹⁷², B. Pearson¹¹⁵, L. E. Pedersen³⁹, M. Pedersen¹²¹, S. Pedraza Lopez¹⁷⁰, R. Pedro^{128a,128b}, S. V. Peleganchuk^{111.c}, O. Penc¹²⁹, C. Peng^{35a}, H. Peng^{36a}, J. Penwell⁶⁴, B. S. Peralva^{26b}, M. M. Perego¹³⁸, D. V. Perepelitsa²⁷, E. Perez Codina^{163a}, L. Perini^{94a,94b}, H. Pernegger³², S. Perrella^{106a,106b}, R. Peschke⁴⁵, V. D. Peshekhonov⁶⁸, K. Peters⁴⁵, R. F. Y. Peters⁸⁷, B. A. Petersen³², T. C. Petersen³⁹, E. Petit⁵⁸, A. Petridis¹, C. Petridou¹⁵⁶, P. Petroff¹¹⁹, E. Petrolo^{134a}, M. Petrov¹²², F. Petrucci^{136a,136b}, N. E. Pettersson⁸⁹, A. Peyaud¹³⁸, R. Pezoa^{34b}, P. W. Phillips¹³³, G. Piacquadio^{145.ah}, E. Pianori¹⁷³, A. Picazio⁸⁹, E. Piccaro⁷⁹, M. Piccinini^{22a,22b}, M. A. Pickering¹²², R. Piegai²⁹, J. E. Pilcher³³, A. D. Pilkington⁸⁷, A. W. J. Pin⁸⁷, M. Pinamonti^{167a,167c.ai}, J. L. Pinfold³, A. Pingel³⁹, S. Pires⁸³, H. Pirumov⁴⁵, M. Pitt¹⁷⁵, L. Plazak^{146a}, M.-A. Pleier²⁷, V. Pleskot⁸⁶, E. Plotnikova⁶⁸, D. Pluth⁶⁷, R. Poettgen^{148a,148b}, L. Poggioli¹¹⁹, D. Pohl²³, G. Polesello^{123a}, A. Poley⁴⁵, A. Policicchio^{40a,40b}, R. Polifka¹⁶¹, A. Polini^{22a}, C. S. Pollard⁵⁶, V. Polychronakos²⁷, K. Pommès³², L. Pontecorvo^{134a}, B. G. Pope⁹³, G. A. Popeneciu^{28c}, A. Poppleton³², S. Pospisil¹³⁰, K. Potamianos¹⁶, I. N. Potrap⁶⁸, C. J. Potter³⁰, C. T. Potter¹¹⁸, G. Poulard³², J. Poveda³², V. Pozdnyakov⁶⁸, M. E. Pozo Astigarraga³², P. Pralavorio⁸⁸, A. Pranko¹⁶, S. Prell⁶⁷, D. Price⁸⁷, L. E. Price⁶, M. Primavera^{76a}, S. Prince⁹⁰, K. Prokofiev^{62c}, F. Prokoshin^{34b}, S. Protopopescu²⁷, J. Proudfoot⁶, M. Przybycien^{41a}, D. Puddu^{136a,136b}, M. Purohit^{27.aj}, P. Puzo¹¹⁹, J. Qian⁹², G. Qin⁵⁶, Y. Qin⁸⁷, A. Quadt⁵⁷, W. B. Quayle^{167a,167b}, M. Queitsch-Maitland⁴⁵, D. Quilty⁵⁶, S. Raddum¹²¹, V. Radeka²⁷, V. Radescu¹²², S. K. Radhakrishnan¹⁵⁰, P. Radloff¹¹⁸, P. Rados⁹¹, F. Ragusa^{94a,94b}, G. Rahal¹⁸¹, J. A. Raine⁸⁷, S. Rajagopalan²⁷, M. Rammensee³², C. Rangel-Smith¹⁶⁸, M. G. Ratti^{94a,94b}, D. M. Rauch⁴⁵, F. Rauscher¹⁰², S. Rave⁸⁶, T. Ravenscroft⁵⁶, I. Ravinovich¹⁷⁵, M. Raymond³², A. L. Read¹²¹, N. P. Readioff⁷⁷, M. Reale^{76a,76b}, D. M. Rebuffi^{123a,123b}, A. Redelbach¹⁷⁷, G. Redlinger²⁷, R. Reece¹³⁹, R. G. Reed^{147c}, K. Reeves⁴⁴, L. Rehnisch¹⁷, J. Reichert¹²⁴, A. Reiss⁸⁶, C. Rember³², H. Ren^{35a}, M. Rescigno^{134a}, S. Resconi^{94a}, O. L. Rezanova^{111.c}, P. Reznicek¹³¹, R. Rezvani⁹⁷, R. Richter¹⁰³, S. Richter⁸¹, E. Richter-Was^{41b}, O. Ricken²³, M. Ridel⁸³, P. Rieck¹⁷, C. J. Riegel¹⁷⁸, J. Rieger⁵⁷, O. Rifki¹¹⁵, M. Rijssenbeek¹⁵⁰, A. Rimoldi^{123a,123b}, M. Rimoldi¹⁸, L. Rinaldi^{22a}, B. Ristić⁵², E. Ritsch³², I. Riu¹³, F. Rizatdinova¹¹⁶, E. Rizvi⁷⁹, C. Rizzi¹³, S. H. Robertson^{90.m}, A. Robichaud-Veronneau⁹⁰, D. Robinson³⁰, J. E. M. Robinson⁴⁵, A. Robson⁵⁶, C. Roda^{126a,126b}, Y. Rodina^{88.ak}, A. Rodriguez Perez¹³, D. Rodriguez Rodriguez¹⁷⁰, S. Roe³², C. S. Rogan⁵⁹, O. Røhne¹²¹, J. Roloff⁵⁹, A. Romaniouk¹⁰⁰, M. Romano^{22a,22b}, S. M. Romano Saez³⁷, E. Romero Adam¹⁷⁰, N. Rompotis¹⁴⁰, M. Ronzani⁵¹, L. Roos⁸³, E. Ros¹⁷⁰, S. Rosati^{134a}, K. Rosbach⁵¹, P. Rose¹³⁹, N.-A. Rosien⁵⁷, V. Rossetti^{148a,148b}, E. Rossi^{106a,106b}, L. P. Rossi^{53a}, J. H. N. Rosten³⁰, R. Rosten¹⁴⁰, M. Rotaru^{28b}, I. Roth¹⁷⁵, J. Rothberg¹⁴⁰, D. Rousseau¹¹⁹, A. Rozanov⁸⁸, Y. Rozen¹⁵⁴, X. Ruan^{147c}, F. Rubbo¹⁴⁵, M. S. Rudolph¹⁶¹, F. Rühr⁵¹, A. Ruiz-Martinez³¹, Z. Rurikova⁵¹, N. A. Rusakovich⁶⁸, A. Ruschke¹⁰², H. L. Russell¹⁴⁰, J. P. Rutherford⁷, N. Ruthmann³², Y. F. Ryabov¹²⁵, M. Rybar¹⁶⁹, G. Rybkin¹¹⁹, S. Ryu⁶, A. Ryzhov¹³², G. F. Rzehorz⁵⁷, A. F. Saavedra¹⁵², G. Sabato¹⁰⁹, S. Sacerdoti²⁹, H.F.-W. Sadrozinski¹³⁹, R. Sadykov⁶⁸, F. Safai Tehrani^{134a}, P. Saha¹¹⁰, M. Sahinsoy^{60a}, M. Saimpert¹³⁸, T. Saito¹⁵⁷, H. Sakamoto¹⁵⁷, Y. Sakurai¹⁷⁴, G. Salamanna^{136a,136b}, A. Salamon^{135a,135b}, J. E. Salazar Loyola^{34b}, D. Salek¹⁰⁹, P. H. Sales De Bruin¹⁴⁰, D. Salihagic¹⁰³, A. Salmikov¹⁴⁵, J. Salt¹⁷⁰, D. Salvatore^{40a,40b}, F. Salvatore¹⁵¹, A. Salvucci^{62a,62b,62c}, A. Salzburger³², D. Sammel⁵¹, D. Sampsonidis¹⁵⁶, J. Sánchez¹⁷⁰, V. Sanchez Martinez¹⁷⁰, A. Sanchez Pineda^{106a,106b}, H. Sandaker¹²¹, R. L. Sandbach⁷⁹, M. Sandhoff¹⁷⁸, C. Sandoval²¹, D. P. C. Sankey¹³³, M. Sannino^{53a,53b}, A. Sansoni⁵⁰, C. Santoni³⁷, R. Santonico^{135a,135b}, H. Santos^{128a}, I. Santoyo Castillo¹⁵¹, K. Sapp¹²⁷, A. Sapronov⁶⁸, J. G. Saraiva^{128a,128d}, B. Sarrazin²³, O. Sasaki⁶⁹, K. Sato¹⁶⁴, E. Sauvan⁵, G. Savage⁸⁰, P. Savard^{161.d}, N. Savic¹⁰³, C. Sawyer¹³³, L. Sawyer^{82.r}, J. Saxon³³, C. Sbarra^{22a}, A. Sbrizzi^{22a,22b}, T. Scanlon⁸¹, D. A. Scannicchio¹⁶⁶, M. Scarcella¹⁵², V. Scarfone^{40a,40b}, J. Schaarschmidt¹⁷⁵, P. Schacht¹⁰³, B. M. Schachtner¹⁰², D. Schaefer³², L. Schaefer¹²⁴, R. Schaefer⁴⁵, J. Schaeffer⁸⁶, S. Schaepe²³, S. Schaezel^{60b}, U. Schäfer⁸⁶, A. C. Schaffer¹¹⁹, D. Schaile¹⁰², R. D. Schamberger¹⁵⁰, V. Scharf^{60a}, V. A. Schegelsky¹²⁵, D. Scheirich¹³¹, M. Schernau¹⁶⁶, C. Schiavi^{53a,53b}, S. Schier¹³⁹, C. Schillo⁵¹, M. Schioppa^{40a,40b}, S. Schlenker³², K. R. Schmidt-Sommerfeld¹⁰³, K. Schmieden³², C. Schmitt⁸⁶, S. Schmitt⁴⁵, S. Schmitz⁸⁶, B. Schneider^{163a}, U. Schnoor⁵¹, L. Schoeffel¹³⁸, A. Schoening^{60b}, B. D. Schoenrock⁹³, E. Schopf²³, M. Schott⁸⁶, J. F. P. Schouwenberg¹⁰⁸, J. Schovancova⁸, S. Schramm⁵², M. Schreyer¹⁷⁷, N. Schuh⁸⁶, A. Schulte⁸⁶, M. J. Schultens²³, H.-C. Schultz-Coulon^{60a}, H. Schulz¹⁷, M. Schumacher⁵¹, B. A. Schumm¹³⁹,

Ph. Schune¹³⁸, A. Schwartzman¹⁴⁵, T. A. Schwarz⁹², H. Schweiger⁸⁷, Ph. Schwemling¹³⁸, R. Schwienhorst⁹³, J. Schwindling¹³⁸, T. Schwindt²³, G. Sciolla²⁵, F. Scuri^{126a,126b}, F. Scutti⁹¹, J. Searcy⁹², P. Seema²³, S. C. Seidel¹⁰⁷, A. Seiden¹³⁹, F. Seifert¹³⁰, J. M. Seixas^{26a}, G. Sekhniaidze^{106a}, K. Sekhon⁹², S. J. Sekula⁴³, D. M. Seliverstov^{125,*}, N. Semprini-Cesari^{22a,22b}, C. Serfon¹²¹, L. Serin¹¹⁹, L. Serkin^{167a,167b}, M. Sessa^{136a,136b}, R. Seuster¹⁷², H. Severini¹¹⁵, T. Sfiligoj⁷⁸, F. Sforza³², A. Sfyrta⁵², E. Shabalina⁵⁷, N. W. Shaikh^{148a,148b}, L. Y. Shan^{35a}, R. Shang¹⁶⁹, J. T. Shank²⁴, M. Shapiro¹⁶, P. B. Shatalov⁹⁹, K. Shaw^{167a,167b}, S. M. Shaw⁸⁷, A. Shcherbakova^{148a,148b}, C. Y. Shehu¹⁵¹, P. Sherwood⁸¹, L. Shi^{153,al}, S. Shimizu⁷⁰, C. O. Shimmin¹⁶⁶, M. Shimojima¹⁰⁴, S. Shirabe⁷³, M. Shiyakova^{68,am}, A. Shmeleva⁹⁸, D. Shoaleh Saadi⁹⁷, M. J. Shochet³³, S. Shojaii^{94a,94b}, D. R. Shope¹¹⁵, S. Shrestha¹¹³, E. Shulga¹⁰⁰, M. A. Shupe⁷, P. Sicho¹²⁹, A. M. Sickles¹⁶⁹, P. E. Sidebo¹⁴⁹, E. Sideras Haddad^{147c}, O. Sidiropoulou¹⁷⁷, D. Sidorov¹¹⁶, A. Sidoti^{22a,22b}, F. Siegert⁴⁷, Dj. Sijacki¹⁴, J. Silva^{128a,128d}, S. B. Silverstein^{148a}, V. Simak¹³⁰, Lj. Simic¹⁴, S. Simion¹¹⁹, E. Simioni⁸⁶, B. Simmons⁸¹, D. Simon³⁷, M. Simon⁸⁶, P. Sinervo¹⁶¹, N. B. Sinev¹¹⁸, M. Sioli^{22a,22b}, G. Siragusa¹⁷⁷, S. Yu. Sivoklov¹⁰¹, J. Sjölin^{148a,148b}, M. B. Skinner⁷⁵, H. P. Skottowe⁵⁹, P. Skubic¹¹⁵, M. Slater¹⁹, T. Slavicek¹³⁰, M. Slawinska¹⁰⁹, K. Sliwa¹⁶⁵, R. Slovak¹³¹, V. Smakhtin¹⁷⁵, B. H. Smart⁵, L. Smestad¹⁵, J. Smiesko^{146a}, S. Yu. Smirnov¹⁰⁰, Y. Smirnov¹⁰⁰, L. N. Smirnova^{101,an}, O. Smirnova⁸⁴, J. W. Smith⁵⁷, M. N. K. Smith³⁸, R. W. Smith³⁸, M. Smizanska⁷⁵, K. Smolek¹³⁰, A. A. Snesarev⁹⁸, I. M. Snyder¹¹⁸, S. Snyder²⁷, R. Sobie^{172,m}, F. Socher⁴⁷, A. Soffer¹⁵⁵, D. A. Soh¹⁵³, G. Sokhranni⁷⁸, C. A. Solans Sanchez³², M. Solar¹³⁰, E. Yu. Soldatov¹⁰⁰, U. Soldevila¹⁷⁰, A. A. Solodkov¹³², A. Soloshenko⁶⁸, O. V. Solovyanov¹³², V. Solovyev¹²⁵, P. Sommer⁵¹, H. Son¹⁶⁵, H. Y. Song^{36a,ao}, A. Sood¹⁶, A. Sopczak¹³⁰, V. Sopko¹³⁰, V. Sorin¹³, D. Sosa^{60b}, C. L. Sotiropoulou^{126a,126b}, R. Soualah^{167a,167c}, A. M. Soukharev^{111,c}, D. South⁴⁵, B. C. Sowden⁸⁰, S. Spagnolo^{76a,76b}, M. Spalla^{126a,126b}, M. Spangenberg¹⁷³, F. Spanò⁸⁰, D. Sperlich¹⁷, F. Spettel¹⁰³, R. Spighi^{22a}, G. Spigo³², L. A. Spiller⁹¹, M. Spousta¹³¹, R. D. St. Denis^{56,*}, A. Stabile^{94a}, R. Stamen^{60a}, S. Stamm¹⁷, E. Stanecka⁴², R. W. Stanek⁶, C. Stanescu^{136a}, M. Stanescu-Bellu⁴⁵, M. M. Stanitzki⁴⁵, S. Stapnes¹²¹, E. A. Starchenko¹³², G. H. Stark³³, J. Stark⁵⁸, P. Staroba¹²⁹, P. Starovoitov^{60a}, S. Stärz³², R. Staszewski⁴², P. Steinberg²⁷, B. Stelzer¹⁴⁴, H. J. Stelzer³², O. Stelzer-Chilton^{163a}, H. Stenzel⁵⁵, G. A. Stewart⁵⁶, J. A. Stillings²³, M. C. Stockton⁹⁰, M. Stoebe⁹⁰, G. Stoicea^{28b}, P. Stolte⁵⁷, S. Stonjek¹⁰³, A. R. Stradling⁸, A. Straessner⁴⁷, M. E. Stramaglia¹⁸, J. Strandberg¹⁴⁹, S. Strandberg^{148a,148b}, A. Strandlie¹²¹, M. Strauss¹¹⁵, P. Strizenc^{146b}, R. Ströhmer¹⁷⁷, D. M. Strom¹¹⁸, R. Stroynowski⁴³, A. Strubig¹⁰⁸, S. A. Stucci²⁷, B. Stugu¹⁵, N. A. Styles⁴⁵, D. Su¹⁴⁵, J. Su¹²⁷, S. Suchek^{60a}, Y. Sugaya¹²⁰, M. Suk¹³⁰, V. V. Sulim⁹⁸, S. Sultansoy^{4c}, T. Sumida⁷¹, S. Sun⁵⁹, X. Sun^{35a}, J. E. Sundermann⁵¹, K. Suruliz¹⁵¹, C. J. E. Suster¹⁵², M. R. Sutton¹⁵¹, S. Suzuki⁶⁹, M. Svatos¹²⁹, M. Swiatlowski³³, S. P. Swift², I. Sykora^{146a}, T. Sykora¹³¹, D. Ta⁵¹, C. Taccini^{136a,136b}, K. Tackmann⁴⁵, J. Taenzer¹⁵⁵, A. Taffard¹⁶⁶, R. Tafirout^{163a}, N. Taiblum¹⁵⁵, H. Takai²⁷, R. Takashima⁷², T. Takeshita¹⁴², Y. Takubo⁶⁹, M. Talby⁸⁸, A. A. Talyshev^{111,c}, K. G. Tan⁹¹, J. Tanaka¹⁵⁷, M. Tanaka¹⁵⁹, R. Tanaka¹¹⁹, S. Tanaka⁶⁹, R. Tanioka⁷⁰, B. B. Tannenwald¹¹³, S. Tapia Araya^{34b}, S. Tapprogge⁸⁶, S. Tarem¹⁵⁴, G. F. Tartarelli^{94a}, P. Tas¹³¹, M. Tasevsky¹²⁹, T. Tashiro⁷¹, E. Tassi^{40a,40b}, A. Tavares Delgado^{128a,128b}, Y. Tayalati^{137e}, A. C. Taylor¹⁰⁷, G. N. Taylor⁹¹, P. T. E. Taylor⁹¹, W. Taylor^{163b}, F. A. Teischinger³², P. Teixeira-Dias⁸⁰, K. K. Temming⁵¹, D. Temple¹⁴⁴, H. Ten Kate³², P. K. Teng¹⁵³, J. J. Teoh¹²⁰, F. Tepel¹⁷⁸, S. Terada⁶⁹, K. Terashi¹⁵⁷, J. Terron⁸⁵, S. Terzo¹³, M. Testa⁵⁰, R. J. Teuscher^{161,m}, T. Theveneaux-Pelzer⁸⁸, J. P. Thomas¹⁹, J. Thomas-Wilsker⁸⁰, P. D. Thompson¹⁹, A. S. Thompson⁵⁶, L. A. Thomsen¹⁷⁹, E. Thomson¹²⁴, M. J. Tibbetts¹⁶, R. E. Ticse Torres⁸⁸, V. O. Tikhomirov^{98,ap}, Yu. A. Tikhonov^{111,c}, S. Timoshenko¹⁰⁰, P. Tipton¹⁷⁹, S. Tisserant⁸⁸, K. Todome¹⁵⁹, T. Todorov^{5,*}, S. Todorova-Nova¹³¹, J. Tojo⁷³, S. Tokár^{146a}, K. Tokushuku⁶⁹, E. Tolley⁵⁹, L. Tomlinson⁸⁷, M. Tomoto¹⁰⁵, L. Tompkins^{145,aq}, K. Toms¹⁰⁷, B. Tong⁵⁹, P. Tornambe⁵¹, E. Torrence¹¹⁸, H. Torres¹⁴⁴, E. Torrón Pastor¹⁴⁰, J. Toth^{88,ar}, F. Touchard⁸⁸, D. R. Tovey¹⁴¹, T. Trefzger¹⁷⁷, A. Tricoli²⁷, I. M. Trigger^{163a}, S. Trincaz-Duvoid⁸³, M. F. Tripiana¹³, W. Trischuk¹⁶¹, B. Trocme⁵⁸, A. Trofymov⁴⁵, C. Troncon^{94a}, M. Trotter-McDonald¹⁶, M. Trovatelli¹⁷², L. Truong^{167a,167c}, M. Trzebinski⁴², A. Trzupek⁴², J.C.-L. Tseng¹²², P. V. Tsiarshka⁹⁵, G. Tsipolitis¹⁰, N. Tsirintanis⁹, S. Tsiskaridze¹³, V. Tsiskaridze⁵¹, E. G. Tskhadadze^{54a}, K. M. Tsui^{62a}, I. I. Tsukerman⁹⁹, V. Tsulaia¹⁶, S. Tsuno⁶⁹, D. Tsybychev¹⁵⁰, Y. Tu^{62b}, A. Tudorache^{28b}, V. Tudorache^{28b}, T. T. Tulbure^{28a}, A. N. Tuna⁵⁹, S. A. Tupputi^{22a,22b}, S. Turchikhin⁶⁸, D. Turgeman¹⁷⁵, I. Turk Cakir^{4b,as}, R. Turra^{94a,94b}, P. M. Tuts³⁸, G. Ucchielli^{22a,22b}, I. Ueda¹⁵⁷, M. Ughetto^{148a,148b}, F. Ukegawa¹⁶⁴, G. Unal³², A. Undrus²⁷, G. Unel¹⁶⁶, F. C. Ungaro⁹¹, Y. Unno⁶⁹, C. Unverdorben¹⁰², J. Urban^{146b}, P. Urquijo⁹¹, P. Urrejola⁸⁶, G. Usai⁸, J. Usui⁶⁹, L. Vacavant⁸⁸, V. Vacek¹³⁰, B. Vachon⁹⁰, C. Valderanis¹⁰², E. Valdes Santurio^{148a,148b}, N. Valencic¹⁰⁹, S. Valentini^{22a,22b}, A. Valero¹⁷⁰, L. Valery¹³, S. Valkar¹³¹, J. A. Valls Ferrer¹⁷⁰, W. Van Den Wollenberg¹⁰⁹, P. C. Van Der Deijl¹⁰⁹, H. van der Graaf¹⁰⁹, N. van Eldik¹⁵⁴, P. van Gemmeren⁶, J. Van Nieuwkoop¹⁴⁴, I. van Vulpen¹⁰⁹, M. C. van Woerden¹⁰⁹, M. Vanadia^{134a,134b}, W. Vandelli³², R. Vanguri¹²⁴, A. Vaniachine¹⁶⁰, P. Vankov¹⁰⁹, G. Vardanyan¹⁸⁰, R. Vari^{134a}, E. W. Varnes⁷, T. Varol⁴³, D. Varouchas⁸³, A. Vartapetian⁸, K. E. Varvell¹⁵², J. G. Vasquez¹⁷⁹, G. A. Vasquez^{34b}, F. Vazeille³⁷, T. Vazquez Schroeder⁹⁰, J. Veatch⁵⁷, V. Veeraraghavan⁷, L. M. Veloce¹⁶¹, F. Veloso^{128a,128c}, S. Veneziano^{134a}, A. Ventura^{76a,76b}, M. Venturi¹⁷², N. Venturi¹⁶¹, A. Venturini²⁵, V. Vercesi^{123a}, M. Verducci^{134a,134b}, W. Verkerke¹⁰⁹, J. C. Vermeulen¹⁰⁹, A. Vest^{47,at}

M. C. Vetterli^{144,d}, O. Viazzo⁸⁴, I. Vichou^{169,*}, T. Vickey¹⁴¹, O. E. Vickey Boeriu¹⁴¹, G. H. A. Viehhauser¹²², S. Viel¹⁶, L. Vigani¹²², M. Villa^{22a,22b}, M. Villaplana Perez^{94a,94b}, E. Vilucchi⁵⁰, M. G. Vinciter³¹, V. B. Vinogradov⁶⁸, C. Vittori^{22a,22b}, I. Vivarelli¹⁵¹, S. Vlachos¹⁰, M. Vlasak¹³⁰, M. Vogel¹⁷⁸, P. Vokac¹³⁰, G. Volpi^{126a,126b}, M. Volpi⁹¹, H. von der Schmitt¹⁰³, E. von Toerne²³, V. Vorobel¹³¹, K. Vorobev¹⁰⁰, M. Vos¹⁷⁰, R. Voss³², J. H. Vossebeld⁷⁷, N. Vranjes¹⁴, M. Vranjes Milosavljevic¹⁴, V. Vrba¹²⁹, M. Vreeswijk¹⁰⁹, R. Vuillermet³², I. Vukotic³³, P. Wagner²³, W. Wagner¹⁷⁸, H. Wahlberg⁷⁴, S. Wahrenmund⁴⁷, J. Wakabayashi¹⁰⁵, J. Walder⁷⁵, R. Walker¹⁰², W. Walkowiak¹⁴³, V. Wallangen^{148a,148b}, C. Wang^{35b}, C. Wang^{36b,88}, F. Wang¹⁷⁶, H. Wang¹⁶, H. Wang⁴³, J. Wang⁴⁵, J. Wang¹⁵², K. Wang⁹⁰, R. Wang⁶, S. M. Wang¹⁵³, T. Wang³⁸, W. Wang^{36a}, C. Wanotayaroj¹¹⁸, A. Warburton⁹⁰, C. P. Ward³⁰, D. R. Wardrope⁸¹, A. Washbrook⁴⁹, P. M. Watkins¹⁹, A. T. Watson¹⁹, M. F. Watson¹⁹, G. Watts¹⁴⁰, S. Watts⁸⁷, B. M. Waugh⁸¹, S. Webb⁸⁶, M. S. Weber¹⁸, S. W. Weber¹⁷⁷, S. A. Weber³¹, J. S. Webster⁶, A. R. Weidberg¹²², B. Weinert⁶⁴, J. Weingarten⁵⁷, C. Weiser⁵¹, H. Weits¹⁰⁹, P. S. Wells³², T. Wenaus²⁷, T. Wengler³², S. Wenig³², N. Wermes²³, M. D. Werner⁶⁷, P. Werner³², M. Wessels^{60a}, J. Wetter¹⁶⁵, K. Whalen¹¹⁸, N. L. Whallon¹⁴⁰, A. M. Wharton⁷⁵, A. White⁸, M. J. White¹, R. White^{34b}, D. Whiteson¹⁶⁶, F. J. Wickens¹³³, W. Wiedenmann¹⁷⁶, M. Wielers¹³³, C. Wigglesworth³⁹, L. A. M. Wiik-Fuchs²³, A. Wildauer¹⁰³, F. Wilk⁸⁷, H. G. Wilkens³², H. H. Williams¹²⁴, S. Williams¹⁰⁹, C. Willis⁹³, S. Willocq⁸⁹, J. A. Wilson¹⁹, I. Wingerter-Seez⁵, F. Winklmeier¹¹⁸, O. J. Winston¹⁵¹, B. T. Winter²³, M. Wittgen¹⁴⁵, T. M. H. Wolf¹⁰⁹, R. Wolff⁸⁸, M. W. Wolter⁴², H. Wolters^{128a,128c}, S. D. Worm¹³³, B. K. Wosiek⁴², J. Wotschack³², M. J. Woudstra⁸⁷, K. W. Wozniak⁴², M. Wu⁵⁸, M. Wu³³, S. L. Wu¹⁷⁶, X. Wu⁵², Y. Wu⁹², T. R. Wyatt⁸⁷, B. M. Wynne⁴⁹, S. Xella³⁹, Z. Xi⁹², D. Xu^{35a}, L. Xu²⁷, B. Yabsley¹⁵², S. Yacoob^{147a}, D. Yamaguchi¹⁵⁹, Y. Yamaguchi¹²⁰, A. Yamamoto⁶⁹, S. Yamamoto¹⁵⁷, T. Yamanaka¹⁵⁷, K. Yamauchi¹⁰⁵, Y. Yamazaki⁷⁰, Z. Yan²⁴, H. Yang^{36c}, H. Yang¹⁷⁶, Y. Yang¹⁵³, Z. Yang¹⁵, W-M. Yao¹⁶, Y. C. Yap⁸³, Y. Yasu⁶⁹, E. Yatsenko⁵, K. H. Yau Wong²³, J. Ye⁴³, S. Ye²⁷, I. Yeletsikh⁶⁸, E. Yildirim⁸⁶, K. Yorita¹⁷⁴, R. Yoshida⁶, K. Yoshihara¹²⁴, C. Young¹⁴⁵, C. J. S. Young³², S. Youssef²⁴, D. R. Yu¹⁶, J. Yu⁸, J. M. Yu⁹², J. Yu⁶⁷, L. Yuan⁷⁰, S. P. Y. Yuen²³, I. Yusufović^{30,au}, B. Zabinski⁴², R. Zaidan⁶⁶, A. M. Zaitsev^{132,ae}, N. Zakharchuk⁴⁵, J. Zalieckas¹⁵, A. Zaman¹⁵⁰, S. Zambito⁵⁹, L. Zanello^{134a,134b}, D. Zanzi⁹¹, C. Zeitnitz¹⁷⁸, M. Zeman¹³⁰, A. Zemla^{41a}, J. C. Zeng¹⁶⁹, Q. Zeng¹⁴⁵, O. Zenin¹³², T. Ženiš^{146a}, D. Zerwas¹¹⁹, D. Zhang⁹², F. Zhang¹⁷⁶, G. Zhang^{36a,ao}, H. Zhang^{35b}, J. Zhang⁶, L. Zhang⁵¹, L. Zhang^{36a}, M. Zhang¹⁶⁹, R. Zhang²³, R. Zhang^{36a,av}, X. Zhang^{36b}, Z. Zhang¹¹⁹, X. Zhao⁴³, Y. Zhao^{36b}, Z. Zhao^{36a}, A. Zhemchugov⁶⁸, J. Zhong¹²², B. Zhou⁹², C. Zhou¹⁷⁶, L. Zhou³⁸, L. Zhou⁴³, M. Zhou¹⁵⁰, N. Zhou^{35c}, C. G. Zhu^{36b}, H. Zhu^{35a}, J. Zhu⁹², Y. Zhu^{36a}, X. Zhuang^{35a}, K. Zhukov⁹⁸, A. Zibell¹⁷⁷, D. Zieminska⁶⁴, N. I. Zimine⁶⁸, C. Zimmermann⁸⁶, S. Zimmermann⁵¹, Z. Zinonos⁵⁷, M. Zinser⁸⁶, M. Ziolkowski¹⁴³, L. Živković¹⁴, G. Zobernig¹⁷⁶, A. Zoccoli^{22a,22b}, M. zur Nedden¹⁷, L. Zwalinski³²

¹ Department of Physics, University of Adelaide, Adelaide, SA, Australia

² Physics Department, SUNY Albany, Albany, NY, USA

³ Department of Physics, University of Alberta, Edmonton, AB, Canada

⁴ (a) Department of Physics, Ankara University, Ankara, Turkey; (b) Istanbul Aydin University, Istanbul, Turkey; (c) Division of Physics, TOBB University of Economics and Technology, Ankara, Turkey

⁵ LAPP, CNRS/IN2P3 and Université Savoie Mont Blanc, Annecy-le-Vieux, France

⁶ High Energy Physics Division, Argonne National Laboratory, Argonne, IL, USA

⁷ Department of Physics, University of Arizona, Tucson, AZ, USA

⁸ Department of Physics, The University of Texas at Arlington, Arlington, TX, USA

⁹ Physics Department, University of Athens, Athens, Greece

¹⁰ Physics Department, National Technical University of Athens, Zografou, Greece

¹¹ Department of Physics, The University of Texas at Austin, Austin, TX, USA

¹² Institute of Physics, Azerbaijan Academy of Sciences, Baku, Azerbaijan

¹³ Institut de Física d'Altes Energies (IFAE), The Barcelona Institute of Science and Technology, Barcelona, Spain

¹⁴ Institute of Physics, University of Belgrade, Belgrade, Serbia

¹⁵ Department for Physics and Technology, University of Bergen, Bergen, Norway

¹⁶ Physics Division, Lawrence Berkeley National Laboratory and University of California, Berkeley, CA, USA

¹⁷ Department of Physics, Humboldt University, Berlin, Germany

¹⁸ Albert Einstein Center for Fundamental Physics and Laboratory for High Energy Physics, University of Bern, Bern, Switzerland

¹⁹ School of Physics and Astronomy, University of Birmingham, Birmingham, UK

- 20 (a)Department of Physics, Bogazici University, Istanbul, Turkey; (b)Department of Physics Engineering, Gaziantep University, Gaziantep, Turkey; (c)Istanbul Bilgi University, Faculty of Engineering and Natural Sciences, Istanbul, Turkey; (d)Bahcesehir University, Faculty of Engineering and Natural Sciences, Istanbul, Turkey
- 21 Centro de Investigaciones, Universidad Antonio Narino, Bogota, Colombia
- 22 (a)INFN Sezione di Bologna, Bologna, Italy; (b)Dipartimento di Fisica e Astronomia, Università di Bologna, Bologna, Italy
- 23 Physikalisches Institut, University of Bonn, Bonn, Germany
- 24 Department of Physics, Boston University, Boston, MA, USA
- 25 Department of Physics, Brandeis University, Waltham, MA, USA
- 26 (a)Universidade Federal do Rio De Janeiro COPPE/EE/IF, Rio de Janeiro, Brazil; (b)Electrical Circuits Department, Federal University of Juiz de Fora (UFJF), Juiz de Fora, Brazil; (c)Federal University of Sao Joao del Rei (UFSJ), Sao Joao del Rei, Brazil; (d)Instituto de Fisica, Universidade de Sao Paulo, Sao Paulo, Brazil
- 27 Physics Department, Brookhaven National Laboratory, Upton, NY, USA
- 28 (a)Transilvania University of Brasov, Brasov, Romania; (b)National Institute of Physics and Nuclear Engineering, Bucharest, Romania; (c)Physics Department, National Institute for Research and Development of Isotopic and Molecular Technologies, Cluj Napoca, Romania; (d)University Politehnica Bucharest, Bucharest, Romania; (e)West University in Timisoara, Timisoara, Romania
- 29 Departamento de Física, Universidad de Buenos Aires, Buenos Aires, Argentina
- 30 Cavendish Laboratory, University of Cambridge, Cambridge, UK
- 31 Department of Physics, Carleton University, Ottawa, ON, Canada
- 32 CERN, Geneva, Switzerland
- 33 Enrico Fermi Institute, University of Chicago, Chicago, IL, USA
- 34 (a)Departamento de Física, Pontificia Universidad Católica de Chile, Santiago, Chile; (b)Departamento de Física, Universidad Técnica Federico Santa María, Valparaiso, Chile
- 35 (a)Institute of High Energy Physics, Chinese Academy of Sciences, Beijing, China; (b)Department of Physics, Nanjing University, Jiangsu, China; (c)Physics Department, Tsinghua University, Beijing 100084, China
- 36 (a)Department of Modern Physics, University of Science and Technology of China, Anhui, China; (b)School of Physics, Shandong University, Shandong, China; (c)Department of Physics and Astronomy, Shanghai Key Laboratory for Particle Physics and Cosmology, Shanghai Jiao Tong University (also affiliated with PKU-CHEP), Shanghai, China
- 37 Laboratoire de Physique Corpusculaire, Université Clermont Auvergne Université Blaise Pascal, CNRS/IN2P3, Clermont-Ferrand, France
- 38 Nevis Laboratory, Columbia University, Irvington, NY, USA
- 39 Niels Bohr Institute, University of Copenhagen, Kobenhavn, Denmark
- 40 (a)Laboratori Nazionali di Frascati, INFN Gruppo Collegato di Cosenza, Frascati, Italy; (b)Dipartimento di Fisica, Università della Calabria, Rende, Italy
- 41 (a)Faculty of Physics and Applied Computer Science, AGH University of Science and Technology, Krakow, Poland; (b)Marian Smoluchowski Institute of Physics, Jagiellonian University, Kraków, Poland
- 42 Institute of Nuclear Physics, Polish Academy of Sciences, Kraków, Poland
- 43 Physics Department, Southern Methodist University, Dallas, TX, USA
- 44 Physics Department, University of Texas at Dallas, Richardson, TX, USA
- 45 DESY, Hamburg and Zeuthen, Germany
- 46 Lehrstuhl für Experimentelle Physik IV, Technische Universität Dortmund, Dortmund, Germany
- 47 Institut für Kern-und Teilchenphysik, Technische Universität Dresden, Dresden, Germany
- 48 Department of Physics, Duke University, Durham, NC, USA
- 49 SUPA-School of Physics and Astronomy, University of Edinburgh, Edinburgh, UK
- 50 INFN Laboratori Nazionali di Frascati, Frascati, Italy
- 51 Fakultät für Mathematik und Physik, Albert-Ludwigs-Universität, Freiburg, Germany
- 52 Section de Physique, Université de Genève, Geneva, Switzerland
- 53 (a)INFN Sezione di Genova, Genoa, Italy; (b)Dipartimento di Fisica, Università di Genova, Genoa, Italy
- 54 (a)E. Andronikashvili Institute of Physics, Iv. Javakhishvili Tbilisi State University, Tbilisi, Georgia; (b)High Energy Physics Institute, Tbilisi State University, Tbilisi, Georgia
- 55 II Physikalisches Institut, Justus-Liebig-Universität Giessen, Giessen, Germany
- 56 SUPA-School of Physics and Astronomy, University of Glasgow, Glasgow, UK

- 57 II Physikalisches Institut, Georg-August-Universität, Göttingen, Germany
- 58 Laboratoire de Physique Subatomique et de Cosmologie, Université Grenoble-Alpes, CNRS/IN2P3, Grenoble, France
- 59 Laboratory for Particle Physics and Cosmology, Harvard University, Cambridge, MA, USA
- 60 ^(a)Kirchhoff-Institut für Physik, Ruprecht-Karls-Universität Heidelberg, Heidelberg, Germany; ^(b)Physikalisches Institut, Ruprecht-Karls-Universität Heidelberg, Heidelberg, Germany; ^(c)ZITI Institut für technische Informatik, Ruprecht-Karls-Universität Heidelberg, Mannheim, Germany
- 61 Faculty of Applied Information Science, Hiroshima Institute of Technology, Hiroshima, Japan
- 62 ^(a)Department of Physics, The Chinese University of Hong Kong, Shatin, NT, Hong Kong; ^(b)Department of Physics, The University of Hong Kong, Hong Kong, China; ^(c)Department of Physics and Institute for Advanced Study, The Hong Kong University of Science and Technology, Clear Water Bay, Kowloon, Hong Kong, China
- 63 Department of Physics, National Tsing Hua University, Taiwan, Taiwan
- 64 Department of Physics, Indiana University, Bloomington, IN, USA
- 65 Institut für Astro- und Teilchenphysik, Leopold-Franzens-Universität, Innsbruck, Austria
- 66 University of Iowa, Iowa City, IA, USA
- 67 Department of Physics and Astronomy, Iowa State University, Ames, IA, USA
- 68 Joint Institute for Nuclear Research, JINR Dubna, Dubna, Russia
- 69 KEK, High Energy Accelerator Research Organization, Tsukuba, Japan
- 70 Graduate School of Science, Kobe University, Kobe, Japan
- 71 Faculty of Science, Kyoto University, Kyoto, Japan
- 72 Kyoto University of Education, Kyoto, Japan
- 73 Department of Physics, Kyushu University, Fukuoka, Japan
- 74 Instituto de Física La Plata, Universidad Nacional de La Plata and CONICET, La Plata, Argentina
- 75 Physics Department, Lancaster University, Lancaster, UK
- 76 ^(a)INFN Sezione di Lecce, Lecce, Italy; ^(b)Dipartimento di Matematica e Fisica, Università del Salento, Lecce, Italy
- 77 Oliver Lodge Laboratory, University of Liverpool, Liverpool, UK
- 78 Department of Physics, Jožef Stefan Institute, University of Ljubljana, Ljubljana, Slovenia
- 79 School of Physics and Astronomy, Queen Mary University of London, London, UK
- 80 Department of Physics, Royal Holloway University of London, Surrey, UK
- 81 Department of Physics and Astronomy, University College London, London, UK
- 82 Louisiana Tech University, Ruston, LA, USA
- 83 Laboratoire de Physique Nucléaire et de Hautes Energies, UPMC and Université Paris-Diderot and CNRS/IN2P3, Paris, France
- 84 Fysiska institutionen, Lunds universitet, Lund, Sweden
- 85 Departamento de Física Teórica C-15, Universidad Autónoma de Madrid, Madrid, Spain
- 86 Institut für Physik, Universität Mainz, Mainz, Germany
- 87 School of Physics and Astronomy, University of Manchester, Manchester, UK
- 88 CPPM, Aix-Marseille Université and CNRS/IN2P3, Marseille, France
- 89 Department of Physics, University of Massachusetts, Amherst, MA, USA
- 90 Department of Physics, McGill University, Montreal, QC, Canada
- 91 School of Physics, University of Melbourne, Melbourne, VIC, Australia
- 92 Department of Physics, The University of Michigan, Ann Arbor, MI, USA
- 93 Department of Physics and Astronomy, Michigan State University, East Lansing, MI, USA
- 94 ^(a)INFN Sezione di Milano, Milano, Italy; ^(b)Dipartimento di Fisica, Università di Milano, Milano, Italy
- 95 B.I. Stepanov Institute of Physics, National Academy of Sciences of Belarus, Minsk, Republic of Belarus
- 96 National Scientific and Educational Centre for Particle and High Energy Physics, Minsk, Republic of Belarus
- 97 Group of Particle Physics, University of Montreal, Montreal, QC, Canada
- 98 P.N. Lebedev Physical Institute of the Russian Academy of Sciences, Moscow, Russia
- 99 Institute for Theoretical and Experimental Physics (ITEP), Moscow, Russia
- 100 National Research Nuclear University MEPhI, Moscow, Russia
- 101 D.V. Skobel'syn Institute of Nuclear Physics, M.V. Lomonosov Moscow State University, Moscow, Russia
- 102 Fakultät für Physik, Ludwig-Maximilians-Universität München, München, Germany
- 103 Max-Planck-Institut für Physik (Werner-Heisenberg-Institut), München, Germany
- 104 Nagasaki Institute of Applied Science, Nagasaki, Japan

- 105 Graduate School of Science and Kobayashi-Maskawa Institute, Nagoya University, Nagoya, Japan
106 (a)INFN Sezione di Napoli, Napoli, Italy; (b)Dipartimento di Fisica, Università di Napoli, Napoli, Italy
107 Department of Physics and Astronomy, University of New Mexico, Albuquerque, NM, USA
108 Institute for Mathematics, Astrophysics and Particle Physics, Radboud University Nijmegen/Nikhef, Nijmegen, The Netherlands
109 Nikhef National Institute for Subatomic Physics and University of Amsterdam, Amsterdam, The Netherlands
110 Department of Physics, Northern Illinois University, DeKalb, IL, USA
111 Budker Institute of Nuclear Physics, SB RAS, Novosibirsk, Russia
112 Department of Physics, New York University, New York, NY, USA
113 Ohio State University, Columbus, OH, USA
114 Faculty of Science, Okayama University, Okayama, Japan
115 Homer L. Dodge Department of Physics and Astronomy, University of Oklahoma, Norman, OK, USA
116 Department of Physics, Oklahoma State University, Stillwater, OK, USA
117 Palacký University, RCPTM, Olomouc, Czech Republic
118 Center for High Energy Physics, University of Oregon, Eugene, OR, USA
119 LAL, Univ. Paris-Sud, CNRS/IN2P3, Université Paris-Saclay, Orsay, France
120 Graduate School of Science, Osaka University, Osaka, Japan
121 Department of Physics, University of Oslo, Oslo, Norway
122 Department of Physics, Oxford University, Oxford, UK
123 (a)INFN Sezione di Pavia, Pavia, Italy; (b)Dipartimento di Fisica, Università di Pavia, Pavia, Italy
124 Department of Physics, University of Pennsylvania, Philadelphia, PA, USA
125 National Research Centre “Kurchatov Institute” B.P.Konstantinov Petersburg Nuclear Physics Institute, St. Petersburg, Russia
126 (a)INFN Sezione di Pisa, Pisa, Italy; (b)Dipartimento di Fisica E. Fermi, Università di Pisa, Pisa, Italy
127 Department of Physics and Astronomy, University of Pittsburgh, Pittsburgh, PA, USA
128 (a)Laboratório de Instrumentação e Física Experimental de Partículas-LIP, Lisboa, Portugal; (b)Faculdade de Ciências, Universidade de Lisboa, Lisboa, Portugal; (c)Department of Physics, University of Coimbra, Coimbra, Portugal; (d)Centro de Física Nuclear da Universidade de Lisboa, Lisboa, Portugal; (e)Departamento de Física, Universidade do Minho, Braga, Portugal; (f)Departamento de Física Teórica y del Cosmos and CAFPE, Universidad de Granada, Granada, Spain; (g)Dep Física and CEFITEC of Faculdade de Ciências e Tecnologia, Universidade Nova de Lisboa, Caparica, Portugal
129 Institute of Physics, Academy of Sciences of the Czech Republic, Praha, Czech Republic
130 Czech Technical University in Prague, Praha, Czech Republic
131 Faculty of Mathematics and Physics, Charles University in Prague, Praha, Czech Republic
132 State Research Center Institute for High Energy Physics (Protvino), NRC KI, Protvino, Russia
133 Particle Physics Department, Rutherford Appleton Laboratory, Didcot, UK
134 (a)INFN Sezione di Roma, Roma, Italy; (b)Dipartimento di Fisica, Sapienza Università di Roma, Roma, Italy
135 (a)INFN Sezione di Roma Tor Vergata, Roma, Italy; (b)Dipartimento di Fisica, Università di Roma Tor Vergata, Roma, Italy
136 (a)INFN Sezione di Roma Tre, Roma, Italy; (b)Dipartimento di Matematica e Fisica, Università Roma Tre, Roma, Italy
137 (a)Faculté des Sciences Ain Chock, Réseau Universitaire de Physique des Hautes Energies-Université Hassan II, Casablanca, Morocco; (b)Centre National de l’Energie des Sciences Techniques Nucleaires, Rabat, Morocco; (c)Faculté des Sciences Semlalia, Université Cadi Ayyad, LPHEA-Marrakech, Marrakech, Morocco; (d)Faculté des Sciences, Université Mohamed Premier and LTPM, Oujda, Morocco; (e)Faculté des Sciences, Université Mohammed V, Rabat, Morocco
138 DSM/IRFU (Institut de Recherches sur les Lois Fondamentales de l’Univers), CEA Saclay (Commissariat à l’Energie Atomique et aux Energies Alternatives), Gif-sur-Yvette, France
139 Santa Cruz Institute for Particle Physics, University of California Santa Cruz, Santa Cruz, CA, USA
140 Department of Physics, University of Washington, Seattle, WA, USA
141 Department of Physics and Astronomy, University of Sheffield, Sheffield, UK
142 Department of Physics, Shinshu University, Nagano, Japan
143 Fachbereich Physik, Universität Siegen, Siegen, Germany
144 Department of Physics, Simon Fraser University, Burnaby, BC, Canada

- 145 SLAC National Accelerator Laboratory, Stanford, CA, USA
- 146 ^(a)Faculty of Mathematics, Physics and Informatics, Comenius University, Bratislava, Slovak Republic; ^(b)Department of Subnuclear Physics, Institute of Experimental Physics of the Slovak Academy of Sciences, Kosice, Slovak Republic
- 147 ^(a)Department of Physics, University of Cape Town, Cape Town, South Africa; ^(b)Department of Physics, University of Johannesburg, Johannesburg, South Africa; ^(c)School of Physics, University of the Witwatersrand, Johannesburg, South Africa
- 148 ^(a)Department of Physics, Stockholm University, Stockholm, Sweden; ^(b)The Oskar Klein Centre, Stockholm, Sweden
- 149 Physics Department, Royal Institute of Technology, Stockholm, Sweden
- 150 Departments of Physics and Astronomy and Chemistry, Stony Brook University, Stony Brook, NY, USA
- 151 Department of Physics and Astronomy, University of Sussex, Brighton, UK
- 152 School of Physics, University of Sydney, Sydney, Australia
- 153 Institute of Physics, Academia Sinica, Taipei, Taiwan
- 154 Department of Physics, Technion: Israel Institute of Technology, Haifa, Israel
- 155 Raymond and Beverly Sackler School of Physics and Astronomy, Tel Aviv University, Tel Aviv, Israel
- 156 Department of Physics, Aristotle University of Thessaloniki, Thessaloniki, Greece
- 157 International Center for Elementary Particle Physics and Department of Physics, The University of Tokyo, Tokyo, Japan
- 158 Graduate School of Science and Technology, Tokyo Metropolitan University, Tokyo, Japan
- 159 Department of Physics, Tokyo Institute of Technology, Tokyo, Japan
- 160 Tomsk State University, Tomsk, Russia, Russia
- 161 Department of Physics, University of Toronto, Toronto, ON, Canada
- 162 ^(a)INFN-TIFPA, Trento, Italy, Italy; ^(b)University of Trento, Trento, Italy, Italy
- 163 ^(a)TRIUMF, Vancouver, BC, Canada; ^(b)Department of Physics and Astronomy, York University, Toronto, ON, Canada
- 164 Faculty of Pure and Applied Sciences, and Center for Integrated Research in Fundamental Science and Engineering, University of Tsukuba, Tsukuba, Japan
- 165 Department of Physics and Astronomy, Tufts University, Medford, MA, USA
- 166 Department of Physics and Astronomy, University of California Irvine, Irvine, CA, USA
- 167 ^(a)INFN Gruppo Collegato di Udine, Sezione di Trieste, Udine, Italy; ^(b)ICTP, Trieste, Italy; ^(c)Dipartimento di Chimica Fisica e Ambiente, Università di Udine, Udine, Italy
- 168 Department of Physics and Astronomy, University of Uppsala, Uppsala, Sweden
- 169 Department of Physics, University of Illinois, Urbana, IL, USA
- 170 Instituto de Física Corpuscular (IFIC) and Departamento de Física Atomica, Molecular y Nuclear and Departamento de Ingeniería Electrónica and Instituto de Microelectrónica de Barcelona (IMB-CNM), University of Valencia and CSIC, Valencia, Spain
- 171 Department of Physics, University of British Columbia, Vancouver, BC, Canada
- 172 Department of Physics and Astronomy, University of Victoria, Victoria, BC, Canada
- 173 Department of Physics, University of Warwick, Coventry, UK
- 174 Waseda University, Tokyo, Japan
- 175 Department of Particle Physics, The Weizmann Institute of Science, Rehovot, Israel
- 176 Department of Physics, University of Wisconsin, Madison, WI, USA
- 177 Fakultät für Physik und Astronomie, Julius-Maximilians-Universität, Würzburg, Germany
- 178 Fakultät für Mathematik und Naturwissenschaften, Fachgruppe Physik, Bergische Universität Wuppertal, Wuppertal, Germany
- 179 Department of Physics, Yale University, New Haven, CT, USA
- 180 Yerevan Physics Institute, Yerevan, Armenia
- 181 Centre de Calcul de l'Institut National de Physique Nucléaire et de Physique des Particules (IN2P3), Villeurbanne, France
- ^a Also at Department of Physics, King's College London, London, UK
- ^b Also at Institute of Physics, Azerbaijan Academy of Sciences, Baku, Azerbaijan
- ^c Also at Novosibirsk State University, Novosibirsk, Russia
- ^d Also at TRIUMF, Vancouver BC, Canada
- ^e Also at Department of Physics and Astronomy, University of Louisville, Louisville, KY, USA
- ^f Also at Physics Department, An-Najah National University, Nablus, Palestine
- ^g Also at Department of Physics, California State University, Fresno, CA, USA

- ^h Also at Department of Physics, University of Fribourg, Fribourg, Switzerland
- ⁱ Also at Departament de Física de la Universitat Autònoma de Barcelona, Barcelona, Spain
- ^j Also at Departamento de Física e Astronomia, Faculdade de Ciências, Universidade do Porto, Portugal
- ^k Also at Tomsk State University, Tomsk, Russia, Russia
- ^l Also at Università di Napoli Parthenope, Napoli, Italy
- ^m Also at Institute of Particle Physics (IPP), Victoria, BC, Canada
- ⁿ Also at National Institute of Physics and Nuclear Engineering, Bucharest, Romania
- ^o Also at Department of Physics, St. Petersburg State Polytechnical University, St. Petersburg, Russia
- ^p Also at Department of Physics, The University of Michigan, Ann Arbor, MI, USA
- ^q Also at Centre for High Performance Computing, CSIR Campus, Rosebank, Cape Town, South Africa
- ^r Also at Louisiana Tech University, Ruston, LA, USA
- ^s Also at Institutio Catalana de Recerca i Estudis Avancats, ICREA, Barcelona, Spain
- ^t Also at Graduate School of Science, Osaka University, Osaka, Japan
- ^u Also at Institute for Mathematics, Astrophysics and Particle Physics, Radboud University Nijmegen/Nikhef, Nijmegen, Netherlands
- ^v Also at Department of Physics, The University of Texas at Austin, Austin, TX, USA
- ^w Also at Institute of Theoretical Physics, Ilia State University, Tbilisi, Georgia
- ^x Also at CERN, Geneva, Switzerland
- ^y Also at Georgian Technical University (GTU), Tbilisi, Georgia
- ^z Also at O Chadai Academic Production, Ochanomizu University, Tokyo, Japan
- ^{aa} Also at Manhattan College, New York, NY, USA
- ^{ab} Also at Academia Sinica Grid Computing, Institute of Physics, Academia Sinica, Taipei, Taiwan
- ^{ac} Also at School of Physics, Shandong University, Shandong, China
- ^{ad} Also at Department of Physics, California State University, Sacramento, CA, USA
- ^{ae} Also at Moscow Institute of Physics and Technology State University, Dolgoprudny, Russia
- ^{af} Also at Section de Physique, Université de Genève, Geneva, Switzerland
- ^{ag} Also at Eotvos Lorand University, Budapest, Hungary
- ^{ah} Also at Departments of Physics and Astronomy and Chemistry, Stony Brook University, Stony Brook, NY, USA
- ^{ai} Also at International School for Advanced Studies (SISSA), Trieste, Italy
- ^{aj} Also at Department of Physics and Astronomy, University of South Carolina, Columbia, SC, USA
- ^{ak} Also at Institut de Física d'Altes Energies (IFAE), The Barcelona Institute of Science and Technology, Barcelona, Spain
- ^{al} Also at School of Physics and Engineering, Sun Yat-sen University, Guangzhou, China
- ^{am} Also at Institute for Nuclear Research and Nuclear Energy (INRNE) of the Bulgarian Academy of Sciences, Sofia, Bulgaria
- ^{an} Also at Faculty of Physics, M.V.Lomonosov Moscow State University, Moscow, Russia
- ^{ao} Also at Institute of Physics, Academia Sinica, Taipei, Taiwan
- ^{ap} Also at National Research Nuclear University MEPhI, Moscow, Russia
- ^{aq} Also at Department of Physics, Stanford University, Stanford, CA, USA
- ^{ar} Also at Institute for Particle and Nuclear Physics, Wigner Research Centre for Physics, Budapest, Hungary
- ^{as} Also at Faculty of Engineering, Giresun University, Giresun, Turkey
- ^{at} Also at Flensburg University of Applied Sciences, Flensburg, Germany
- ^{au} Also at University of Malaya, Department of Physics, Kuala Lumpur, Malaysia
- ^{av} Also at CPPM, Aix-Marseille Université and CNRS/IN2P3, Marseille, France
- * Deceased